Modelling germination and early seedling growth of radiata pine

A thesis
submitted in partial fulfilment
of the requirements for the Degree of
Doctor of Philosophy
at
Lincoln University
by
Mark Bloomberg

Lincoln University
2008

Abstract of a thesis submitted in partial fulfilment of the
requirements for the degree of Ph.D.

Modelling germination and early seedling growth of radiata pine

by

Mark Bloomberg

Background: This study seeks to model aspects of the regeneration of radiata pine (*Pinus radiata* D.Don) seedlings under a range of environmental conditions. This study investigated whether "hybrid" mechanistic models, which predict plant growth and development using empirical representations of plant physiological responses to the environment, could provide a realistic alternative to conventional empirical regeneration models.

Objectives: The objectives of this study were to 1) identify the functional relationships between the environmental conditions controlling germination, establishment and growth of radiata pine seedlings, under a range of those environmental conditions as specified by temperature and available light and soil water; and 2) specify those functional relationships in hybrid mechanistic ("hybrid") models.

Methods: Radiata pine seedling germination and growth were measured under controlled environmental conditions (incubators for seed germination, growth cabinets for seedlings), and results used to adapt, parameterise and test two published hybrid models; one for germination (the hydrothermal time model); and one for seedling growth in the first six months after germination, based on plant radiation use efficiency (RUE).

The hydrothermal model was tested by incubating commercial radiata pine seeds under factorial combinations of temperature and water potentials where germination was likely to occur (12.5 ºC to 32.5 ºC and 0 MPa to –1.2 MPa.). 100 seeds were germinated for each factorial combination. The hydrothermal germination model was fitted to the germination data using non-linear regression modles, will allowed simultaneous estimation of all modle parameters.

Seedlings were grown in controlled growth cabinets, and their RUE was calculated as the ratio of net primary production (NPP, specified in terms of an increase in oven dry biomass), to PAR intercepted or absorbed by a seedling. Estimation of seedling RUE required development of novel techniques for non-destructive estimation of seedling oven

dry weight, and measurement of PAR interception by seedlings. The effect of varying PAR flux density on RUE was tested by measuring RUE of seedlings grown at 125, 250 and 500 μmol m^{-2} s^{-1}. In a second experiment, the effect of deficits in available soil water on RUE was tested by measuring RUE of seedlings grown under 250 μmol m^{-2} s^{-1} PAR flux, and at different levels of available soil water. Available soil water was specified by a soil moisture modifier factor (f_θ) which ranges between 1 for moist soils and 0 for soils where there is insufficient water for seedling growth. This soil moisture modifier had not previously been applied in studies of tree seedling growth.

Temperatures for both seedling experiments were a constant 17.5 ºC (day) and 12.5 ºC (night).

Results: Hydrothermal time models accurately described radiata pine seed germination. Model predictions were closely correlated with actual seed germination over the full range of temperature and water potentials where germination was likely to occur (12.5 ºC to 32.5 ºC and 0 MPa to –1.2 MPa. The minimum temperature for germination (base temperature) was 9.0 ºC. Optimum temperatures for germination ranged from ~20ºC for slow-germinating seeds to ~27 ºC for the fastest germinating seeds. The minimum water potential for seed germination varied within the seed population, with an approximately normal distribution (base water potential = –1.38 MPa, standard deviation of 0.48 MPa). In the process of developing the model, a novel explanation for the decline in germination rates at supra-optimal temperatures was developed (Section 3.4.6), based on earlier models proposed by Alvarado & Bradford (2002) and Rowse & Finch-Savage (2003). This explanation was that the decline in germination rate was not driven just by temperature, but by accumulated hydrothermal time above the base temperature for germination (T_o). This in turn raised the base soil water potential (Ψ_b) towards 0, so that the reduction in germination rate arose from a reduced accumulation of hydro-time, rather than from thermal denaturation of enzymes facilitating germination – the conventional explanation for non-linear accumulation of thermal time at supra-optimal temperatures for plant development. Upwards adjustment (towards 0 MPa) of base water potentials of germinating seeds occurred also at very cold temperatures in combination with high water potentials. In both cases (very cold or else supra-optimal temperatures) this upwards adjustment in base water potentials prevented germination of part of the

seed population, and is proposed as a mechanism which enables seed populations to "hedge their bets" when germinating under less than ideal germination conditions.
RUE of young germinated radiata pine seedlings growing in a controlled growth cabinet was not significantly different over a range of constant PAR flux densities. Mean RUE's were 3.22, 2.82 and 2.58 g MJ^{-1} at 125, 250 and 500 μmol m^{-2} s^{-1} respectively.
In the second experiment, the novel use of a soil moisture modifier (f_θ) to predict RUE of seedlings subjected to water stress proved successful within a limited range of soil water stress conditions. Measured seedling transpiration and stomatal conductance were closely correlated but seedling photosynthesis was less correlated with available soil water. This result suggests that photosynthesis was not coupled with stomatal conductance when PAR flux was 250 μmol m^{-2} s^{-1}, which is well below saturating irradiance for C_3 plants.
Conclusions: The use of hybrid, quasi-mechanistic models to describe tree seedling growth has been seldom explored, which necessitated the development of novel experimental and analytical techniques for this study. These included a predictive model of germination decline at sub- and supra-optimal temperatures; a method for accurately estimating seedling dry weights under a range of PAR flux densities; and a novel method for estimating light interception by small seedlings.
The work reported in this thesis showed that existing hybrid models (the hydrothermal time germination model and the RUE model) can be adapted to model germination and growth of radiata pine seedlings under controlled environmental conditions. Nonetheless, further research is needed before the models can be confidently used as an alternative to conventional empirical models to model regeneration in "real-world" forests. Research priorities are the performance of hydrothermal germination models under variable field conditions, and the use of the soil moisture modifier for seedlings growing on a range of soil textures and under a range of PAR fluxes.
Keywords: mechanistic model; hybrid model; RUE; hydrothermal time models; *Pinus radiata*.

Table of Contents

List of Figures

List of Tables

List of Appendices

Appendices are recorded on a CD which is stored on the inside back cover.

Notation and Abbreviations

Abbreviations	Definitions	Units
[PEG]	Concentration of PEG in water	g PEG/g H_20
A	Silhouette area of the seedling	cm^{-2}
A_p	Net photosynthesis	μmol m^{-2} s^{-1}
AB model	Alvarado & Bradford hydrothermal germination model	
RFS model	Rowse & Finch-Savage hydrothermal germination model	
AIC	Akaike information criterion	
Ancova	Analysis of covariance	
Ap (1-g)	Projected area Ap of the tree crown	m^2
A_β	Projected area of the seedling in the direction β	cm^2
A_φ	Projected area of the seedling in the direction φ	cm^2
C_s	CO_2 concentration at the leaf surface	μmol mol^{-1}
c_θ	Location parameter for the soil moisture modifier f_θ	
D	Ground level stem diameter of seedling	mm
D_l	Vapour pressure deficit between the leaf and the surrounding air	kPa
dS	A small area element of the radiant hemisphere surrounding the plant	m^2
D_s	Vapour pressure deficit at the leaf surface	kPa
Et	Evapotranspiration	mmol m^{-2} s^{-1}
f_D	Vapour pressure deficit modifier	
f_N	Tree nutrition modifier	
f_T	Temperature modifier	
f_θ	Soil water availability modifier	
G	Seed percentile	
gf(ω)	Gap fraction, the proportion of visible sky in the hemisphere above the shoot (the non-visible part of the sky is obscured by surrounding plant canopy)	
GPP	Gross primary production	g
GR	Germination Rate	d^{-1}
g_s	Stomatal conductance	mmol m^{-2} s^{-1}
H	Top height of the seedling	mm
HTI	Hydro-time index	MPa d
I	Downwelling PAR intercepted by an object	W

Abbreviations	Definitions	Units
$I_{(dS)}$	Diffuse radiant flux from dS that is intercepted by the crown of the tree (W)	W
k and k′	Rate of change in Ψ_b with respect to time or temperature	MPa d^{-1}
N	Radiance	W m^{-2} sr^{-1}
NPP	Net primary production	g
n_θ	Shape parameter for the soil moisture modifier f_θ	
p	Probability	
PAR	Photosynthetically active radiation	
PAW	Plant available water	
PEG 8000	Polyethylene glycol 8000	
PPFD	Photosynthetic photon flux density	μmol m^{-2} s^{-1}
Probit (G)	The probit function which calculates the standard normal deviate (z) for a specified cumulative probability (= G) in a normally distributed population	
Q	Incident irradiance	W m^{-2}
Q_φ	Incident PPFD at elevation angle φ	μmol m^{-2} s^{-1}
$q(\omega)$	Seasonal amount of PAR from the direction of ω	J m^{-2} sr^{-1}
r	Radius of a radiant hemisphere	m
R^2	Coefficient of determination	
R_a	Autotrophic respiration	μmol m^{-2} s^{-1}
R_d	Day respiration	μmol m^{-2} s^{-1}
RH	Relative Humidity	%
RPE	Relative Prediction Error	%
RUE		G MJ^{-1}
r_θ	Soil moisture ratio	
SD	Standard deviation	
SLA	Specific leaf area	m^2/kg
SMC	Soil moisture characteristic curve	
SSA(ω)	Shoot silhouette area (on a plane normal to the direction ω	m^2
SOHTI	Supra-optimal hydrothermal time	ºC MPa d^{-1}
t(G)	Time for the G^{th} percentile to germinate	d
T_{air}	Ambient air temperature	ºC
T_b	Base temperature for seed germination	ºC
T_c	Ceiling temperature for seed germination	ºC
T_d	Deviation temperature for seed germination	ºC
T_{leaf}	Temperature of the leaf surface	ºC
T_o	Optimum temperature for germination	ºC
v/v	Volume/volume ratio	

Abbreviations	Definitions	Units
V_c	Rate of carboxylation	μmol m^{-2} s^{-1}
V_m	Coefficient in Michaelis-Menten equation	
VPD	Vapour pressure deficit	kPa
W	Seedling oven-dry biomass	g
W_a	Total above-ground biomass(calculated oven dry weights of foliage and stem)	g
W_r	Root oven dry weight	g
WU	Water use (% of maximum)	%
z	Standard normal deviate	
β	Zenith angle of dS from the vertical	degrees or radians
έ	Radiation Use Efficiency	G MJ^{-1}
θ	Azimuth angle on the horizontal plane	degrees or radians
θ	Volumetric soil water content (v/v)	mm mm^{-1}
θ (w/w)	Gravimetric soil moisture content	kg/kg
θ_{HT}	Hydrothermal time constant that has a unique value for the seed population	ºC MPa d^{-1}
θ_{max}	Soil water content at field capacity	mm mm^{-1}
θ_{min}	Soil water content (v/v) at wilting point	mm mm^{-1}
θ_s	Saturated water content (v/v)	mm mm^{-1}
ρ_b	Soil dry bulk density	kg m^{-3}
ρ_w	Density of water	kg m^{-3}
$\Sigma\varphi_{p.a}$	Cumulative absorbed PAR ($\varphi_{p.}$) summed over a time interval	MJ
$\Sigma\varphi_{p.i}$	Cumulative intercepted PAR summed over a time interval	MJ
$\sigma_{\Psi b}$	Standard deviation of Ψ_b	MPa
φ	Elevation angle of the direction in which the quantum sensor was aimed	Degrees or radians
$\varphi_{p\,a}$	Absorbed PAR	MJ
$\varphi_{p.i}$	Intercepted PAR	MJ
Ψ	Water potential	MPa
Ψ_b	Base water potential	MPa
Ψ_b (50)	Median (mean) base water potential	MPa
Ψ_b (G)	Base water potential for the G^{th} percentile of the seed population	MPa
Ψ_e	Soil water suction below which $\theta = \theta_s$	kPa
Ψ_{soil}	Soil matric potential	kPa
ω	A solid angle within a hemisphere above the shoot	sr
Ω	Total solid angle of a hemisphere	sr

1 INTRODUCTION

1.1 Overview

This study seeks to model aspects of the regeneration of radiata pine (*Pinus radiata* D.Don) seedlings under a range of environmental conditions. The term "regeneration" as used by ecologists and foresters includes the production and dispersal of seeds, their storage in seed banks until conditions are favourable for germination, followed by their germination and the establishment of seedlings on the forest floor (Barnes *et al.* 1998d; Price *et al.* 2001).

Radiata pine grows both in natural forests within its limits of natural distribution in California and in approximately four million hectares of managed plantations which are principally located in the Southern Hemisphere (Lavery & Mead 1998). These radiata pine plantation forests may regenerate themselves (natural regeneration) or be regenerated by human intervention, for example by planting of nursery raised seedlings. This means that radiata pine may regenerate into a wide range of environments where previous studies of radiata pine regeneration in its natural range do not necessarily apply. An example of this which is particularly relevant to plantation grown pines, is the spread of wildings, naturally regenerated seedlings originating from plantations but dispersing into adjacent vegetation as an invasive plant (Richardson & Higgins 1998).

Therefore, this study aims to develop general models which will be robust enough to describe germination and seedling growth in the wide range of regeneration niches now available to radiata pine within and beyond its natural range. Conventional empirical regeneration models may not meet this criterion of generality. Reynolds *et al.* (2001) criticise empirical regeneration models on these grounds, and call for greater use of mechanistic models to study forest regeneration. In contrast to empirical models, mechanistic models of plant growth and development specify the responses of plant physiological processes to variation in environmental factors, such flux density of

photosynthetically active radiation (PAR), soil water availability and ambient air temperature. Mechanistic models are usually considered to be more general than empirical models, because they are based on physiological processes that are always determinants of plant growth and development, rather than empirical relationships between environment and plant growth that cannot be safely extrapolated outside the boundaries of the data from which they were derived (Korzukhin *et al.* 1996).
This study investigates the use of mechanistic models–a promising alternative to conventional empirical regeneration models–to describe two important aspects of regeneration, namely seed germination and early seedling growth. Mechanistic models were chosen for investigation because they seemed more likely than empirical models to achieve the generality and robustness required to model germination and seedling growth of radiata pine seedlings under the wide range of environmental conditions where radiata pine now grows.

1.2 Summary of thesis objectives and structure

1.2.1 Thesis objectives

Objectives: The objectives of this study were to 1) identify the functional relationships between environmental conditions and germination, establishment and growth of radiata pine seedlings, under a range of those conditions specified by temperature and available light and soil water; and 2) specify those functional relationships in mechanistic models.

To meet these objectives, radiata pine seed germination and seedling growth were measured under controlled environmental conditions (incubators for seed germination, growth cabinets for seedlings). The results were used to develop and parameterise two mechanistic models-one for germination, one for seedling growth in the first six months after germination. The validity of the models was assessed using model explanatory power and/or the statistical significance of model parameters as criteria.

1.2.2 Thesis structure

Chapter 2 reviews the scientific literature relevant to this study and develops the objectives set out in Section 1.2.1 above.
Chapter 3 describes the development of a mechanistic germination model for radiata pine seed.
Chapter 4 describes the development of a mechanistic model relating seedling growth to PAR intercepted by the seedling. Chapter 5 describes the development of functions which modify this relationship between growth and intercepted PAR when available soil water is suboptimal.
While the effects of temperature and soil nutrients on this relationship between seedling growth and PAR are also important, it was not possible to investigate them within the time available for this study.
Chapter 6 reviews the results of this study and discusses potential future research to study temperature and soil nutrient effects on plant growth, as well as other future research suggested by the results of this study.

2 LITERATURE REVIEW

2.1 Background

The overall aim of this study was to model aspects of regeneration of radiata pine seedlings under a range of environmental conditions. The term "regeneration," as used by forest ecologists and foresters, includes the following aspects: 1) the production and dispersal of seeds; 2) their storage in "seed banks" until conditions favourable for germination occur; followed by 3) their germination; and 4) the establishment of seedlings on the forest floor (Barnes *et al.* 1998d).

This study is not a broad investigation of regeneration of radiata pine but instead focuses on aspects 3 and 4 above (germination and seedling establishment). However germination and seedling growth are not isolated processes and occur in the context of forest regeneration. Therefore this chapter will look firstly at broader aspects of regeneration of radiata pine, so as to illustrate the relevance of the germination and seedling growth models that are discussed in the second part of the chapter.

The next three sections describe where and how radiata pine forests regenerate themselves (natural regeneration) or are regenerated by human intervention e.g. in managed plantations.

2.1.1 Natural regeneration of radiata pine

Radiata pine originates from the "fog belt" along the coast of central California, where the climate is classified as cool mediterranean (Dallman 1998). Air temperatures are relatively uniform and moderate throughout the year and although summer droughts are the norm, these are tempered by sea fogs which moderate air and soil temperatures (Forde 1966). Despite the occurrence of sea fogs, radiata pine seed (which is retained on the tree in closed (serotinous) cones (Roy 1966)) may be released during the summer due to either hot dry weather (Roy 1966) or episodic wildfires (Stephens *et al.* 2004; O'Brien *et al.* 2007).

After a dry summer, the rainy season typically begins in late autumn and continues throughout a mild winter. Radiata pine seed has no physiological or physical dormancy (Kusmintardjo *et al.* 1991) and given adequate soil aeration, will commence germination as soon as soil moisture and temperature are suitable. Therefore, although there is no published study of germination and seedling emergence in natural radiata pine forests, it is safe to assume that the released radiata pine seeds commence imbibition at the onset of the rainy season and that germination and initial seedling growth may continue throughout the winter and the following spring. This germination and regeneration pattern was reported for radiata pine plantations growing in South Australia (Fielding 1947) which experiences a similar mediterranean climate pattern to that in California. The same pattern has also been reported for *Pinus halapensis* Miller, a species with serotinous cones growing on coastal Mediterranean sites which also regenerates prolifically after stand-replacing fires (Daskalakou & Thanos 2004).

Because of radiata pine's serotinous cone habit and suitable mild moist weather in autumn and spring after seed has been released, complete stand replacement occurs successfully in natural radiata pine forests after large-scale summer fires (Stephens *et al.* 2004). However, seed may also be released from radiata pine's serotinous cones after smaller scale disturbances e.g. loss of canopy trees due to disease or patchy fires which do not kill all the parent trees (Roy 1966; Storer *et al.* 2001; O'Brien *et al.* 2007). In these situations radiata pine seedlings may germinate and grow in the shade of a partial overstorey or in small gaps where solar radiation is partially intercepted by surrounding trees (Storer *et al.* 2001). In a survey of U.S forest managers in 1947, radiata pine was classified as having intermediate shade tolerance (Baker 1949), whereas most common pines growing in the Western United States were classified as intolerant or very intolerant. Baker's (1949) assessment of radiata pine's shade tolerance is consistent with Baker (1945) and Moulds (1955) who reported vigorous growth of radiata pine seedlings

under reduced light in a greenhouse (in California) and beneath existing plantations (in South Australia) provided the seedlings had adequate water[1].

2.1.2 Plantations

In New Zealand, Chile, Australia and South Africa, radiata pine is an important exotic plantation species and is typically regenerated after clearfelling. Historically in New Zealand this was achieved by natural regeneration but this gave variable results (Page 1970). Since the late 1960's replanting of clearfelled forests with nursery-raised seedlings has predominated. Planting of seedlings in New Zealand is accompanied by intensive weed control measures in order to reduce competition from fast-growing weed species such as gorse (*Ulex europaeus* L.) and buddleia (*Buddleja davidii* Franchet) (Richardson 1993). This seems consistent with radiata pine's regeneration strategy in its natural habitat where it is adapted for regeneration after large-scale stand-replacing fires. Similarly, in New Zealand natural regeneration can be prolific after sheet disturbance from large scale wildfires (Fenton 1951; Thomson & Prior 1958). However, as noted in Section 2.1.1, radiata pine is also capable of regenerating in the shade of small forest gaps or under partial overstories which gives it the potential to regenerate after partial forest disturbance or even invade established forests and shrublands.

2.1.3 Radiata pine as an invasive plant

Radiata pine can be an invasive plant. Typically this occurs in the form of fringe spread of "wildings" (naturally regenerated seedlings) from radiata pine plantations into ungrazed, low-stature grasslands and shrublands such as *fynbos* in South Africa and native tussock grassland in New Zealand (Richardson & Higgins 1998); and some types of eucalypt forest in Australia (Minko & Aeberli 1986). In these cases radiata pine exhibits sufficient tolerance of competition for light, water and nutrients that it can naturally regenerate itself beneath an existing vegetative canopy.

[1] In this context it is worth mentioning that the original concept of shade tolerance has been broadened to include tolerance of root competition (Barnes *et al.* 1998a**,** p399 *et seq.*), and that water and nutrients may be major limiting factors for seedlings regenerating beneath a partial overstorey or in a small forest gap.

2.1.4 Summary of regeneration behaviour of radiata pine

To characterise the regeneration behaviour of radiata pine one has to account for the germination of radiata pine seed and growth of the germinated seedling in four different circumstances i.e.

1. As a germinating seedling on open sites created by stand-replacing fires or clearfelling.
2. As a germinating wilding beneath grassland, shrub and forest canopies e.g. in South Africa, New Zealand and Australia.
3. As a naturally regenerating seedling in gaps or under a partial overstorey in its native habitat.
4. Finally, it may not be fanciful to include the germination and growth of seedlings in nursery seedbeds and their planting out on clearfelled plantation sites as an important category of regeneration, subject to the same physical limitations as the other three categories above. Certainly this last is likely to be the most important form of regeneration in radiata pine forests, because managed plantations in New Zealand, Chile, Australia and elsewhere are far greater in area than the remnant native populations of this species (Lavery & Mead 1998).

2.2 The Regeneration Niche

2.2.1 The concept of the regeneration niche

The concept of the regeneration niche will be used in this study to understand the regeneration of radiata pine, described in Section 2.1. The concept of the regeneration niche was first advanced by Watt (1947) and expounded by Grubb (1977). Grubb (1977) noted that a plant's ecological niche has three aspects: 1) the habitat niche, which is "the physical and chemical limits tolerated by the mature plant in nature"; 2) the plant's form and function which define its role within the ecosystem, described by Grubb (1977) as the life-form and phenological niches, and 3) the regeneration niche, "an expression of the requirements for a high chance of success in the replacement of one mature individual by a new mature individual of the next generation."

Therefore an understanding of regeneration by a plant species is predicated on an understanding of both the site where regeneration occurs (habitat), and the way in which seed and seedling form and function (life-form and phenology) are adapted to give the best chance of success for regeneration on that site. Grubb (1977) noted that the regeneration niche included elements of the habitat, life-form and phenological niches, which suggests that his scheme does not properly account for variation in these niches with time. It may be more rigorous to say that the niche of a plant species has three aspects: 1) its habitat; 2) its life-form and phenology; and 3) a temporal aspect, which recognises that aspects 1 and 2 may vary throughout the life of a plant (Barnes *et al.* 1998b). For example, a common observation is that the habitat niche of a regenerating plant is usually narrower than the niche occupied by a mature plant, because of the sensitivity of the regenerating seedling to minor fluctuations in environmental factors such as soil moisture (Farmer 1997, p155).

Grubb also noted Hutchinson's (1957) idea of the potential niche (where the plant is able to survive and regenerate) versus the realised niche (where the plant actually grows). The realised niche is often more geographically restricted than the potential niche. This is due to predation and competition, or to limits on the dispersal of a species arising from historical events e.g. glaciation, which mean that the species has not yet re-colonised sites which are highly suited to its growth (Perry 1994, p186-187). The concept of the realised niche implies that the regeneration niche defined by the regenerating plant's habitat, life-form and phenological niches may be further narrowed by biotic factors such as competition, seed predation, herbivory and pathogens. It may also be widened through beneficial interactions with other organisms e.g. root symbioses (Perry 1994, p186-187).

2.2.2 Defining the regeneration niche for radiata pine

The adaptation of a plant species' regeneration strategy to its physical niche necessarily evolves within the natural range of the species. This adaptedness may be impaired (or enhanced) by human influence on the physical niche. This last point is illustrated by radiata pine in its natural range, which consists of three small separate populations on the central Californian coast, as well as two island populations (Figure 2.1). The mainland

radiata pine forests are now surrounded by urban areas and other human developments (Lavery & Mead 1998) and consequently forest wildfires are controlled to protect human life and property. Predictably, the control of fire has interrupted the normal regeneration process of radiata pine in these native forests which depends on regular wildfires to stimulate seed release and to clear competing vegetation from the regeneration site (Storer *et al.* 2001).

Figure 2.1. Natural distribution of radiata pine.

Most cultivated populations are descended from the three populations on mainland California. 1= Año Nuevo Point, 2 = Monterey, 3 = Cambria. In addition there are two island populations, 4= Guadelupe Island, 5 = Cedros Island (both islands are under Mexican sovereignty). Source: Bannister (1973).

One other consequence of human activity is that radiata pine has been widely planted as a plantation and ornamental species throughout the temperate Southern hemisphere (South America, Australia, New Zealand) and in limited areas in the northern hemisphere such as northern Spain (Lavery & Mead 1998, p439 *et seq*). In many cases, radiata has been successful in habitats which are quite different from those in its natural range e.g. radiata exhibits very high growth rates on deep volcanic soils in the Central North Island of New Zealand where rainfall is well-distributed throughout the year and totals approximately 1500 mm yr^{-1}, in contrast to its natural range where a Mediterranean climate pattern results in prolonged summer droughts (although mitigated by sea fogs) and annual rainfall ranges from 400-800 mm yr^{-1} (Lavery & Mead 1998, p435).

This suggests that radiata pine's realised niche in California is narrower than its potential niche which is expressed in the wide range of sites on which radiata has been successful as a plantation species. On the other hand radiata pine has typically been first established as a plantation species by planting well-conditioned nursery seedlings, obviating the need for successful regeneration from seed. In contrast to the success of radiata pine as a planted crop, subsequent natural regeneration of radiata pine after clearfelling the first planted crop has been highly variable in New Zealand (Page 1970), suggesting that exotic forest plantations do not always provide a suitable regeneration niche for radiata pine.

Faced with the diversity of habitats where radiata pine is now growing, and with human interference (clearfell harvesting, fire control) in the adaptation of radiata pine to its regeneration niche, trying to characterise that niche may seem a difficult task. However the task is simplified by radiata pine's serotinous habit and absence of seed dormancy which means that seedfall is not dependent on the timing of flowering and seed development; nor is germination dependent on winter chilling of seed or other dormancy-release mechanisms. Instead, successful regeneration of radiata pine depends solely on seed release from an aerial seedbank (seeds held in serotinous cones) and the degree to which the seed and seedling's life form and phenology are adapted to the physical niche available at the time the seed is released. How best to study this relationship between the

physical niche and a seedling's life form and phenological adaptations to its physical niche is discussed in the next section.

2.3 Study Methods

The concept of the regeneration niche implies that if seeds or seedlings at the same phenological stage experience the same physical conditions (habitat niche) in two different locations, their germination and growth will proceed at the same rate and follow the same course in both locations. This in turn suggests that if the relationships between the physical and life form/phenological niches are known, then specifying the physical niche at any location should enable predictions to be made about the germination and growth of the seedling. The next section discusses how best to specify the habitat and life form/phenological niches in order to make these predictions.

2.3.1 Modelling regeneration

Models of plant growth and development can be broadly categorised as either empirical or mechanistic. Empirical models treat underlying physiological processes as a "black box," and "describe statistical relationships among the data with limited regard to the object's internal structure, rules or behaviour" (Korzukhin *et al.* 1996). In contrast, mechanistic models describe data "using a current understanding of key mechanisms or processes that determine the object's internal structure, rules and behaviour" (Korzukhin *et al.* 1996). For example, mechanistic models of plant growth and development specify the responses of plant physiological processes (such as photosynthesis, uptake of soil water and nutrients, and respiration and transpiration) to variations in environmental factors such as flux density of PAR, soil water availability and ambient air temperature. For this reason, mechanistic models are usually considered to be more general because they are based on physiological processes that are always determinants of plant growth and development. In contrast, empirical models are only applicable within the data domain used to estimate their parameters. Extrapolation outside this domain has the pitfalls attendant on any extrapolation (Korzukhin *et al.* 1996).

Price *et al*., (2001), Reynolds, Bugmann, & Pitelka, (2001),Wullschleger *et al*., (2001) and Mason *et al*. (2007) have criticized empirical forest regeneration models on grounds of generality, stating that: 1) they will not be robust if they can not model future effects of climatic change and elevated CO_2 and 2) processes such as germination and weed competition are determined by small-scale environmental variations in the regeneration site, which are not captured by empirical models. This second criticism is supported by the findings of Gray & Spies (1997) that variations in microsite had as much if not more influence than seedling position within forest gaps, on regeneration of Douglas fir (*Pseudotsuga menziesii* (Mirb.) Franco) and western hemlock (*Tsuga heterophylla* (Raf.) Sarg.) in the Pacific Northwest of the U.S.A.

This study aims to explain and predict the regeneration behaviour of radiata pine under a wide range of conditions. To achieve this requires a model of the regeneration niche which has generality in the sense defined by Sharpe (1990)−"the applicability of a concept to a whole range of instances". A mechanistic model relating germination and growth of seedlings to physical site variables will probably have greater generality than an empirical model in that it should enable 1) comparison between different sites on a consistent basis and 2) simulation of the effects of human intervention, both deliberate (silviculture and fire control) and inadvertent (climate change), provided these can be specified in terms of their effects on the physical characteristics of the site.

However, mechanistic models are not without disadvantages. Mason *et al*. (2007) contend that 1) they are inherently complex and require inputs of numerous measurement variables that may be expensive or difficult to obtain; and 2) they may be recursive, meaning that their complex structure leads to model outputs being re-used as inputs to generate further outputs. This second disadvantage may lead to compounded errors in model predictions.

The overcomplexity of mechanistic models, coupled with the abovementioned limitations of conventional empirical models, has led to the development of quasi-mechanistic or "hybrid" models (Mason *et al*. 2007), which use empirical mathematical representations

of physiological processes to model plant growth and development. A well-known example of a hybrid model is the "thermal time" concept, where thermal time above a defined base temperature is used as the independent variable when modelling many plant growth and development processes (Bonhomme 2000; Trudgill *et al*. 2005). The thermal time concept has a mechanistic component, in that plant physiological processes proceed at a rate that is temperature dependent; however, the relationship between temperature and these plant processes is complex and non-linear. Thermal time simplifies these complex physiological relationships into an empirical linear relationship that is approximately correct within a defined temperature range.
Hybrid models are simpler than equivalent mechanistic models, but retain at least some of their generality and ability to represent how plant physiological processes respond to the environment. For this reason "hybrid" models, rather than conventional empirical or mechanistic models, were used in this study to model aspects of radiata pine regeneration.

The germination niche for a seed is usually different from the niche for the growing seedling, in that seedling growth occurs both above and below the ground and depends on photosynthesis and root uptake of soil nutrients, processes which do not occur during seed germination. In other words, the physical site variables controlling germination of most conifer seeds are not identical with those that subsequently control growth of the seedling. This implies two separate hybrid models will be needed to characterise radiata pine's regeneration niche, one for germination and one for seedling growth.

2.4 Modelling of germination

2.4.1 Germination processes

Germination begins with imbibition of water by the seed and continues until either 1) the radicle emerges from the seed coat or 2) the growing embryo does not have enough turgor pressure to rupture the tissues that enclose the embryo within the seed, in which case it becomes quiescent (Bradford 2002).

The environmental factors which are critical to germination of a non-dormant seed are water availability, the physical nature of the germination seedbed (including drainage and porosity as they both influence soil aeration) and seedbed temperature (Finch-Savage 2004). Water availability must be sufficient for imbibition and subsequent development of the germinating seed. Soil water also influences the physical resistance of the substrate to penetration e.g. germination may fail when the strength of a dry soil exceeds a threshold resistance and it therefore impedes emergence of the germinating seedling (Minko 1986) or downward growth of the radicle and subsequent seedling root growth (Pomeroy 1949; Zou *et al.* 2000a).

Germination is also strongly controlled by temperature (Bewley & Black 1983).
Even if non-dormant, seeds typically have threshold temperatures beyond which germination will not occur. Base temperature (T_b) is the temperature where the seedbed becomes too cold for germination: ceiling temperature (T_c) is the temperature at which the seedbed becomes too hot and germination is prevented (Roberts 1988).
In addition, seeds have a base water potential (Ψ_b), below which the seedbed becomes too dry for seeds to germinate (Finch-Savage 2004). There is no ceiling threshold for seedbed water potential because a seedbed with a water potential of ~0 MPa provides optimum conditions for seed germination, assuming adequate aeration.

Under ideal seedbed conditions, seeds germinate rapidly. As seedbed conditions tend towards threshold values (T_b, T_c, Ψ_b), seeds germinate more slowly. Furthermore germination rates vary within the seed population, even when all seeds are subjected to identical conditions. Therefore germination models usually include a function which directly or indirectly predicts the frequency distribution of germination rates within the population. Similarly, under adverse seedbed conditions not all seeds may germinate, even if the population is non-dormant and has high seed viability (Finch-Savage 2004). Germination models must therefore also predict the frequency distribution of the seeds' ability to germinate, under a range of seedbed conditions.

Forcella *et al*. (2000) reviewed a number of published empirical and mechanistic models of seed germination response to seedbed conditions. In particular, they noted that many empirical models did not adequately describe germination in variable wild seed populations, or in seedbeds with varying soil water potential. This latter deficiency may be in part due to the greater difficulty of measuring soil water (and especially water potential) compared to soil temperature. However, they state that the hydrothermal time model first proposed by Gummerson (1986) does provide a method for modelling the cumulative effects of water deficits on germination, commenting that the model was "so appealing that rapid adoption can be expected by those involved with modelling seedling emergence" (Forcella *et al*. 2000).

Because of its ability to dynamically model effects on germination of both seedbed temperature and seedbed water potential, the hydrothermal germination model was chosen for closer investigation in this study.

2.4.2 Hydrothermal germination models

In hydrothermal models, germination rate and percentage germination are explained by seed population characteristics and by the water potential (Ψ) and temperature (T) of the seed's environment.

The hydrothermal germination model (Gummerson 1986) can be specified mathematically as:

$$\theta_{HT} = [\Psi - \Psi_b(\mathrm{G})]\,(T - T_b)\,t(\mathrm{G}) \qquad (2.1)$$

where θ_{HT} is a hydrothermal time constant that has a unique value for the seed population, $\Psi_b(\mathrm{G})$ is the base water potential for the G^{th} percentile of the seed population, T_b is the base temperature for seed germination and $t(\mathrm{G})$ is the time for the G^{th} percentile to germinate. The hydrothermal time model falls into the "hybrid" category because it uses empirical variables (thermal time = $(T - T_b)\,t(\mathrm{G})$ and the conceptually equivalent "hydro-time" = $[\Psi - \Psi_b(\mathrm{G})]\,t(\mathrm{G})$) to predict the time course of the physiological processes involved in germination. Germination is completed when the seed has

accumulated hydrothermal time ([$\Psi - \Psi_b$(G)] (T–T_b) t(G)) equal to the hydrothermal time constant θ_{HT}.

The model predicts that under constant conditions of T and Ψ, the Gth percentile in the population will germinate at t(G), when the seeds in that percentile have accumulated hydrothermal time equal to the population hydrothermal time constant θ_{HT}. It also specifies that Ψ_b varies within the population (with each seed percentile G having a unique value for its base water potential, Ψ_b(G)); but base temperature has a common value for all percentiles (T_b). Hence all seeds in the population will accumulate the same thermal time (θ_T) under any temperature regime in the seed's environment. In contrast, because Ψ_b differs between percentiles, each percentile will accumulate different amounts of "hydro-time" (θ_H) within a specific time period under any moisture regime applied to the whole seed population. Therefore it is the variation in Ψ_b that results in a spread of seed germination times within the population (Bradford 2002; Finch-Savage 2004). Furthermore, if Ψ_b is normally distributed, then the median base water potential (Ψ_b (50)) will equal the mean Ψ_b for the seed population.

These specifications of Ψ_b and T_b are not arbitrary but have held true in many germination studies (Covell *et al.* 1986; Bradford 2002).

The features of the hydrothermal germination model described in the preceding paragraph are illustrated in Figure 2.2A (overleaf).

For most seed plants there is an optimum temperature (T_o) for germination, where both the germination rate (GR) of seeds and their germination percentage are maximal. Above T_o both GR and germination percentage decline, eventually reaching zero at a ceiling temperature (T_c) (Roberts 1988). The hydrothermal germination model (Equation 2.1) only applies when temperatures are below the optimum temperature because it implies that germination rate will increase indefinitely with increasing T i.e. if the term ($T - T_b$) becomes larger and if θ_{HT} is a constant, then t(G) must become smaller. To account for the decline in GR at supra-optimal temperatures, additional terms must be included in the hydrothermal model.

Removed for copyright reasons

Figure 2.2. A. Relationship between germination rates and temperature, B. Relationship between germination rates and water potential (Ψ).

A. At sub-optimal temperatures, germination rates (*GRg*) for different fractions (percentages) of the seed population increase linearly with temperature above a common base temperature (T_b). The slopes of the lines are equal to the inverses of the thermal times to germination ($1/\theta_T(g)$), which vary among individual seeds in a normal distribution (inset 1). The maximum *GRg* occurs at the optimum temperature (T_o), and above this temperature *GRg* decreases linearly. The ceiling temperatures for germination ($T_c(g)$) vary among seed fractions in a normal distribution (inset 2).
B. As Ψ decreases, germination rates for different percentages decrease linearly with a common slope of $1/\theta_H$, intercepting the *x*-axis at different threshold or base water potential values ($\Psi_b(g)$), which are normally distributed among seeds in the population (inset). Source: Bradford (2002).

2.4.3 Hydrothermal models for supra-optimal temperatures

Alvarado & Bradford (2002) and Rowse & Finch-Savage (2003) have proposed hydrothermal models which account for declining *GR* and germination percentage above T_o. Both models achieve this by adjusting the base water potential of seeds (Ψ_b(G)) towards zero with increasing temperature above T_o. This adjustment reduces the hydro-time accumulated by the seed during germination and so the seed takes longer to accumulate hydrothermal time equal to the θ_{HT} which it must do before it can germinate.

In the conventional hydrothermal model, seed base water potentials are normally distributed around Ψ_b(50). Therefore at sub-optimal temperatures the slower germinating seeds (G > 50%) will have a Ψ_b(G) value that is closer to zero and so will accumulate hydrothermal time more slowly than the faster seeds (G < 50%), whose Ψ_b(G) values are at the other end of the frequency distribution. Alvarado & Bradford (2002) and Rowse & Finch-Savage (2003) propose that at supra-optimal temperatures, the upwards-adjusted value of Ψ_b for the slow seeds may approach or even exceed 0 MPa and so they cannot germinate even under optimum conditions. Bradford & Somasco (1994) use this model to explain thermo-inhibition in lettuce (*Lactuca sativa* L.) seed, where some strains of lettuce will not germinate even at 0 MPa if exposed to high temperatures (≈ 35 °C). The behaviour of the supra-optimal hydrothermal time model proposed by Bradford (2002) is shown in Figure 2.2A.

One advantage of the hydrothermal models proposed by Alvarado & Bradford (2002) and Rowse & Finch-Savage (2003) is that they give a mechanistic explanation for germination rates at both sub- and supra-optimal temperatures, as follows. Ψ_b has been linked to the resistance of tissues surrounding the embryo (such as the endosperm) to radicle elongation, so that seeds with more resistant tissues require higher turgor pressures in the radicle in order to emerge (Bradford 1995; Bradford 2002). High radicle turgor pressures result from moist seedbeds which allow the seed to fully imbibe, therefore an increase in the resistance of surrounding tissues necessitates moister seedbed conditions for germination, which means that the seed's Ψ_b is closer to zero. Thermo-inhibition at supra-optimal temperatures is also explicable using this model, because there

are physiological processes (mediated by abscisic acid (ABA)) within the seed that increase endosperm resistance, effectively raising the value of Ψ_b towards zero and therefore causing reduced germination at supra-optimal temperatures (Tamura *et al.* 2006).

2.5 Modelling of seedling growth

2.5.1 Seedling growth processes

Germination is completed and the seedling phase commences once the radicle emerges from the seed and begins to elongate (Bradford 1995). Pine seed germinates epigeally and the cotyledons emerge from the seed coat once the radicle has commenced downward extension into the soil (see Figure 2.3).

Once the cotyledons have emerged, the germinating seedling begins to photosynthesise. In pines, the cotyledons may also contribute to seedling growth from stored reserves (Sasaki & Kozlowski 1968). However the germinant now also relies on light–or more specifically, on photosynthetically active radiation (PAR). PAR is that part of incident light which, when absorbed by the plant's foliage, provides the energy to drive photosynthetic processes.

Removed for copyright reasons

Figure 2.3. Emergence of a pine seedling.

The seed (*a*) germinates epigeally, either on or just below the seedbed surface. The radicle (*c*) emerges and commences rapid downwards growth into the seedbed. The hypocotyl (*b*) elongates which lifts the seed coat and cotyledons (*d*) free of the seedbed. Finally the cotyledons emerge by shedding the seed coat. Source: Barnes *et al.* (1998d, p110).

Landsberg & Gower (1997) describe a mechanistic model of the relationship between PAR absorbed by the seedling's foliage and seedling growth:

$$\mathrm{NPP} = \acute{\varepsilon}\Sigma\varphi_{\mathrm{p.a}} \qquad (2.2)$$

where NPP = net primary dry mass production over a specified time interval, $\acute{\varepsilon}$ = radiation use efficiency and $\Sigma\varphi_{\mathrm{p.a}}$ = total absorbed PAR summed over the specified time interval.

Note that NPP = GPP – R_{a}, where GPP is net photosynthetic production and R_{a} is autotrophic (non-photosynthetic) respiration by the plant. NPP is therefore the

photosynthetic production that is available for growth (and subsequent litterfall) after the plant has met its requirement for metabolic energy.

All mechanistic models of plant growth have the structure implied by Equation 2.2, where plant NPP is governed by the amount of PAR absorbed by the plant (APAR or $\varphi_{p.a}$) and the efficiency with which it is converted into dry matter (radiation use efficiency or RUE, $\acute{\varepsilon}$). RUE is governed by the rate of leaf photosynthesis, less the rate of autotrophic respiration for the whole plant. Leaf photosynthetic rate in turn is governed by leaf age, the temperature of the leaf and leaf water and nutritional status; whereas autotrophic respiration is primarily influenced by temperature (Landsberg & Gower 1997). Mechanistic models therefore specify the linkages between RUE and environmental factors such as air temperature, relative humidity and soil nutrient and water availability in terms of their influence on the temperature of the leaf and leaf water and nutritional status.

The Farquhar-von Caemmerer-Berry photosynthetic model (Farquhar *et al.* 1980) can be used to illustrate this point. This model, which has become the most widely used mechanistic model for analysis of photosynthesis in C_3 plants (Landsberg & Gower 1997, p130), gives the net rate of photosynthesis as (von Caemmerer 2000):

$$A_p = V_c/(1 - \Gamma_*/c_i) - R_d \qquad (2.3)$$

where A_p is the net rate of photosynthesis, V_c is the rate of carboxylation (CO_2 fixation) by the leaf, Γ_* is the CO_2 compensation point in the absence of R_d (="day" respiration, defined as all mitochondrial respiration other than photorespiration (von Caemmerer 2000)) and c_i is the intercellular concentration of CO_2.

In terms of environmental factors, carboxylation rate (V_c) is controlled by both temperature and leaf nitrogen (von Caemmerer 2000), and R_d is controlled by temperature (Landsberg & Gower 1997, p139). c_i is influenced by c_a (the ambient concentration of CO_2) and by stomatal conductance, which in turn is controlled by leaf water status and the vapour pressure deficit (Landsberg & Gower 1997, p133). Low soil water and nutrient availability, low temperatures and high vapour pressure deficits

therefore combine to reduce V_c and c_i, which in turn results in reduced leaf photosynthesis. At the same time, R_d decreases with lower temperatures ((Landsberg & Gower 1997, p139), and this may counteract to some extent reductions in V_c.
The next section describes a classification of mechanistic plant growth models, based on the way in which the models specify the relationship between absorbed PAR and net photosynthesis, and how they model the influence of environmental factors on this relationship.

2.5.2 Mechanistic models of seedling growth

Medlyn (2004, p33), provides a useful classification of mechanistic models used for simulating forest growth in Australia into four categories. In order of increasing complexity they are: 1) maximum productivity models, where multipliers which are functions of environmental deficits are used to reduce the postulated maximum net primary dry mass production (NPP) that occurs under ideal conditions; 2) Radiation use efficiency (RUE) models; 3) "big-leaf" models i.e. where the forest canopy is treated as a single leaf for the purposes of calculating PAR absorption and gross primary production (R_d is calculated separately) and 4) sun-shade models which divide the forest canopy into sections with similar incident PAR and then calculate the photosynthetic rate in each section.

Medlyn (2004) notes that both the maximum productivity and the RUE models have the advantage of simplicity, but the simplifying assumptions used in the models may mean a loss of generality (e.g. ability to predict forest growth under a wide range of present and future conditions). They have also been criticised on grounds of reality; in particular the simple linear relationship between absorbed PAR and NPP in the RUE model (NPP = $\acute{\varepsilon}\Sigma\varphi_{p.a}$, where $\acute{\varepsilon}$ is the slope constant) does not seem consistent with the non-linear response of photosynthesis to increasing PPFD (Medlyn 2004). In this repect, RUE models can be classified as belonging to the "hybrid" category, because the linear relationship between absorbed PAR and NPP is a simplifying assumption that is used to model the complex and non-linear response of photosynthesis and respiration to environmental conditions.

In contrast the big-leaf and sun-shade models use non-linear mechanistic functions, such as the Farquhar-von Caemmerer-Berry photosynthetic model (Farquhar *et al.* 1980; Sands 1995), to describe photosynthetic response to PPFD. The Farquhar-von Caemmerer-Berry photosynthetic model is commonly used in big-leaf models to simulate GPP of forest stands (see for example (McMurtrie & Landsberg 1992).

Notwithstanding the greater sophistication (and therefore generality and reality) of the big-leaf and sun-shade models compared with the "hybrid" RUE and maximum productivity models, Medlyn (2004) notes that there has been no published comparison showing a clear advantage in using any of the four types of model. Kirschbaum (1999) listed a number of published reviews of the very extensive literature on mechanistic plant growth models, including a comparison by Ryan *et al.* (1996) where a range of models was validated using two observational data sets from Australia and Sweden. Ryan *et al.* (1996) reported disagreement between the reviewed models and that none of the models could adequately simulate the full range of data from the Australian and Swedish data sets. It seems that most of the models reviewed lacked generality because they did not model all important processes in the forest ecosystem. For example, Kirschbaum (1999) subsequently developed CenW (a big-leaf model) in order to remedy the lack of a model which simulated nutrient uptake characteristics of the Australian and Swedish stands.

2.5.3 Choice of modelling strategy

In comparing alternative mechanistic models for simulating seedling growth of radiata pine under varying levels of light and environmental deficits, the choice of modelling strategy can be narrowed to the use of either RUE or big-leaf models. This is because the maximum productivity models lack generality especially with respect to variation in incident radiation levels (Medlyn 2004); the sun-shade models will be unnecessarily complex because there will be little variation in absorbed PAR within the small and quite open crowns of young radiata pine seedlings.

There have been several published big-leaf modelling simulations of radiata pine photosynthesis and growth. Walcroft *et al.* (1997) calculated parameters for the Farquhar-von Caemmerer-Berry photosynthetic model (Farquhar *et al.* 1980) based on gas-exchange measurements of two-year-old radiata pine seedlings. Walcroft *et al.* (1997) demonstrated that the Farquhar-von Caemmerer-Berry photosynthetic model could be applied to radiata pine seedlings, although the model was confined to predicting the effect of atmospheric CO_2 concentration and leaf temperature and nitrogen concentration on GPP. A big-leaf modelling approach has also been used to simulate growth of established radiata pine stands (McMurtrie & Landsberg 1992).

RUE models have also been successfully used to predict NPP in established radiata pine stands (Coops *et al.* 1998) and to study initial growth of planted radiata pine and Douglas fir seedlings (Mason 2004; Mason *et al.* 2007). In the end, the choice of modelling strategy comes down to the simplicity of the "hybrid" RUE approach versus the greater mechanistic reality of the big-leaf models. Dzierzon & Mason (2006) reviewed various strategies for modelling vegetation management for establishment of tree seedlings and concluded that the RUE models were computationally efficient but had "sufficient complexity to represent the results of scientific studies associated with vegetation management for use by managers."

2.5.4 RUE models

RUE is a concept first developed by Monteith (1972; 1977), and although initially employed for crop research it has more recently been used to estimate biomass productivity over a variety of scales (DeLucia *et al.* 2002; Medlyn 2004). RUE models predict a constant ratio of NPP to absorbed PAR ($\varphi_{p.a}$), which is equal to RUE ($\acute{\varepsilon}$, Equation 2.2). RUE has been found to be approximately constant during unstressed plant vegetative growth for a range of species (Monteith 1977; Landsberg & Gower 1997).

However, light-response curves (instantaneous photosynthesis versus the flux density of photosynthetic photons, or PPFD) are markedly non-linear. For C_3 plants, they reach an

asymptote (light saturation) at $\leq$ 50% of the PPFD level experienced in bright sunshine (Fitter & Hay 2002).

In temperate latitudes, total daily incident PAR in the open may have a coefficient of variation ranging from ~0.1 in summer to >0.4 in winter (Dewar *et al*. 1998). Additional variation in incident PAR occurs 1) diurnally and 2) hourly, especially under forest canopies, where seedlings may experience only short periods of direct full sunlight (sunflecks). Since photosynthetic response to PPFD is non-linear, the varying amounts of PAR received by seedlings over hourly, daily and seasonal time scales should undermine the assumption of linearity underpinning the RUE model.

There are three candidate explanations for this apparent contradiction between approximately constant RUE and non-linear light response in plants:

1. Plant canopies are structured so that PAR is distributed through the canopy in such a way that most leaves are exposed to non-saturating PPFD i.e. PPFD is low enough that the light response curve is essentially linear.
2. Variability in RUE decreases with increasing time scales, such that RUE should be close to constant when calculated on a monthly or annual basis (Landsberg & Gower 1997).
3. Plants maximise their overall RUE by differentially allocating leaf nitrogen (N) in the canopy, so that leaves exposed to full sunlight have markedly higher levels of leaf photosynthetic N and therefore do not reach the saturated phase of their light response curves even at quite high PPFD's.

Medlyn (1998) reviewed these candidate explanations and concluded that 1) explanation 1 was inadequate, because model-based simulations of RUE showed that it varied widely with PPFD regardless of canopy structure; 2) explanation 2 was valid to "some extent", although model simulations of annual mean RUE showed that it was influenced by variations in light climate; 3) given the inadequacy of explanations 1 and 2, explanation 3 (differential allocation of leaf photosynthetic N) deserved closer attention.

In a companion paper, Dewar *et al*. (1998) used elegant manipulations of established mechanistic models of photosynthesis and plant nitrogen and carbon dynamics to demonstrate how differential allocation of leaf photosynthetic N allows plants to acclimate to variations in PPFD. This acclimation occurs in a way that maintains an approximately constant RUE independent of variations in the light climate. Figure 2.4 (Figure 2(c), Dewar *et al*. 1998) shows how gross daily leaf photosynthesis responds linearly to varying levels of daily PAR, because of acclimation in the instantaneous light response curves of the leaf to different levels of PPFD.

Removed for copyright reasons

Figure 2.4. Simulation of leaf acclimation under a constant "square-wave" light regime.

PPFD is at three levels (I_d =25, 50 and 100W PAR m^{-2} leaf area, equivalent to 115, 230 and 460 μmol m^{-2} s^{-1} respectively). Solid curves: non-linear, instantaneous light responses of gross leaf photosynthesis (P) for three leaves acclimated to different constant values of daylight leaf absorbed PAR (I_d). Broken line and boxes: linear relationship between gross daylight photosynthesis, P_d, and the constant daylight leaf PAR to which it is acclimated, I_d. Source: Dewar *et al.* (1998).

As noted by Dewar *et al*. (1998), the linearity of the relationship between gross daylight photosynthesis (P_d) and constant daylight absorbed PAR is due to "leaf protein acclimation to light which tends to desaturate the instantaneous light response of *P*." Dewar *et al*. (1998) were also able to demonstrate that the leaf acclimation response demonstrated in Figure 2.4 for a constant "square-wave" (12 h day, 12 h night) diurnal light regime could be generalised to:

1. Describe leaf RUE under an actual light climate for a location near Canberra, Australia (35° 21′ S), where PPFD varied on a diurnal, daily and seasonal basis.
2. Whole plant RUE under both constant and varying light climates.

This second point addresses another inconsistency between the instantaneous light response curves (such as those shown in Figure 2.4) and the assumption that RUE is approximately constant under all light climates. The light response curves are for gross leaf photosynthesis, and pass through the origin i.e. when PPFD = 0, gross photosynthesis is equal to zero. However, if respiration losses are subtracted from gross photosynthesis to calculate net photosynthesis, then net photosynthesis will fall to zero at the "compensation point" where gross photosynthesis is > 0 but equal to respiration.

In contrast, carbon budgets for forests in contrasting climates indicate that respiration scales with photosynthesis (Landsberg & Gower 1997). The same authors note that the ratio of respiration to net canopy photosynthesis is "surprisingly" stable. These results imply that plant NPP (whole plant photosynthesis minus respiration) will scale linearly with absorbed PAR, with an intercept of zero. Similarly, Kruger and Volin (2006) reviewed data from 18 controlled-environment studies of photosynthesis and plant growth for a range of herbaceous and woody species, and compared measured plant growth rate with net leaf photosynthesis. Figure 2.5 shows a close linear relationship between net leaf photosynthesis and plant growth rate over a range of PPFD from 90-1000 μmol m^{-2} s^{-1}. Note that the intercept for this relationship is slightly greater than zero, rather than the negative intercept which would result if respiration did not scale with whole-plant net canopy photosynthesis.

Removed for copyright reasons

Figure 2.5. General relationship between relative growth rate (RGR) and estimated daily integrals for leaf net photosynthesis.

Source: Kruger and Volin (2006).

Theoretical support for the results reported by Kruger and Volin (2006), Landsberg and Gower (1997) and other authors, is offered by the model developed by Dewar *et al*. (1998), who conclude that plant RUE is independent of absorbed PAR and photosynthetic rates. In this model, whole-plant respiration associated with synthesis of proteins and structural compounds scales with production of labile carbon, which in turn scales with PPFD and gross canopy photosynthesis.

In summary, the assumption that RUE is approximately constant for a single plant or stand of plants, over a range of PPFD, seems to be well justified on the basis of both the

empirical data presented in this section, and the theoretical analysis of Dewar *et al*. (1998).

Variation in RUE due to environmental factors other than light

While approximately constant for a specific crop growing under specific environmental conditions, RUE values vary between plant species and also between crops growing under different site conditions. Landsberg & Waring (1997) propose a modified model to account for variation in RUE due to non-optimal site factors:

$$\text{NPP} = \acute{\varepsilon}\Sigma\varphi_{\text{p.a}} f_{\theta,} f_{\text{D}} f_{\text{T}} f_{\text{N}} \qquad (2.4)$$

where $f_{\theta,}$ f_{D}, f_T and f_{N} are modifying factors describing reductions in $\acute{\varepsilon}$ resulting from deficits in soil water and nutrient availability (f_θ and f_{N} respectively), the vapour pressure deficit of the air (f_{D}) and deviations from optimal air temperature (f_{T}). These factors have values between 0 and 1, where the factor value of 1 applies to optimal soil water or nutrient availability, vapour pressure deficit or temperature; and a factor value of 0 means that the factor value is insufficient for the plant to grow and NPP = 0. This conceptual approach to modelling effects of environmental deficits, where the value of $\acute{\varepsilon}$ is modified by $f_{\theta,}$, f_{D}, f_{T} and $f_{\text{N,}}$ is used in the 3-PG model (Landsberg & Waring 1997), a stand-based mechanistic model designed to predict NPP of forests over long time periods.

Note that the modifiers in 3-PG are assumed to act multiplicatively, with no interaction between them (except in the case of $f_{\theta,}$and f_{D}, where the model uses the minimum of these two variables). Further, they do not account for acclimation responses, where the response of plant photosynthesis to water and temperature deficits depends on antecedent conditions experienced by the plant. Rook (1969) showed that light response curves for radiata pine seedlings differed for seedlings growing at different temperatures, as might be expected. However, the effect of temperature on light response curves depended in turn on antecedent temperatures. For example, radiata pine seedlings raised at day/night temperatures of 15ºC/10ºC showed a reduced light response when subjected to a temperature of 30 ºC but showed no change in light response at 9ºC. In contrast,

seedlings raised at 24/19ºC showed a reduced light response when subjected to a temperature of 9 ºC, but no change in light response when subjected to a temperature of 30 ºC.

Similarly, the light response of radiata pine seedlings is influenced not just by current soil water, but by the preceding watering regime (Wood & Brittain 1973; Squire *et al.* 1988). For example, after two cycles of droughting (4 and 12 days), watering restored the relative water content of seedling foliage to 88% and net photosynthesis to 77% of the initial (maximum) values. After a third longer drought period (17 days), rewatering restored the relative water content of the foliage to 85%, but net photosynthesis to only 61% of the original maximum (Wood & Brittain 1973).

In summary, the modifiers proposed by Landsberg and Waring (1997) represent a simple but general way to model the effects of environmental deficits on seedling growth. However, as with all "hybrid" models they require simplifying assumptions (in this case, 1) simple multiplicative interactions between modifiers, and 2) absence of acclimation effects on modifier functions) which may depart from the reality of plant physiological and growth processes. The efficiency and accuracy of the RUE model and the modifiers proposed by Landsberg and Waring (1997) for modelling seedling growth therefore need testing, to ensure that their advantages of simplicity are not gained at the expense of model efficiency and generality.

2.5.5 Modelling seedling mortality

As well as growth in biomass, a model of forest growth also needs to model mortality. This seems to be a more difficult task (J. Landsberg pers. comm.) as tree death is less deterministic than the rate of growth of a healthy tree. However, it is especially important to predict mortality in young seedlings as the period following germination is a vulnerable one (Farmer 1997). 3-PG (Landsberg & Waring 1997) relies on empirical mortality functions based on tree size and spacing between trees (the -3/2 power law which predicts mortality as a power-function of tree size in pure even-aged stands (Yoda

et al. 1963)). However this approach is more suited to older stands where canopy closure has occurred.

For seedlings, the approach used by Milner & Coble (1996) seems more appropriate i.e. use an index of vigour (net photosynthesis minus respiration) to predict death of young trees. In other words, seedlings are more likely to die when NPP approaches zero, because they have less reserves available for maintenance respiration when photosynthesis is temporarily inhibited e.g. by a short-term drought. Not included in this hypothesis are the effects of extreme climatic events e.g. frost, or extreme high temperatures at the soil surface. These cause mortality by mechanically damaging the young seedling or else permanently damaging or inhibiting biochemical reactions within the plant (Fitter & Hay 2002, p205 *et seq*.). However, the Milner & Coble (1996) hypothesis does partly account for seedling mortality due to disease, because a healthy seedling with adequate reserves has more resources with which to combat pathogens e.g. by production of secondary metabolites or mechanical defences (Coley *et al.* 1985; Waring 1987).

2.6 Research objectives

The objectives of this study were to 1) identify the functional relationships between environmental conditions and germination, establishment and growth of radiata pine seedlings, under a range of those conditions specified by temperature and available light and soil water; and 2) specify those functional relationships in hybrid models.

To meet these objectives, radiata pine seedling germination and growth were measured under controlled environmental conditions (incubators for seed germination, growth cabinets for seedlings), and used to develop, parameterise and test two hybrid models; one for germination and one for seedling growth in the first six months after germination. Note that a full comparison of the big-leaf versus the RUE modelling approaches is beyond the scope of this study, and a simple RUE model (including modifier functions proposed by Landsberg and Waring (1997)) was used to model seedling growth.

Chapter 3 describes the development of a hybrid germination model. Chapter 4 describes the development of a hybrid (RUE) model relating seedling NPP to intercepted or absorbed PAR. Chapter 5 describes the development of modifier functions ($f_{\theta,}$, f_D) which modify the relationship between NPP and intercepted or absorbed PAR when available soil water and atmospheric vapour pressure deficit are suboptimal.

3 HYDROTHERMAL GERMINATION MODEL

3.1 Background

The objective of the work described in this chapter was to examine the functional relationships between the rate of germination of radiata pine seed and the temperature and moisture regime experienced by the seed. These relationships were tested fitting a hybrid hydrothermal germination model to germination data for a seedlot of radiata pine. The hydrothermal model used in this study was that specified by Equation 2.1 in the previous chapter i.e $\theta_{HT} = [\ \Psi - \Psi_b(G)]\ (T\text{-}T_b)\ t(G)$, where θ_{HT} is a hydrothermal time constant that has a unique value for the seed population, $\Psi_b(G)$ is the base water potential for the G^{th} percentile of the seed population, and varies according to a frequency distribution, T_b is the base temperature for seed germination and $t(G)$ is the time for the G^{th} percentile to germinate.

The model specified by Equation 2.1 applies only at seedbed temperatures less than or equal to the optimum temperature. This study also tested whether the decline in germination percentage and germination rate (*GR*) in radiata pine seed observed at supra-optimal seedbed temperatures could be accurately predicted using a similar hydrothermal model to that proposed by Alvarado & Bradford (2002) and Rowse & Finch-Savage (2003), where $\Psi_b(G)$ is adjusted upwards with increasingly supra-optimal temperatures. The Alvarado and Bradford and Rowse and Finch-Savage models will henceforth be referred to as the AB and RFS models respectively.

3.2 Methods

3.2.1 Germination

A commercial radiata pine seedlot (seedlot no. 075/780 supplied by Proseed NZ Ltd, Amberley, New Zealand) was germinated for 50 d in incubators at constant temperatures from 12.5 to 32.5 °C, on germination media with constant water potentials from 0 to –1.2 MPa. Pilot experiments with seedlot no. 075/780 suggested that base temperature and

mean base water potential for germination were approximately 10 ºC and –1.5 MPa respectively, and that optimum germination was obtained at temperatures of 20-22 ºC and a water potential of 0 MPa.

For each combination of water potential and temperature there were four replicates, each comprising a 750 ml plastic snap-top tray with 25 seeds on the germination medium. This resulted in 100 seeds per water potential/temperature combination, which enabled germination percentages to be easily calculated for each treatment combination. Before placement in the trays, the germination media (Whatman No 2 filter papers) were soaked in trays containing an osmotic solution of the desired water potential for 48 hours (the length of time necessary for equilibration of the filter paper with the osmotic solution (Hardegree & Emmerich 1990)). The filter papers were then placed on a 5 mm thick glass plate in the trays which were filled with freshly mixed osmotic solution until the solution just made contact with the filter paper. This reservoir of osmotic solution was intended to further buffer the filter paper from changes in water potential due to evaporation of water. Osmotic solutions of water potential = 0, –0.3. –0.6, –0.9 and –1.2 MPa were made up using polyethylene glycol 8000 (PEG 8000) according to the formula in Equation 3.1 (Hardegree & Emmerich 1990):

$$\Psi = 0.130[\mathrm{PEG}]^2 T - 13.7[\mathrm{PEG}]^2 \qquad (3.1)$$

where Ψ is the osmotic potential of a solution of PEG 8000 in water (MPa), [PEG] is the concentration of PEG 8000 in water (g PEG 8000 / g H_20) and T is the solution temperature in ºC.

Note that the value of the solution osmotic potential (Ψ) in this formula is temperature dependent, so that solutions with slightly different concentrations were required to achieve a specific value of Ψ at different germination temperatures. The osmotic solution with 0 MPa was reverse osmosis water with no PEG 8000 added.

Seeds were screened to remove any obvious empty or broken seeds and then lightly dusted with Thiram before being carefully placed onto the germination medium. Seeds were expected to have better than 95% germinability based on seed-testing results provided by Proseed NZ Ltd. Radiata pine seed has no stratification-sensitive seed dormancy (Rimbawanto *et al.* 1988), therefore seeds received no stratification or other pre-treatment prior to sowing (ISTA 2003).

Once the seeds were placed in the germination trays, the tops of the trays were sealed with a sheet of cling-wrap to prevent loss of water vapour and the plastic snap-top lid was firmly placed on the top of the tray. Trays were then placed in eight incubators which were set to run at constant temperatures of 12.5, 15, 17.5, 20, 22.5, 25, 27.5 and 32.5 °C respectively. All water potential treatments were present in each incubator, except for −1.2 MPa which was only replicated for three incubators (T = 17.5, 20 and 22.5 °C). Within each incubator, each tray was randomly placed and its position was rotated systematically every three days in order to mitigate any small spatial variations in air temperature due to inefficient air circulation. Temperatures were monitored continuously within the incubators using either Tiny-Tag temperature loggers (Gemini Data Loggers, Chichester, U.K.) or temperature probes interfaced with a HOBO data logger (Onset Computer Corporation, Bourne, MA, U.S.A.). No consequential deviations from target incubator temperatures occurred during the experiment, as shown by the datalogger data summarised in Table 3.1.

Table 3.1. Incubator temperature data during the 50 d germination period.

Nominal Temperature (°C)	Mean actual temperature (°C)	Standard Deviation (°C)
12.5	12.4	0.52
15.0	14.8	0.49
17.5	17.6	0.34
22.5	22.4	0.09
25.0	25.1	0.42
27.5	27.4	0.27
32.5	32.6	0.41

There were no data for the 20 °C incubator due to a shortage of dataloggers. However, temperature within the 20 °C incubator was monitored using a mercury thermometer

which was checked whenever seed germination was measured. Observed thermometer values were always within ± 0.5 ºC of 20 ºC.

Water potentials of the germination media were monitored by measuring samples of the osmotic solutions in the trays twice-weekly, using a Wescor 5520 vapour pressure osmometer (Wescor Inc, Logan, Utah, U.S.A.). Osmotic potentials for solutions at $T \leq$ 25 ºC were stable and did not deviate from specified treatment levels by > 0.05 MPa. For $T >$ 25 ºC, solutions began to deviate from specified treatment levels by > 0.05 MPa within 7–14 days, in which case the incorrect osmotic solutions were discarded and replaced with fresh solutions.

3.2.2 Germination counts and seed mortality

Germination counts were continued for a 50 day period. Seeds were inspected twice daily for the first nine days of the germination period, and thereafter daily until 27 d, when seeds were inspected once every two days. In the first nine days many seeds in the near-optimum treatments were germinating rapidly and a twice-daily count was needed to avoid a result where large numbers of seeds shared the same time to germination. After 27 d, the opposite case applied. Fewer seeds were germinating and a daily inspection would frequently yield a zero count of germinated seeds. Seeds were considered to have germinated when the radicle protruded more than 2 mm from the seed coat. The number of days to germination was recorded as well as the seed's order of germination within the tray (1, 2, 3…25). Seed counting required that the lid of the tray be lifted in order to carefully inspect the seeds and remove any germinated individuals. This also served to aerate the seed tray, which was otherwise quite effectively sealed by the snap-top lid and sheet of cling-wrap covering the top of the tray.

3.2.3 Assessment of dormancy

Most seeds germinated within 50 d in the near-optimum treatments. However for treatments with extremely high or low temperatures and/or low water potentials, many seeds remained ungerminated after 50 d. This may have been due to 1) secondary dormancy acquired after the seeds began to germinate or 2) at supra-optimal

temperatures, the occurrence of an upwards shift towards zero in seed Ψ_b as predicted by the AB and RFS models.

The extent of secondary dormancy was tested at the end of 50 d by placing all remaining ungerminated seeds in trays with moist substrate (Ψ = 0 MPa) and incubating them at optimum temperature (20^{o}C) for a further 75 d. Counts of germination were taken at regular intervals, and as with the main experiment, germinated seeds were counted and discarded, as were any seeds that were clearly dead. Seeds that germinated under ideal conditions within 75 d were considered non-dormant. Seeds that had not germinated by 75 d were considered completely dormant, although they may simply have been non-viable.

3.3 Data analysis

3.3.1 Germination rate at suboptimal temperatures

Germination rate (*GR*) of a seed is defined as the inverse of the time taken by the seed to germinate i.e. $1/GR = t$ (G). The hydrothermal model can be linearized by substituting $1/GR$ for t (G) in Equation 1 i.e.

$$GR = [\Psi - \Psi_b(G)]\,(T-T_b)/\,\theta_{HT} \qquad \text{for } \Psi > \Psi_b(G) \qquad (3.2a)$$

$$GR = 0 \qquad \text{for } \Psi < \Psi_b(G) \text{ or } T < T_b \qquad (3.2b)$$

Equation 3.2 implies that if T is constant, then for any seed percentile (G), GR is a linear function of Ψ because Ψ_b (G) is constant at suboptimal temperatures. Similarly, if Ψ is constant, then GR is a linear function of T because T_b is constant. By plotting GR versus Ψ and T, data can be checked for its conformity to the hydrothermal model i.e. for all percentiles: 1) GR vs T should be linear and converge to a single base temperature T_b, and 2) for GR versus Ψ, GR should increase linearly as the substrate water potential increases from $\Psi = \Psi_b$ (where $GR = 0$) to $\Psi = 0$ (where GR reaches its maximum value). In addition, for GR versus Ψ, the trend lines for the different percentiles should be parallel

with each percentile having a common slope but a differing intercept (= Ψ_b(G)) with the *x*-axis (Bradford 2002; Finch-Savage 2004).

The hydrothermal germination model

In order to estimate parameter values for the hydrothermal model (Equation 2.1), germination data for the four 25-seed replicates for each temperature/water potential treatment were amalgamated into one set of data (i.e. 100 seeds). Within each treatment, seeds were allocated a percentile number, beginning with 1 for the fastest seed to germinate, 2 for the second-fastest and so on. It was assumed that all seeds were potentially germinable, and so the maximum percentile number for any treatment was 100. Menzies *et al.* (1991) and Anon. (1997) report germination percentages > 95% in commercial radiata pine seedlots in New Zealand.

If base water potentials for each percentile (Ψ_b(G)) within the population are normally distributed, then:

$$\text{Probit (G)} = [\Psi_b(\text{G}) - \Psi_b(50)]/\ \sigma_{\Psi b} \qquad (3.3)$$

where Probit (G) is the probit function which calculates the standard normal deviate (z) for a specified cumulative probability (= G) in a normally distributed population, Ψ_b(50) is the mean Ψ_b, $\sigma_{\Psi b}$ is the standard deviation of Ψ_b for the seed population, and from Equation 2.1, $\Psi_b(\text{G}) = \Psi - (\theta_{HT}/[(T\text{-}T_b)\ t(\text{G})])$

The Probit(G) statistics for all seeds were calculated, then Equation 3.3 was fitted to the germination data using the "nls" function in programme R (R Development Core Team 2004). This function simultaneously estimated θ_{HT}, Ψ_b(50), T_b and $\sigma_{\Psi b}$ using an iterative least-squares procedure.

The frequency distribution for Ψ_b

If Ψ_b is normally distributed around Ψ_b (50), the expected value for Ψ_b(G) can be predicted from the hydrothermal model parameters as follows:

$$\Psi_b\,(\mathrm{G}) = \Psi_b(50) + \mathrm{Probit}\,(\mathrm{G})\,\sigma_{\Psi b}. \qquad (3.4)$$

The expected base water potential (Equation 3.4) was compared with the actual base water potential to test whether Ψ_b was normally distributed around Ψ_b (50). If this was the case, then there should be no systematic trends in the deviations between actual Ψ_b and expected Ψ_b (Crawley 2002). Note that "actual" base water potential for the G^{th} seed is a virtual value calculated from model parameters (θ_{HT} , T_b) and germination data (Ψ, T, t(G)) as follows:

$$\Psi_b\,(\mathrm{G}) = \Psi - [\theta_{HT}/(T - T_b)\,t(\mathrm{G})\,] \qquad (3.5)$$

3.3.2 Germination rate at supra-optimal temperatures

Both the Alvarado and Bradford (AB) and Rowse and Finch-Savage (RFS) models propose that the decline in *GR* at supra-optimal temperatures results from a temperature dependent increase in Ψ_b. This temperature dependent increase shifts the mean population value of the base water potential (Ψ_b (50)) towards zero, but does not change the standard deviation of the Ψ_b values about the mean value (Bradford 2002). Therefore if Ψ_b is normally distributed around Ψ_b (50) the expected value for Ψ_b(G) can be predicted using Equation 3.4 ($\Psi_b\,(\mathrm{G}) = \Psi_b(50) + \mathrm{Probit}(\mathrm{G})\,\sigma_{\Psi b}$). Both $\Psi_b(50)$ and $\sigma_{\Psi b}$ are population parameters estimated from fitting a hydrothermal model to germination data from sub-optimal temperatures (Section 3.3.1).

In the AB model, the upwards adjustment to Ψ_b (G) at supra-optimal temperatures is estimated by Equation 3.6:

$$\Psi_b(\mathrm{G})' = \Psi_b\,(\mathrm{G}) + k[T - T_o] \quad \text{when } T > T_o \qquad (3.6)$$

where $\Psi_b(G)'$ is the adjusted base water potential for the G^{th} percentile in the seed population and k is a constant.

The AB model also assumes that the maximum rate of thermal time accumulation occurs at T_o, and that supra-optimal temperatures do not contribute additional hydrothermal time i.e. for $T > T_o$, thermal time = $(T_o - T_b)\ t(G)$. The effect of this assumption together with the linear upwards adjustment in Ψ_b predicted by Equation 3.6, is that: 1) the relationship between *GR* and temperature follows a "broken-stick" pattern, with a linear upwards trend in *GR* from T_b to T_o followed by an abrupt linear decline in *GR* down to T_c; and 2) the peak of the "broken stick" occurs at the same temperature (T_o) for all seed percentiles, although the actual value of the *GR* at T_o is dependent on the seed percentile i.e. low seed percentiles have a high maximum *GR*, the higher seed percentiles have a somewhat lower maximum *GR* (Alvarado & Bradford 2002). A graphical representation of the AB model is shown in Figure 3.1 (a).

Removed for copyright reasons

Figure 3.1. Graphical representation of the Alvarado-Bradford (AB) and Rowse and Finch-Savage (RFS) models.

(a) The AB model shows a 'broken-stick' inflexion at the optimum temperature in contrast to (b) the broader maximum at T_o predicted by the RFS model. Both models 1) use a linear increase in Ψ_b (shown as Ψ_b(g) in Figure 3.1(a)) to predict the reduction in germination rate at supra-optimal temperatures; and 2) predict a range of values for ceiling temperature (T_c in Figure 3.1(b)) where germination rate = 0.
Source: (a) Bradford (2002); (b) Rowse & Finch-Savage (2003).

The RFS model also uses a linear function to calculate the upwards adjustment in Ψ_b above optimum temperatures, but it differs importantly from the AB model in that there is no maximum temperature for calculating thermal time i.e thermal time accumulates increasingly rapidly with increasing temperature above T_o. This means that predicted *GR* continues to increase above the temperature at which Ψ_b is assumed to increase as function of supra-optimal temperature, because the extra thermal time accumulated at higher temperatures counteracts the effect of an upwards adjustment in Ψ_b towards zero (Rowse & Finch-Savage 2003). However, the upwards-adjusting effect of temperature on Ψ_b occurs at a faster rate per unit of temperature than thermal time accumulation, and so there is an inflexion point where *GR* begins to decline. These assumptions mean that for the RFS model the temperature threshold where Ψ_b begins to increase as a function of temperature ("deviation temperature" or T_d) must be less than T_o, where *GR* is at a peak. Therefore the adjustment to Ψ_b is calculated as shown in Equation 3.7:

$$\Psi_b(\mathrm{G})' = \Psi_b(\mathrm{G}) + k[T - T_d] \quad \text{when } T > T_d . \tag{3.7}$$

The assumptions of the RFS model also mean that 1) the plot of predicted *GR* vs *T* has a broad rounded peak (rather than a sharp "broken-stick" profile); and 2) T_o occurs at a higher temperature for the faster than for slower germinating seeds, because for faster germinating seeds the increase in Ψ_b due to temperature has less effect on the magnitude of the term $[\Psi - \Psi_b(\mathrm{G})]$ in Equation 3.2 (see Figure 3.1 (b)).
However, for both models the shift in Ψ_b is a simple linear function of either $T - T_o$ (AB model) or $T - T_d$ (RFS model). This assumption of linearity can be checked by plotting the deviations of actual Ψ_b from expected Ψ_b, as a function of temperature. If the AB or RFS models hold for radiata pine at supra-optimal temperatures then the deviations should closely follow a linear trend in relation to temperature above either T_o (AB model) or T_d (RFS model).

Equation 3.8 calculates "actual" base water potential for the G^{th} seed from hydrothermal model parameter values for θ_{HT} and T_b at sub-optimal temperatures and from germination

data from the supra-optimal temperature treatments (Ψ, t(G) and T where $T = T_o$ in the AB model or T = germination temperature in the RFS model) :

$$\Psi_b\,(\mathrm{G}) = \Psi - [\theta_{HT}\,/(T - T_b)\,t(\mathrm{G})\,]. \qquad (3.8)$$

This approach assumes that the hydrothermal model parameter values for seedlot 075/780 at sub-optimal temperatures (Section 3.3.1) apply to seeds from the same seedlot which have been germinated at supra-optimal temperatures.

3.4 Results

3.4.1 Germination rate for suboptimal temperatures

Plots of seed *GR* vs temperature (at optimum $\Psi = 0$ MPa) and water potential (at optimum $T = 20^{o}$ C) are shown in Figure 3.2. Rates are plotted for the 10th, 30th, 50th 70th and 90th percentiles, to show trends in data across the entire seed population. In general, *GR* of the radiata pine seeds conform to the assumptions of the hydrothermal model i.e. for all percentiles 1) *GR* vs *T* appears to be linear and to converge to a single base temperature T_b; and 2) *GR* versus Ψ appears to be linear with parallel trend lines for the different percentiles but each percentile has a different intercept ($=\Psi_b$(G)) with the *x*-axis. However the data for slower germinating radiata pine seeds appear to depart from the assumptions of the hydrothermal model. The linear trends in Figure 3.2(a) predict that 70% germination should have occurred within 50 d at 12.5 ºC and 90% germination should have occurred within 50 d at 15 ºC and 17.5 ºC. However, in Figure 3.2(a) there are no data for the 50th and 70th percentiles at $T = 12.5$ ºC nor for the 90th percentile at $T =$ 15 ºC and 17.5 ºC i.e. seeds did not reach 50% germination at 12.5 ºC nor 90% germination at 15 ºC and 17.5 ºC, within the 50 d duration of the experiment.

Similarly, in Figure 3.2(b) the linear *GR* versus Ψ trends for the 70th and 90th percentiles suggest that seeds should have reached 70% germination within 50 d at –0.9 MPa, and 90% germination within 50 d at –0.3 MPa. Actual germination percentages at –0.9 MPa and –0.3 MPa were 59% and 87% respectively.

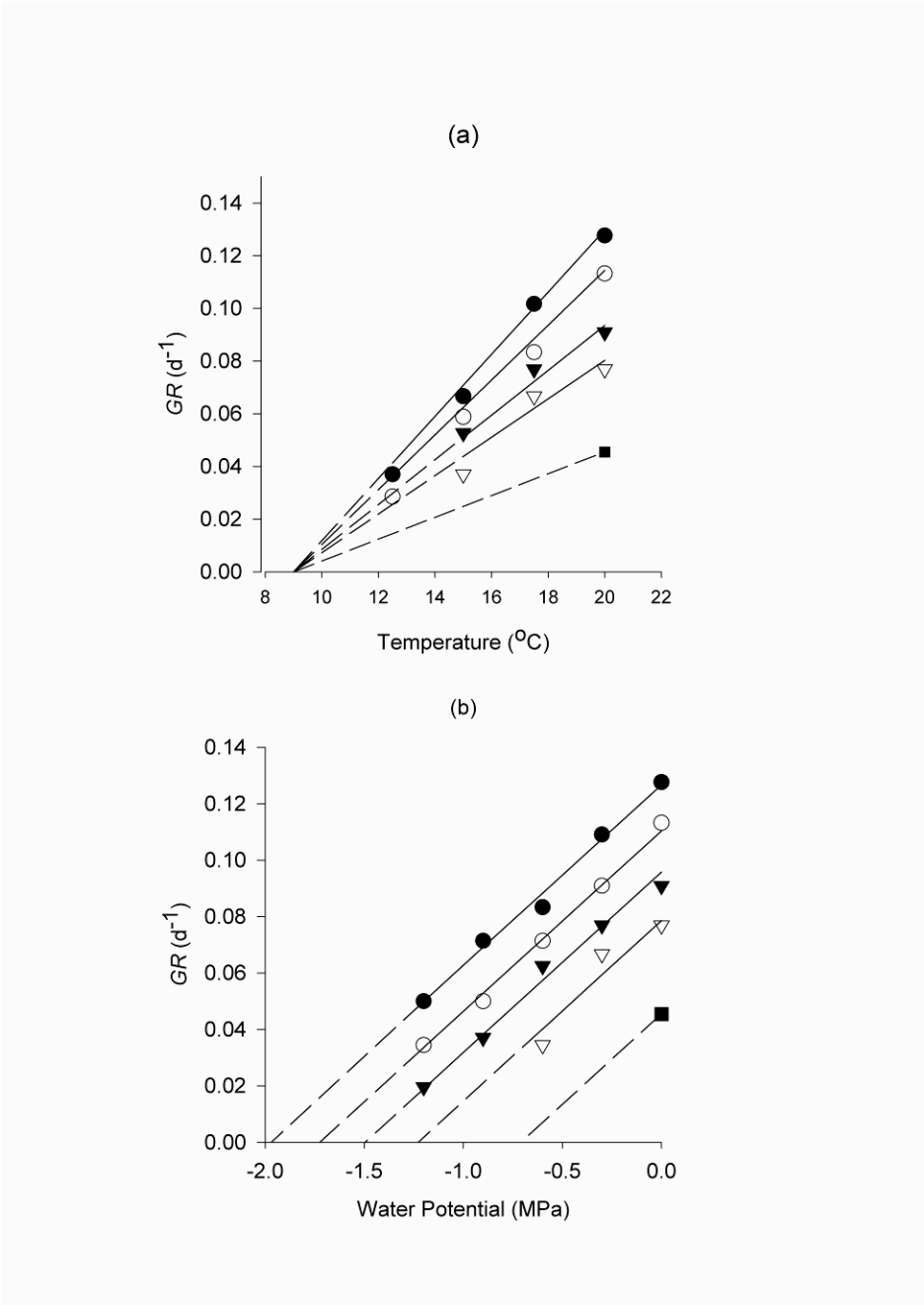

Figure 3.2. Germination rates (GR) for 10th – 90th percentiles (a) versus temperature when Ψ = 0 MPa, (b) versus water potential when T = 20ºC.

Percentile symbols: ● = 10th, ○ = 30th , ▼ = 50th, ▽ = 70th, ■ = 90 th. The solid lines are linear regressions fitted to the data points. Dashed lines are extrapolations of the regression lines, drawn to indicate the location of base temperatures and water potentials. Regression lines in (a) are constrained to pass through a single T_b of 9.0 ºC. Regression lines in (b) are constrained to a common slope.

3.4.2 Hydrothermal models at sub-optimal temperatures.

Although the data for slow-germinating seeds (70th and 90th percentiles) appeared to depart from model assumptions, Figures 3.2(a) and (b) showed that the data generally conformed to the assumptions of the hydrothermal model (Equations 3.2 and 3.3). Therefore Equation 3.3 was fitted to the germination data. Estimated model parameters are shown in Table 3.2 (Model 1). The model fitted the germination data quite well, with a coefficient of determination (R^2) = 92%. However examination of the residuals revealed that model predictions of germination percent were biased upwards–the model was predicting higher germination percentages than actually occurred within 50 d during the experiment. This seemed to arise from the model underestimating Ψ_b(G) values for these seeds. In other words the model predicted lower (more negative) Ψ_b (G) values which then resulted in the model predicting that seeds accumulated more hydrothermal time than was actually the case. Consequently, higher seed percentiles (> 70th percentile) were predicted to accumulate enough hydrothermal time to germinate when in fact they had not.

Table 3.2. Model parameter and Akaike Information Criterion (AIC) values for hydrothermal models.

Parameter	Model 1 Unadjusted	Model 2 Time-adjusted Ψ	Model 3 Hydro-time index adjusted Ψ
θ_{HT} (°C MPa d)	149	168	176
T_b (°C)	9.7	9.4	9.0
$\Psi_b(50)$ (MPa)	–1.38	–1.50	–1.53
$\sigma_{\Psi b}$ (MPa)	0.48	0.47	0.42
k	--	1.17×10^{-2}	1.30×10^{-2}
AIC	67.6	–136	-449

A plot of deviations of "actual" Ψ_b (G) from expected Ψ_b (G) (calculated from Equations 3.5 and 3.4 respectively) showed that these deviations were unevenly distributed around zero (Figure 3.3 (a)), suggesting that the incorrect model predictions were due to a non-normal distribution of "actual" Ψ_b around Ψ_b (50) when the distribution used in the model was normal in form. Figure 3.3(a) (deviations vs germination percentile) showed that the

deviations for a specific percentile were not consistent between the different temperature or water potential treatments. In other words, the frequency distribution of "actual" Ψ_b was not normally distributed around Ψ_b (50), and with the shape of the frequency distribution varying with temperature and water potential.

While not consistent with seed percentile, the deviations of "actual" from expected Ψ_b did appear to be related to the time to germination for the seed. For seeds that took longer than 25 d to germinate, the deviations for all temperatures increased at approximately the same rate with respect to germination time (Figure 3.3(b)). In other words, slow-germinating seeds (t(G) > 25 d) underwent an apparent increase in "actual" Ψ_b from $t \approx$ 25 d onwards, which meant they germinated even slower. This shift in Ψ_b appeared to be related to chronological time to germination rather than thermal time, because Figure 3.3(c) shows an inconsistent relationship between deviations and thermal time to germination.

Figure 3.3(b) also shows that the relationship of the deviations of "actual" from expected Ψ_b vs time varied with Ψ and became weak for the driest treatment (Ψ = –1.2 MPa). Plotting the deviations against a calculated "hydro-time index" (HTI, =[(Ψ– Ψ_b) t (G)]), where Ψ_b = –1.5 MPa, normalized the deviations across all water potential treatments (Figure 3.3(d)). In this case, the deviation of "actual" from expected Ψ_b occurs from HTI ≈ 20 MPa d onwards for all the water potential treatments.

To account for the deviations between "actual" and expected Ψ_b, two alternative hydrothermal models were fitted with an additional term for the increase of Ψ_b with time to germination, as follows:

$$\Psi_b(\mathrm{G})\ ' = \Psi_b\ (\mathrm{G}) + k[t\ (\mathrm{G}) - 25] \text{ for } t\ (\mathrm{G}) > 25 \text{ d} \qquad (3.9)$$

$$\Psi_b(\mathrm{G})\ '' = \Psi_b\ (\mathrm{G}) + k'[(\Psi - (-1.5))\ t\ (\mathrm{G}) - 20] \text{ for } (\Psi - (-1.5))\ t\ (\mathrm{G}) > 20 \text{ MPa d} \qquad (3.10)$$

where k and k' are constants. Equation 3.9 adjusts Ψ_b as a function of chronological time to germination, Equation 3.10 adjusts Ψ_b as a function of hydro-time index (*HTI*) to germination. The increase in Ψ_b was modelled as a function of chronological time or *HTI* rather than thermal time because Figure 3.3(c) indicated no clear relationship between the deviation of "actual" from expected Ψ_b and thermal time (calculated using T_b for the unadjusted model= 9.7 °C (Table 3.2)).

The alternative hydrothermal time models (i.e. without adjustment to Ψ_b, or with adjustments to Ψ_b as specified in Equations 3.9 and 3.10) were compared for their likelihood using the Akaike Information Criterion (AIC). The AIC is a penalized log-likelihood criterion i.e. it calculates the likelihoods of alternative models fitted to the same data, but reduces the likelihood of each model in proportion to the number of parameters that it uses (Akaike 1974; Burnham & Anderson 2001). The lower (more negative) the AIC value, the greater the likelihood of the model.

The AIC values (Table 3.2) suggest that Model 3, which adjusts Ψ_b as a function of *HTI*, gives the best fit to the measured data. Model 2 is also superior to Model 1. Models 2 and 3 also have the advantage, compared with Model 1, of offering a mechanistic explanation of the non-normality of the frequency distribution for Ψ_b in the seed population i.e. an initial normal distribution is skewed by increases in the Ψ_b values for the slower germinating seeds, which occur as part of the germination process. This point will be returned to in the discussion section.

Figure 3.4 shows predicted germination time courses at 0 and –0.6 MPa for Models 1, 2 and 3, compared with actual germination data. These clearly show that the model with the *HTI* adjusted Ψ_b (Model 3) more correctly predicts germination at all temperatures, whereas the unadjusted model incorrectly predicts higher germination percentages than actually occurred in most cases. Model 2 makes generally correct predictions but incorrectly predicts germination at 12.5 °C/ 0 MPa. The comparisons between models shown in Figure 3.4 were consistent with results for other water potentials i.e. Ψ = –0.3, –0.9 and –1.2 MPa.

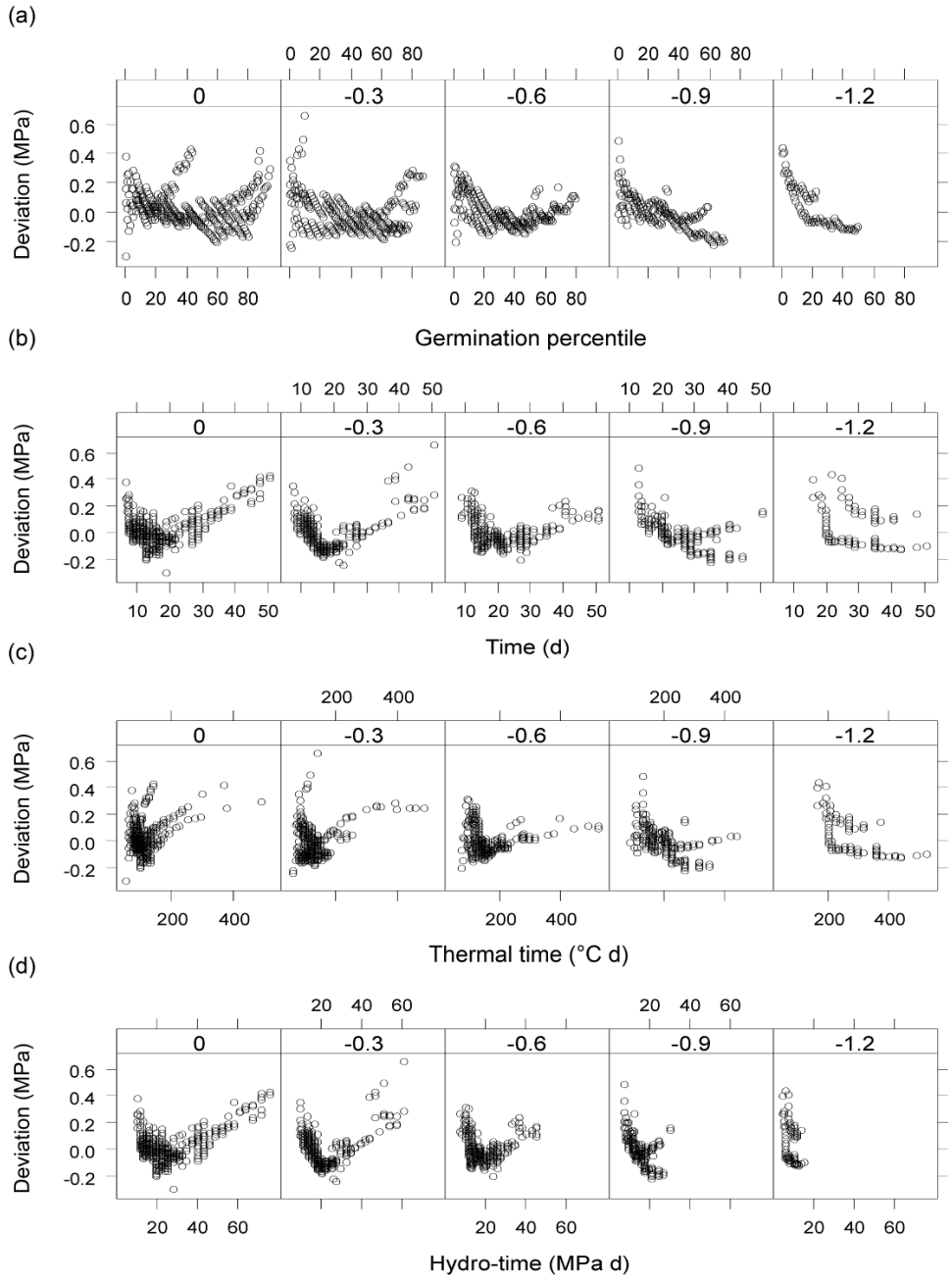

Figure 3.3. Deviation of "actual" from expected Ψ_b.

Deviations are plotted against (a) Germination percentile, (b) Time to germination t(G), (c) Thermal time $(T\text{-}T_b)t$(G), (d) Hydro-time index = $(\Psi - \Psi_b)\ t$(G), where $\Psi_b = -1.5$ MPa. Data are plotted for Ψ treatments (L to R): 0, –0.3, –0.6, –0.9 and –1.2 MPa.

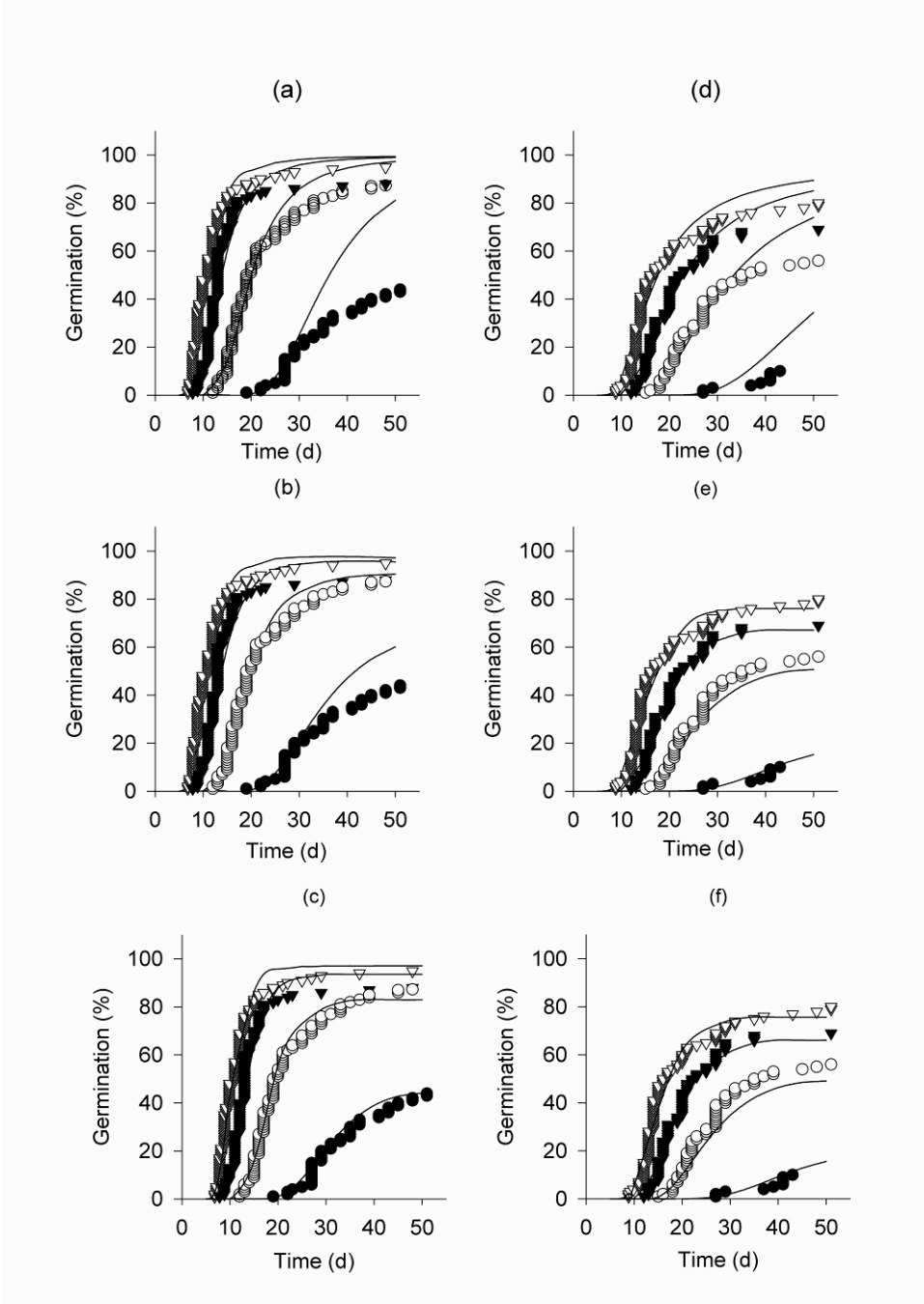

Figure 3.4. Germination time course data compared with hydrothermal model predictions.

(a) $\Psi = 0$ MPa, Model 1; (b) $\Psi = 0$ MPa, Model 2; (c) $\Psi = 0$ MPa, Model 3; (d) $\Psi = -0.6$ MPa, Model 1; (e) $\Psi = -0.6$ MPa, Model 2; (f) $\Psi = -0.6$ MPa, Model 3. Data are plotted for each temperature as follows: ● = 12. 5 ºC, ○ = 15 ºC, ▼= 17.5 ºC, ▽ = 20 ºC. Model predictions are shown by the solid lines.

3.4.3 Ungerminated seeds at suboptimal temperatures

For germination treatments at low temperatures (12.5 or 15 ºC), the higher seed percentiles did not germinate. The unadjusted hydrothermal model predicted that most of these seeds should have germinated, because they should have accumulated sufficient hydrothermal time (Figures 3.4(a) and 3.4 (d)). In contrast, the adjusted models correctly predicted no germination by the higher seed percentiles at 12.5 or 15 ºC (Figures 3.4(b), 3.4(c), 3.4(e), 3.4(f)) because they adjusted Ψ_b upward during germination as described in the previous section. This shift in Ψ_b towards zero resulted in the high percentile seeds failing to germinate because they accumulated insufficient hydrothermal time to germinate, even under moist conditions.

An alternative explanation for this lack of germination might be that the seeds had become dormant during the germination process (secondary dormancy). The extent of dormancy in all remaining ungerminated seeds was tested at the end of 50 d by placing the seeds in germination trays with moist germination substrate (Ψ_b = 0 MPa) and incubating at optimum temperature (20^{o}C) for a further 75 d.

For ungerminated seed from the sub-optimal T and Ψ treatments, > 90% germinated within 20 d of being placed in optimal conditions. Seeds from the driest treatments (–1.2 and –0.9 MPa) were slower to respond, typically requiring more than 30 d to reach >90% germination. This suggests that the lack of germination during the experimental period of 50 d was due to insufficient hydrothermal time being accumulated by the seeds, rather than dormancy.

3.4.4 Germination rates at supraoptimal temperatures

Figure 3.5 shows trends in *GR* vs temperature for both sub-optimal temperatures and supra-optimal temperatures (for Ψ = 0 MPa). Data are plotted for the 10th, 30th, 50th and

70th percentiles but not for the 90th percentile because no treatment with supra-optimal temperature achieved ≥ 90 % germination.

Germination rates in Figure 3.5 show the following responses to temperature:
1) *GR* increases linearly from a common T_b until temperature approaches 20°C (as shown by Figure 3.2(a)).
2) The increase in *GR* then declines non-linearly until T_o (the optimum temperature where *GR* is at a maximum).
3) Beyond T_o, *GR* declines (quite rapidly for the higher percentiles) to zero at the ceiling temperature T_c. However, the value of T_o and T_c are different for each percentile of the seed population. T_o and T_c are typically highest for the fastest germinating seeds (ie the lowest percentiles in the population). Figure 3.5 shows that *GR* for the 10th percentile only just began to decline after 27.5 °C and it is therefore not possible to estimate T_c for this percentile by extrapolation from the data.

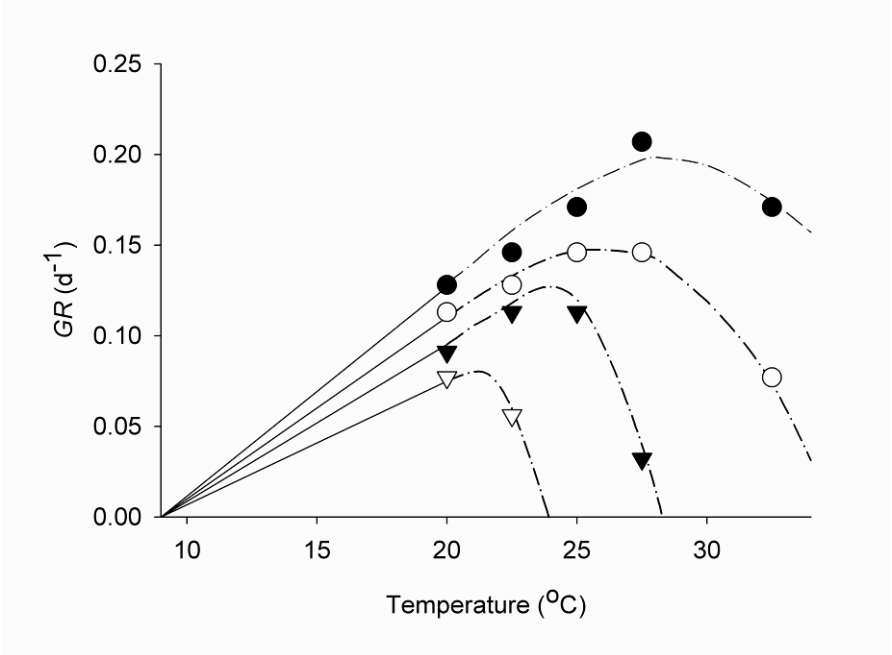

Figure 3.5. Germination rates (GR) vs temperature.

Data are for 10th – 70th percentiles when $\Psi = 0$ MPa. Percentile symbols: ● = 10th, ○ = 30th, ▼ = 50th, ▽ = 70th. The solid lines are linear regressions derived from data for

germination at sub-optimal temperatures, constrained to pass through a single T_b of 9.0 °C. The dashed lines are freehand curves drawn to illustrate trends in *GR* for supra-optimal temperatures.

These trends strongly suggest that germination in radiata pine at supra-optimal temperatures conforms more closely to the RFS model than to the AB model (these models are described in Section 3.3.2), because there is a broad range of optimum temperatures which vary between different seed percentiles, rather than a unique value for T_o which applies to all percentiles. They also suggest that the deviation temperature (T_d) where Ψ_b begins to decline is ≈ 20 °C.

3.4.5 Germination percentages at supraoptimal temperatures

The response of germination percentage to supra-optimal temperature is shown in Figure 3.6(a). Germination percentage declines from 20 °C to the maximum temperature in this experiment (32.5 °C). Similarly, germination percentage declines from the moistest treatment (Ψ = 0 MPa) down to the driest treatment (Ψ = –1.2 MPa), at each temperature. The hydrothermal model for radiata pine has a $\Psi_b(50)$ parameter value of approximately –1.5MPa, and a $\sigma_{\psi b}$ parameter value of 0.4-0.5 MPa (Table 3.2). Assuming a normal distribution for Ψ_b, then at least 95% of the seed population should have Ψ_b less than –0.6 MPa, so that nearly complete germination should occur for water potential treatments 0, –0.3 and –0.6 MPa. This does not happen because Ψ_b adjusts upwards at supra-optimal temperatures as described in the previous section. If the shift is large enough, Ψ_b of some seed percentiles will approach 0, meaning that these seeds cannot accumulate hydrothermal time and therefore will not germinate even under ideal moisture conditions i.e. thermo-inhibition of germination has occurred.

At the end of the 50 d germination period, the extent and reversibility of this putative thermo-inhibition were tested by placing all remaining ungerminated seeds in germination trays with moist germination substrate (Ψ = 0 MPa) and incubating at optimum temperature (20 °C) for a further 75 d. If these seeds were able to germinate under optimum conditions, then thermo-inhibition would clearly not have resulted in seed

dormancy. The effects of the optimum moisture and temperature treatment on further germination are shown in Figure 3.6(b).

For initial temperature treatments of 27.5 ^{o}C and 32.5 ^{o}C, and for all initial supra-optimal temperature treatments where Ψ was $\leq$ –0.6 MPa, seed germination during the 50 d germination period was markedly reduced (Figure 3.6(a)). After a further 75 d under optimum conditions, seeds from treatments where $\Psi \geq$ –0.6 MPa achieved ~ 80% germination except for the 32.5 ^{o}C treatments. Towards the end of the 75 d ungerminated seeds began to decompose, especially seeds from 27.5 ^{o}C and 32.5 ^{o}C treatments (note: for seeds from the 32.5^{o}C/ 0 MPa and 32.5 ^{o}C/–0.3 MPa treatments, 58% and 23% of the seeds respectively were already decomposed at the end of the 50 d germination period). The cause of seed death was not ascertained in this study. However dead seeds showed no sign of fungal infection to the naked eye, suggesting that death was not due to pathogenic causes.

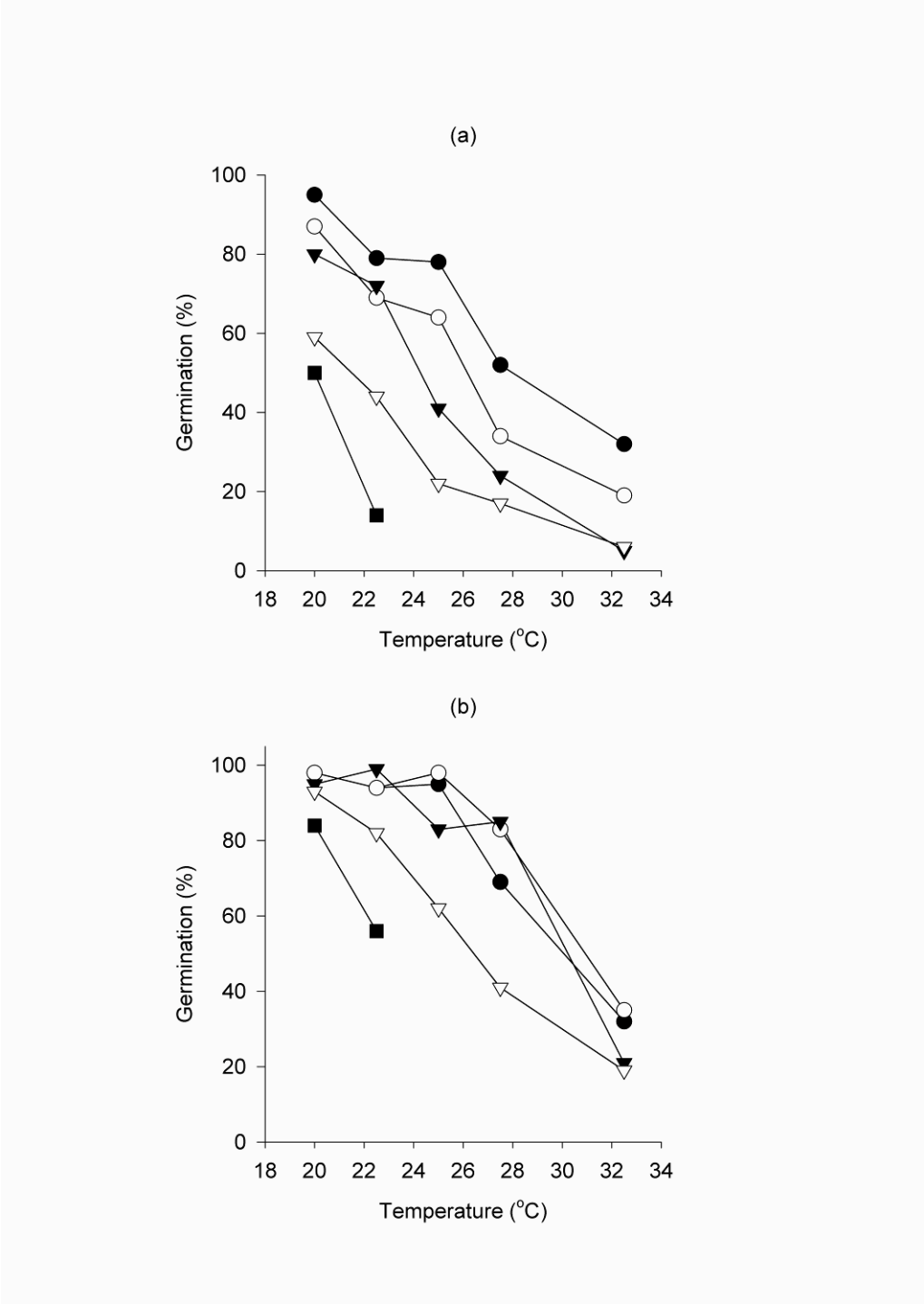

Figure 3.6. Cumulative germination percentage vs initial (50 d) temperature.

Data are plotted for different levels of initial (50d) water potential: (a) after 50 d at the specified initial water potential and temperature and (b) after a further 75 d at 20 ºC and 0 MPa. Initial (50 d) water potentials: ● = 0 MPa, ○ = –0.3 MPa, ▼ = –0.6 MPa, ▽ = –0.9 MPa, ■ = –1.2 MPa.

3.4.6 Hydrothermal models at supra-optimal temperatures

The AB and RFS models account for reduced germination at supra-optimal temperatures by an upwards shift in seed Ψ_b as a function of supra-optimal temperature (respectively $T - T_o$, Equation 3.6 and $T - T_d$, Equation 3.7). This assumption can be checked by plotting deviations of "actual" from expected Ψ_b at supra-optimal temperatures against germination temperature (Figure 3.7(a)). "Actual" Ψ_b is calculated using Equation 3.5 with T = germination temperature, as in the RFS model. Expected Ψ_b is calculated using Equation 3.4 i.e. Ψ_b (G) = $\Psi_b(50)$ + Probit(G) $\sigma_{\Psi b}$. Deviations of "actual" from expected Ψ_b can be specified mathematically by subtracting the right hand side (RHS) of Equation 3.4 from the RHS of Equation 3.5 i.e.:

$$\text{Deviation} = \Psi - [\theta_{HT} /(T-T_b)\, t(\text{G})] - [\Psi_b(50) + \text{Probit(G)}\, \sigma_{\Psi b}]. \qquad (3.11)$$

Figure 3.7(a) shows that the deviations between "actual" and expected Ψ_b show an increase in magnitude with temperature as predicted by the AB and RFS models, but the deviations vary widely for each temperature level. It appears that temperature alone does not account for the deviations from the expected values for Ψ_b. At sub-optimal temperatures, Ψ_b of germinating radiata pine seed shifted upwards towards zero as a function of time during germination (Section 3.4.2). A similar increase may occur at supra-optimal temperatures. Figure 3.7(b) shows deviations of actual from expected Ψ_b vs time to germination, for each supra-optimal temperature. This shows that deviations increase with time to germination but the form of the relationship does vary with temperature.

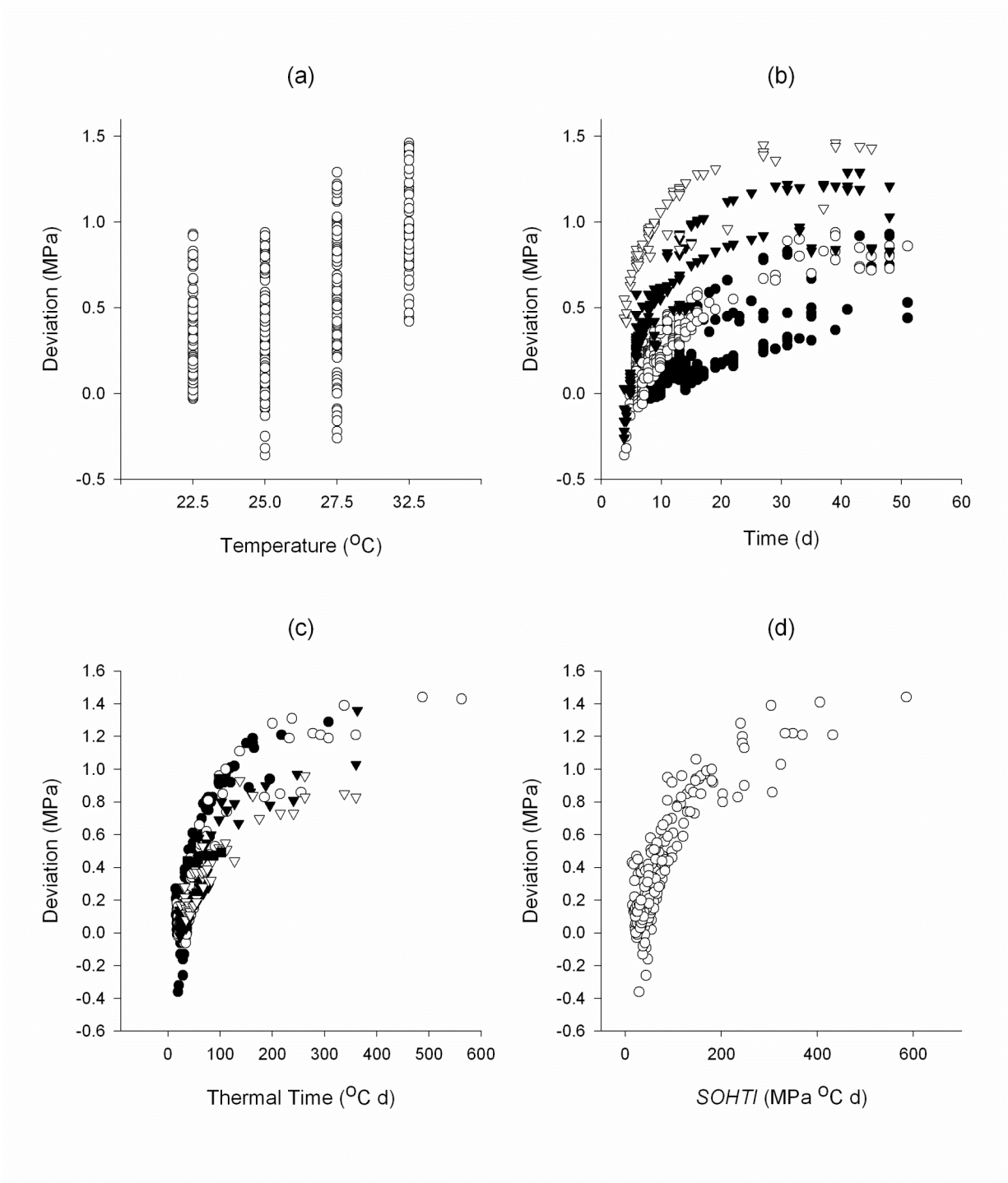

Figure 3.7. Deviation of "actual" from expected Ψ_b at supra-optimal temperatures.

Data are plotted against (a) Temperature; (b) Time to germination for each temperature level (● = 22.5 ºC, ○ = 25 ºC, ▼ = 27.5 ºC, ▽ = 32.5 ºC); (c) Thermal time $(T - T_d)\,t$, for each water potential level (● = 0 MPa, ○ = –0.3 MPa, ▼ = –0.6 MPa, ▽ = –0.9 MPa, ■ = –1.2 MPa); (d) Supra-optimal hydrothermal time index (*SOHTI*).

To account for this, deviations were plotted against thermal time accumulated above T_d i.e. $[T - T_d]\ t(\mathrm{G})$, for each level of water potential in the experiment (Figure 3.7(c)). Doing this revealed that deviations are strongly correlated with thermal time, although the form of the relationship varies between water potential treatments. Figure 3.7(c) shows that this variation between water potential treatments follows a consistent trend, with deviations increasing at a slower rate per unit of thermal time as water potential becomes drier. Therefore the deviations were also plotted against a "supra-optimal hydrothermal time index" (*SOHTI*) calculated using thermal time accumulated above T_d ($\theta' = [\Psi - (-1.5)][T\text{-}T_d]\ t(\mathrm{G})$). *SOHTI* differs from the population hydrothermal time constant θ_{HT}, because it is a variable calculated from a base temperature of $T_d = 20$ ºC rather than T_b, and the base water potential (–1.5 MPa) is an approximation for $\Psi_b(50)$ rather than the base water potential of a particular seed percentile ($\Psi_b(\mathrm{G})$).

The relationship between deviations ("actual" minus expected Ψ_b) and *SOHTI* is quite consistent for all data, and appears to have an asymptotic exponential form with an asymptote of 1.5 MPa (Figure 3.7(d)). This suggests that the temperature-driven shift in Ψ_b (50) proposed by Alvarado & Bradford (2002 and by Rowse & Finch-Savage (2003) is 1) not instantaneous but occurs over time and 2) is also influenced by the water potential of the seed's environment. Accounting for these additional effects of time and water potential using *SOHTI* eliminates much of the variation in "actual" minus expected Ψ_b shown in Figure 3.7(a), which only accounts for the effect of supra-optimal temperatures on the Ψ_b of seeds.

In order to specify a mathematical relationship between deviations ("actual" minus expected Ψ_b) and *SOHTI*, a regression was fitted to the data for deviations vs *SOHTI* using two alternative models for modelling asymptotic curves i.e. the asymptotic exponential equation (Equation 3.12) and the Michaelis-Menten equation (Equation 3.13) (Crawley 2002):

$$y = a - (be^{-\mathrm{c}\,SOHTI}) \tag{3.12}$$

$$y = (V_m\ SOHTI) / (K + SOHTI) \tag{3.13}$$

where y is "actual" minus expected Ψ_b, *SOHTI* is supra-optimal hydrothermal time index, a, b and c are parameters for Equation 3.12, and V_m and K are parameters for Equation 3.13.

The models were fitted using the "nls" function in programme R (R Development Core Team 2007). This function simultaneously estimated all model parameters using an iterative least-squares procedure. Table 3.3 summarizes parameters and Akaike Information Criterion (AIC) values (Akaike 1974; Burnham & Anderson 2001) for the two models.

Table 3.3. Model parameters and Akaike Information Criterion (AIC) values for alternative models of the relationship between deviations ("actual" minus expected Ψ_b) and SOHTI.

Michaelis-Menten Model		Asymptotic exponential model	
Equation 3.13		Equation 3.12	
Parameter	Value	Parameter	Value
V_m	2.63	a	1.45
K	379	b	1.56
		c	0.00596
AIC	–664	AIC	–745

The AIC value for the asymptotic exponential model was more negative than that for the Michaelis-Menten model, indicating that the asymptotic exponential model was a more likely explanation of the relationship between deviations (actual minus expected Ψ_b) and *SOHTI*. Therefore the asymptotic exponential model was used to adjust seed Ψ_b (50) towards zero as a function of *SOHTI* as shown in Equation 3.14:

$$\Psi_b (50)' = \Psi_b(50) + (1.448 - 1.562\, e^{-0.00596\, SOHTI}). \qquad (3.14)$$

The adjusted $\Psi_b (50)'$ was then used as an input into a hydrothermal time model, with other model parameters derived from germination data for sub-optimal temperatures (Section 3.5) i.e. θ_{HT} = 176 ºC MPa d, T_b = 9.0 ºC, $\sigma_{\psi b}$ = 0.42 MPa. Figure 3.8 shows predicted germination percentage vs time using this model, compared with actual germination data for supra-optimal temperatures. Agreement between model predictions

and actual data is generally good, except for the 22.5 ^{o}C/–1.2 MPa treatment. One general discrepancy is that the adjusted hydrothermal model predicts that germination percentage reaches an asymptote and remains there for the remainder of the 50 d germination period. In contrast actual germination quite often quickly reached an asymptote, but after a hiatus a small amount of further germination (typically ≤ 10%) also occurred for many treatments.

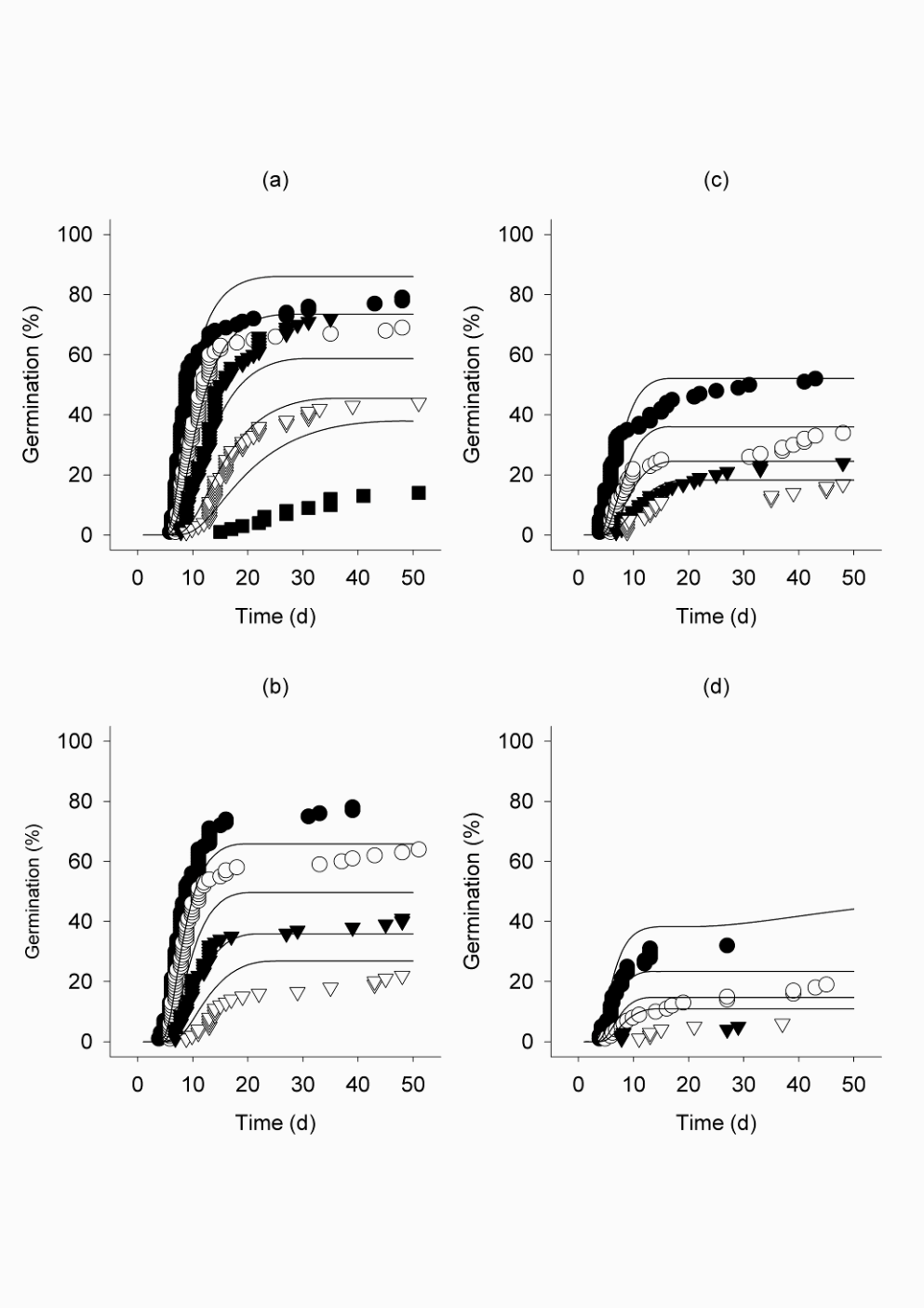

Figure 3.8. Germination time course data compared with hydrothermal model predictions.

Data are plotted for each level of temperature and water potential as follows:(a) = 22.5 ºC, (b) = 25 ºC, (c)= 27.5 ºC, (d) = 32.5 ºC. ● = 0 MPa, ○ = –0.3 MPa, ▼ = –0.6 MPa, ▽ = –0.9 MPa, ■ = –1.2 MPa. Model predictions use the asymptotic exponential function (Equation 3.14) to adjust Ψ_b. Predictions are shown by the solid lines.

3.5 Discussion and conclusions

3.5.1 The suboptimal hydrothermal model

A conventional hydrothermal model (Equation 2.1) gave a reasonable fit to the germination data, but over-predicted germination rates for slower germinating seeds, and consequently over-predicted germination percentages. Modified models which adjusted Ψ_b upward as a linear function of time or hydro-time index (*HTI*) to germination were markedly more accurate for all combinations of T and Ψ used in this study.

Departures of actual seed behaviour from the conventional hydrothermal model are frequently reported in the literature (Dahal & Bradford 1994; Phelps & Finch-Savage 1997; Kebreab & Murdoch 1999; Grundy *et al.* 2000). Kebreab & Murdoch (1999) described results for germinating *Orobanche aegytiaca* where 1) T_b varied with ambient water potential, in contrast to the conventional hydrothermal model assumption of a single T_b value for the whole seed population, and 2) the mean base water potential Ψ_b (50) was found to vary with temperature, being –2 MPa between 14-23^{o}C but increasing towards zero at both higher and lower temperatures. These variations in T_b and Ψ_b for *O. aegyptiaca* were modelled by the authors as functions of ambient water potential. This represents a departure from the assumptions of the conventional hydrothermal model, where T_b and Ψ_b are assumed to be characteristics of the seed population which are independent of seedbed temperature and water potential.

However an explanation for many of the reported departures from the conventional hydrothermal model is suggested by the modified hydrothermal model fitted to radiata pine germination in this study. In the case of *O. aegyptiaca* (Kebreab & Murdoch 1999), the apparent increase in Ψ_b (50) for *O. aegyptiaca* at high (> 23^{o}C) and low (< 14^{o}C) temperatures could be caused by time (when T <14^{o}C) or temperature (when T >23^{o}C) driven shifts in Ψ_b.

These shifts in Ψ_b can, in turn, explain the apparent influence of water potential on T_b. Seeds germinating slowly at low temperatures e.g. where T < 14^{o}C, will eventually reach

the point where their Ψ_b approaches ambient Ψ and their *GR* will fall to zero. Seeds germinating at low temperature in moist conditions will take longer before their Ψ_b approaches the seedbed water potential (because seedbed water potential (Ψ) is closer to 0 MPa) and are therefore more likely to complete germination under cold conditions. For this reason the apparent T_b for the moister seeds is lower than for the seeds growing in drier conditions. In fact, both seedlots could have the same underlying T_b, and the apparent difference in T_b actually results from a time-dependent shift in Ψ_b. This is in contrast to the conclusion of Kebreab & Murdoch (1999) that T_b varies with seedbed water potential.

Several authors have suggested that declining *GR* and seed germination percent at supra-optimal temperatures arises from a temperature-driven increase in Ψ_b towards zero e.g. Alvarado & Bradford (2002) and Rowse & Finch-Savage (2003). In contrast, the hypothesis that Ψ_b varies as a function of germination time at suboptimal temperatures has not been widely reported in the literature. Allen *et al.* (2000) reported that for a range of dry climate plant species, Ψ_b (50) of seeds appears to increase when germinated at temperatures close to T_b. This behaviour was successfully modelled by allowing Ψ_b (50) to increase under these conditions although the authors do not describe the methods used to calculate that increase.

A more detailed paper by Gianinetti and Cohn (2007) describes the induction of secondary dormancy in red rice (*Oryza sativa* L.) in terms of an upwards shift in Ψ_b(G). This upwards shift was modelled as a function of hydrotime accumulated during germination, an approach equivalent to Model 3 (Table 3.2) in this study.

In contrast, Ni & Bradford (1992) and Dahal & Bradford (1994) report a downwards adjustment in Ψ_b for tomato (*Lycopersicon aesculentum* Mill.) seeds incubated under low water potentials, so that seeds became more germinable under these conditions. Dahal & Bradford (1994) accounted for this adjustment by fitting two separate hydrothermal models to the data, one for germination data where Ψ was drier than –0.5 MPa (with a lower mean Ψ_b) and one for data when Ψ was moister than –0.5 MPa (with a higher

mean Ψ_b). However, the data reported by Dahal & Bradford (1994) also indicate a marked downward shift in Ψ_b at low temperatures (10 °C), even under moist conditions ($\Psi > -0.5$ MPa). This suggests that seedbed water potential was not the only factor causing the shift in Ψ, and that chronological time to germination may have also controlled the magnitude of the downwards shift in Ψ_b.

While the shift in Ψ_b reported by Dahal & Bradford (1994) is in the opposite direction to that which was found for radiata pine in this study, it does lend support to the concept that for some plant species Ψ_b is not a fixed parameter, but may vary with seedbed conditions. There may be ecological implications from this ability to vary Ψ_b. Imbibed radiata pine seeds whose Ψ_b shifts above the ambient soil water potential when conditions do not allow rapid germination, will remain ungerminated until they experience sustained moisture and warmth – at which time germination and seedling growth conditions will be ideal. This seems to be a useful "bet-hedging" adaptation for radiata pine seed, which has no dormancy mechanism (Kao & Rowan 1970; Rimbawanto *et al.* 1988). However the adaptive value of this hydro-time index (*HTI*) or time-dependent adjustment to Ψ_b would need to be tested under field conditions similar to radiata pine's natural habitat on the Central Californian coast, if only to verify that it is a real adaptation to radiata pine's regeneration niche and not an artefact of the constant germination conditions used in this study.

3.5.2 The supra-optimal hydrothermal model

Supra-optimal temperatures are temperatures greater than optimum temperature (T_o), the temperature at which the seed germination rate (*GR*) is at a maximum. However for radiata pine seeds, Figure 3.5 shows that T_o occurs at ≈ 27.5 ^{o}C for the lowest percentiles (fastest germinating seeds) and at progressively lower temperatures as the seed percentile value increases.

Figure 3.5 also shows that the maximum *GR* occurs over a wider temperature range for the low percentile seeds, whereas the maximum *GR* for the higher seed percentiles occurs at a narrow peak, before a *GR* declines rapidly to zero for temperatures greater than T_o.

These results suggest that the model proposed by Rowse & Finch-Savage (2003) for germination at supra-optimal temperatures is more appropriate than the broken-stick model proposed by Alvarado & Bradford (2002). In particular, the AB model posits a single T_o for the seed population, above which no further thermal time is accumulated. However Figure 3.5 suggests that for radiata pine, the lower seed percentiles continue to accumulate thermal time above the generally accepted T_o for radiata of 20 ^{o}C, because they germinate most rapidly at 25-27.5^{o}C. This is consistent with the RFS model (Rowse & Finch-Savage 2003), which assumes that thermal time continues to accumulate at supra-optimal temperatures.

Comparison of supra-optimal model predictions with actual germination data

Plots of deviations of actual Ψ_b from an unadjusted (expected) Ψ_b showed that the adjustment to Ψ_b used in the AB and RFS models i.e. $k(T - T_o)$ and $k(T - T_d)$ respectively, would not accurately predict the upwards shift in Ψ_b in radiata pine seed germinated at optimum temperatures (Figure 3.7(a)). However the deviation plots showed a strong correlation with a supra-optimal hydrothermal time index (*SOHTI*), calculated from a base temperature = 20 ^{o}C and from a base water potential = –1.5 MPa (Figure 3.7(d)). This is because the shift in Ψ_b was also influenced by the water potential at which the seeds were germinated, and increased as an asymptotic exponential function of time to germination (t(G)).

Although the adjusted hydrothermal model (using Equation 3.14 to adjust Ψ_b) made reasonably accurate predictions of time to germination for radiata pine seeds at supra-optimal temperatures, Figure 3.8 shows that predictions were less accurate than those made for radiata pine at sub-optimal temperatures. One likely reason for this is that the upwards adjustment in Ψ_b at supra-optimal temperatures occurs at a rapid rate within a few days from the beginning of germination, before the rate declines and the upwards adjustment reaches an asymptote at 1.5 MPa (Figure 3.7(d)). Therefore any error in predicting this upwards adjustment will have a large effect on predicted germination time for the whole seed population. In contrast, the upwards adjustment in Ψ_b at sub-optimal temperatures predicted as a function of hydro-time index did not occur until $t \approx$ 25d and

proceeded at a slower rate (Figure 3.3(b)). Therefore any errors in predicting this shift had less bearing on the predicted time to germination, and predicted times to germination were consistently accurate for all water potentials at sub-optimal temperatures.

The other noteworthy result was the small amount of further germination that occurred late in the germination time course at most supra-optimal temperatures, after germination percentage had apparently reached a plateau. This behaviour was not predicted by the hydrothermal model, except for 32.5 ºC /0 MPa (Figure 3.8(d)). However the late, small increase in predicted germination for 32.5 ºC /0 MPa suggests a possible mechanism for this "second wind" of germination. It may be that the first plateau in germination occurs because of the initial very rapid upwards adjustment in Ψ_b, which makes for a slow rate of hydrothermal time accumulation for higher-percentile seeds whose Ψ_b(G) may end up very close to the ambient Ψ. However, once the upwards adjustment has reached the asymptote, and provided the seed's adjusted Ψ_b is still less than ambient Ψ, the seed will eventually accumulate enough hydrothermal time to germinate. Under warm, moist conditions, for example 32.5/ 0 MPa, it is possible that the seed will die before this occurs because seed respiration rates will be rapid and seed reserves will be exhausted before the seed has accumulated sufficient hydrothermal time to germinate. In contrast, for cooler and/or drier seedbeds where seed reserves may not been exhausted before the seed has accumulated sufficient hydrothermal time, some additional seed will germinate. The reasons for lack of seed germination at both supra- and suboptimal temperatures are discussed at greater length in the next section.

3.5.3 Ungerminated seeds

For temperature treatments of 27.5ºC and 32.5ºC, and for all supra-optimal temperature treatments where Ψ was $\leq$ –0.6 MPa, seeds did not achieve full germination after further incubation for 75 d under optimum conditions, although seeds from T = 27.5 ºC and $\Psi \leq$ –0.6 MPa did make substantial progress towards it (Figure 3.6). By the end of the 75 d incubation period any remaining ungerminated seeds were nearly all dead and had begun to decompose. In contrast, seed from the T = 22.5 or 25 ºC and Ψ = 0 or –0.3 MPa treatments achieved > 90% germination within 21 d of being placed in optimum

conditions. The higher germinability of seeds from cooler treatments (22.5 and 25 ºC) suggests that seeds had not germinated after 50 d because they had not accumulated enough hydrothermal time to germination, due to an upwards shift in Ψ_b driven by supra-optimal temperatures. At the same time, the death of ungerminated seeds at 32.5ºC /0 or –0.3 MPa during the 50 d germination period, and the death of ungerminated seeds during the subsequent 75 d germination test, suggests that germination was also reduced by seed death. As mentioned in Section 3.4.2, there was no sign of fungal infection on the dead seeds. It seems likely that imbibed radiata pine seeds, while not able to completely germinate under warm ($T \geq 27.5$ ºC) and moist conditions, are nonetheless undergoing metabolic processes which lead to the eventual death of some of the ungerminated seeds.

The adaptive value of reduced germination with $T > 20$ ºC is therefore a matter for speculation, because young radiata pine seedlings can grow successfully at daytime temperatures ≈ 30 ºC if acclimated to warm growing temperatures (Rook 1969). More generally, Bradford (2002) comments that the reasons for the decrease in seed *GR* and inhibition of germination at supra-optimal temperatures are not obvious, and that the most commonly offered explanation i.e. non-linearity in thermal time accumulation due to denaturation of proteins, is unlikely to occur at temperatures as low as 20 ºC. In this study, plots of *GR* vs *T* indicated that radiata pine seeds can accumulate thermal time linearly up to 27.5 ºC (Figure 3.5), suggesting that seeds would be able to germinate very rapidly at this temperature, in the absence of an upwards adjustment in Ψ_b caused by temperatures where $T > T_d$.

The regeneration niche of radiata pine within its natural range in Central California was discussed in Section 2.1. Germination of radiata pine seed released from cones commences with the rainy season in California, which typically begins in late autumn and continues throughout a mild winter (Forde 1966; Dallman 1998). Assuming the released radiata pine seeds commence imbibition at the onset of the rainy season, it is unlikely that soil temperatures will exceed 20-25 ºC while germination is taking place. Under these conditions the advantage of thermo-inhibition at $T > 20$ ºC is not clear. One possibility is that it is an adaptation to cope with a "false break", a feature of mediterranean climates

where unseasonal late summer rains may trigger seed germination but germinated seedlings subsequently die because the rains do not persist and soil evaporation rates are still high (Norman *et al.* 1998). One may speculate that radiata pine seeds that imbibe and commence germination during a "false break" 1) will not germinate due to thermo-inhibition by supra-optimal temperatures in the subsequent dry spell, but 2) will germinate once autumn rains bring moister soils and cooler temperatures, when seedling survival is more likely.

However, as noted in Section 3.5.1, seed behaviours observed under constant laboratory conditions (such as the shift in Ψ_b at supra-optimal conditions reported in this study) would need to be observed under field conditions similar to radiata pine's natural habitat in order to properly assess their adaptive value.

3.5.4 Conclusions

1. When germinated under conditions of constant suboptimal temperatures and water potentials, a commercial radiata pine seedlot exhibited germination behaviour consistent with the assumptions of the conventional hydrothermal model proposed by Gummerson (1986). However, the accuracy of the hydrothermal model was improved by including a function for an upwards shift in seed base water potential as a function of hydro-time (the hydro-time index) accumulated by the seed. This kind of shift is not widely reported in the literature, but seems a useful adaptation in species that do not have physiological dormancy mechanisms to prevent germination when seedbed and environmental conditions are far from ideal.
2. When germinated under constant supra-optimal temperatures, the commercial radiata pine seedlot exhibited germination behaviour more consistent with the RFS hydrothermal germination model proposed by Rowse & Finch-Savage (2003) than with the AB model proposed by Alvarado & Bradford (2002). In particular, seeds appeared to accumulate thermal time at temperatures well above the "optimum" temperature for germination of radiata pine (20–22 ^{o}C), which violates a key assumption of the AB model.

3. The accuracy of the hydrothermal model at supra-optimal temperatures was improved by a modification of the RFS model, where the upwards shift in seed base water potential at supra-optimal temperatures occurred as an asymptotic function of hydrothermal time. This meant that the upwards adjustment in seed base water potential occurred fastest when the seedbed was moist. It seems counter-intuitive that germination should be inhibited most strongly under moist conditions, but it makes sense when one considers that warm seedbed conditions mean rapid drying of the seedbed so that by the time the seed germinates, soil moisture may be insufficient for seedling survival. This is a particularly useful adaptation for plants growing in mediterranean climates, where "false breaks" (early autumn rain followed by a further period of drought) are a potential cause of premature germination of seedlings.
4. Overall, the study described in this chapter has successfully applied a hydrothermal model to describe germination of a radiata pine seedlot under constant laboratory conditions, and in the process revealed adaptations in germination behaviour which may be of great importance under field conditions. The implications of these findings are discussed further in Chapter 6.

4 RADIATION INTERCEPTION AND SEEDLING RUE

4.1 Background

The aim of this experiment was to test aspects of the radiation use efficiency (RUE) model discussed in Section 2.5. This was achieved by fitting Equation 2.4 to measurements of seedling NPP and intercepted PAR ($\varphi_{p.i}$), for seedlings grown under low, medium and high levels of PPFD but uniform temperature, nutrition, vapour pressure deficit and water availability. Because 1) ambient temperature and vapour pressure deficit and 2) available water and nutrients did not vary between seedlings, it was expected that $f_{\theta,}$ f_D f_T and f_N would also not vary. Therefore the amount of growth in seedling biomass (NPP) was expected to be directly related to the amount of PAR ($\Sigma\varphi_{p.i}$) intercepted by a seedling–which in turn was determined by the PPFD in the seedling's environment.

The next two sections discuss how NPP and $\varphi_{p.i}$ may be measured for young pine seedlings under different levels of PPFD.

4.1.1 Estimation of seedling NPP

To estimate RUE, NPP in the form of increases in seedling dry biomass need to be measured or estimated. Henceforth, seedling dry biomass will be denoted by the symbol W. An increase in seedling dry biomass is calculated as the difference between W at an initial time t_o, and W at a later time t_1. W at time t_o cannot be obtained by the usual method of destructive measurement (cutting the seedling into its constituent parts and oven-drying to equilibrium weight). W at time t_1 could be measured destructively, but this would preclude growing the seedling on to estimate W increases over subsequent time intervals $t_2 \ldots t_f$ where t_f is the final time of measurement.

Historically the alternative to destructive measurement has been the use of allometric relationships between biomass (W) and seedling measurement variables which can be

measured non-destructively. For example, ground-level stem diameter (D), top height (H) or variables derived from these, such as D^2 or $D^2 H$ have proved good predictors for both total W and W of seedling components (foliage, stem, branches, roots) (Ruehle *et al.* 1984; Zutter *et al.* 1986). Relationships between W and seedling measurement variables have been specified as linear or power-law functions e.g.:

$$W = a + bX \quad (4.1)$$

$$W = aX^b \quad (4.2)$$

where $X = D$ or D^2H, and a and b are constants (Ruehle *et al.* 1984; Ter-Mikaelian & Parker 2000).

Where power-law relationships are log transformed, the model is specified as:

$$\mathrm{Ln}W = a + b\,\mathrm{Ln}X \quad (4.3)$$

(Ruehle *et al.* 1984; Zutter *et al.* 1986; Norgren *et al.* 1995; Ter-Mikaelian & Parker 2000).

Typically these allometric relationships have reasonably good predictive power. In many cases the coefficient of determination (R^2) values for the models exceed 90%, and in some cases R^2 values of 96- 97% have been obtained (Ruehle *et al.* 1984; Norgren *et al.* 1995; Ter-Mikaelian & Parker 2000).

An alternative to D and H as seedling measurement variables is the silhouette area of the seedling (A), which can be measured using digital imaging software. A photographic image of the seedling to be measured is converted by the software to a black and white silhouette by 'thresholding' ((Norgren *et al.* 1995); see Figure 4.1). The digital imaging software estimates the area of the silhouette as a proportion of the total picture frame. A linear scale placed in the photo then allows this proportional area to be converted into the

two-dimensional projected area of the seedling, from the angle from which the photograph was taken.

This technique has been used to estimate leaf area of large trees in urban settings (Peper & McPherson 2003), but has also been used to estimate total and component *W* for conifer seedlings (Norgren *et al.* 1995; Ter-Mikaelian & Parker 2000). It should give good estimates of above-ground biomass, as *A* is a good estimator of the volume of all above-ground components (Ter-Mikaelian & Parker 2000). Assuming a reasonably consistent ratio of *W* to above-ground volume for seedlings, then *A* will also be highly correlated with above-ground biomass.

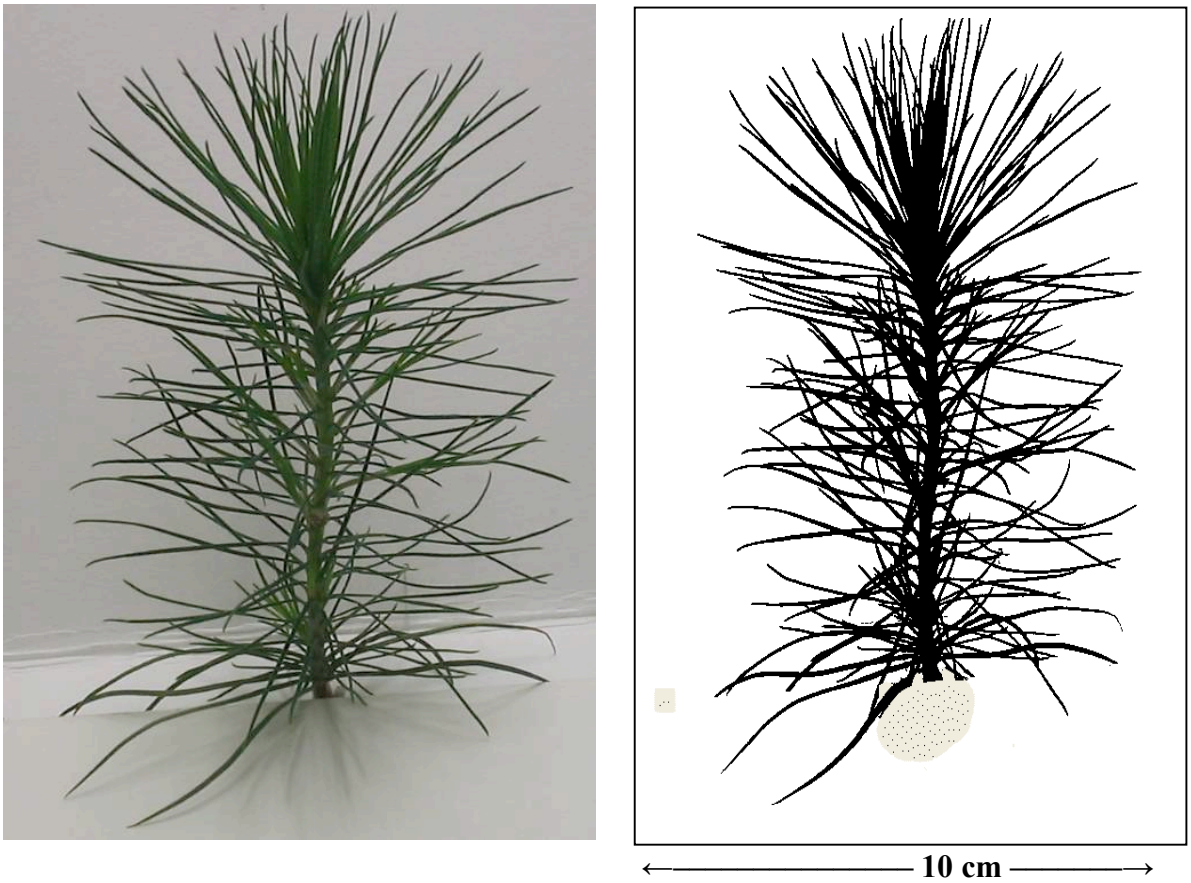

Figure 4.1. (a) A digital photograph of a young radiata pine seedling; (b) the same seedling converted to a silhouette image by thresholding.

Actual size of the seedling is indicated by the scale line.

One important question is whether models relating W to seedling measurement variables (D^2, D^2H, A) are general models, meaning that they can be applied to seedlings growing on different sites and under different conditions. Models which give unbiased estimates of W for all sites are seen as more useful as they can be used for a range of sites without having to derive locally valid allometric models (Ruehle *et al.* 1984).
There are reasons to suspect that allometric equations may vary with site. In general, plants respond to variations in available resources (light, water, nutrients) with allometric or anatomical responses in order to optimize resource capture and utilization (Poorter & Nagel 2000; Weiner 2004). Allometric or anatomical variations between seedlings growing under different levels of photosynthetic photon flux density (PPFD) may result in differences in the parameters of allometric equations relating different seedling measurements such as W, D, H and A.

This study: 1) investigated whether one general allometric equation could be used to predict the total biomass of young radiata pine seedlings grown under three different levels of PPFD; and 2) attempted to identify which variable or variables (D^2, D^2H or A) were the best predictors of seedling biomass under these varying conditions.

4.1.2 Measurements of PAR absorption by seedlings

To calculate seedling RUE, not only seedling NPP but also the PAR absorbed or intercepted by the seedling ($\varphi_{p.a}$ or $\varphi_{p.i}$) must be estimated (Equation 2.2). In this section, three alternative methods are evaluated for their efficacy in estimating the absorption of PAR by newly germinated radiata pine seedlings. These methods are as follows:

1. The Net PAR integration method
   This method was developed by Green (1993) and (McNaughton *et al.* (1992) for the measurement of PAR absorption on large single trees in the field. The crown of the tree is enclosed by a large semi-circular frame which rotates about the crown, such that quantum sensors on the frame measure the net photosynthetic photon flux density (inward PPFD entering the sphere minus outward PPFD exiting the sphere) integrated over the spherical surface described by the rotating semi-circle. If no PAR is absorbed within the sphere, the net PPFD should equal

zero i.e. PAR entering the sphere equals PAR leaving the sphere. If an object within the sphere absorbs a proportion of the PAR entering the sphere, then the PAR leaving the sphere is reduced by the amount that the object has absorbed.

2. The "Wilson" method

   This method was first suggested by Wilson (1981a,;1981b), and is an adaptation of the methods used to estimate light interception by continuous plant canopies (grasslands, field crops). It has been used by many authors since e.g. (Grace *et al.* 1987). In this method, PAR sensors are laid in a grid pattern on an area open to full sky radiation. Sensors are also placed in the same pattern beneath the canopy of the tree. The differences between the PPFD values under the open sky and those under the tree are assumed to result from interception of PAR by the tree crown. These differences are integrated over the area measured to estimate PAR intercepted by the crown.

3. Estimation of intercepted downwelling PAR using photographic method*s*

   This approach assumes that the seedling is surrounded by an envelope surface of foliage, and that the sum of all incident downwelling PAR intersecting this surface is therefore the total intercepted downwelling PAR for the seedling. The envelope surface of the foliage as seen from a specific viewpoint, can be represented by the silhouette of the seedling from that viewpoint, as shown in Figure 4.1.

Method 3 was first described by Elsacker *et al.* (1983) who proposed that the total interception of diffuse PAR by an upright plant growing at the centre of an equatorial plane can be obtained by integrating Equation 4.4 over an imaginary radiant hemisphere surrounding the plane:

$$I_{(dS)} = N\, dS\, A\mathrm{p}\, (1\text{-}g) \qquad (4.4)$$

where dS is a small area element of the radiant hemisphere surrounding the plant (m^2), $I_{(dS)}$ is the diffuse radiant flux from dS that is intercepted by the crown of the tree (in Watts, W); N is the radiance expressed as a flux density(W m^{-2}) per unit solid angle

(steradians, sr) emitted from *dS*; and *A*p (1-*g*) is the projected area *A*p (m^2) of the crown perpendicular to the radiance from *dS*, reduced by the photographically measured fractional area of gaps in the canopy (1-*g*). For a small seedling, *A*p (1-*g*) is equivalent to the silhouette area of the tree in a photograph, which can be measured digitally.

Elsacker *et al.* (1983) state that total intercepted flux *I* (in Watts) is calculated by integrating Equation 4.4 with respect to *dS* over the whole hemisphere, but do not show the details of this calculation. Furthermore, Equation 4.4 appears to be dimensionally inconsistent since it includes two area terms (*dS* and *A*p (1-*g*)), implying that $I_{(dS)}$ is in units of W m^{-2} sr^{-1} rather than W.

However, an alternative solution can be derived from Monteith & Unsworth (1990, p31-32), as follows. In many environments the measured value of radiance *N* of a hemisphere above an equatorial plane varies with the position of *dS* i.e. with the zenith angle of *dS* from the vertical (β), and its azimuth angle on the horizontal plane (θ) (Figure 4.2). At the same time, the seedling has a variable area *A* (projected silhouette area at right angles to the incoming light) for each *dS*.

Removed for copyright reasons

Figure 4.2.Method for calculating irradiance of a unit area (=1) at the centre of an equatorial plane by a radiant surface element dS at zenith angle β to the vertical axis and azimuth angle θ to the horizontal axis.

Source: Monteith & Unsworth (1990)

Then multiplying N (W m^{-2} sr^{-1}) × A (m^2) as measured for each dS gives the light intercepted by the seedling in units of W sr^{-1} for any dS, but this must now be integrated over the solid angle of the hemisphere above the seedling ($\Omega = 2\pi$ steradians), to obtain the total intercepted flux.

Equation 4.5 (derived from Monteith & Unsworth (1990, Equation 3.24, p 32) shows how this integration may be done, for the case where the intercepting object is a flat horizontal disc of unit area (area=1) at the centre of the plane beneath the hemisphere i.e. the integral is expressed in terms of the irradiance $N(\beta, \theta)$ from the direction of dS, the azimuth angle from the direction of dS (θ) and the zenith angle of dS from the vertical (β).

$$I = \int_{\theta=0}^{2\pi} \int_{\beta=0}^{\frac{\pi}{2}} N(\beta,\theta) \sin\beta \cos\beta d\beta d\theta \qquad (4.5)$$

where I is the downwelling PAR intercepted by the flat horizontal disc.

However Equation 4.5 needs to be modified to account for the difference between a flat disc and a 3-dimensional upright seedling. The projected area of the flat disc (area=1) in the direction which is at an angle β to the zenith, is represented by the term cos β (i.e. the horizontal area of the disc (=1), multiplied by cos β) in Equation 4.5. For an upright seedling, this term (cos β) can be replaced by A_β which is the projected area of the seedling in the direction β. This results in the following:

$$I = \int_{\theta=0}^{2\pi} \int_{\beta=0}^{\frac{\pi}{2}} N(\beta,\theta) A_\beta \sin\beta d\beta d\theta \qquad (4.6)$$

which is integrated with respect to azimuth angle (θ=0-2π) and the zenith angle (β=0-π/2).

To simplify analysis, Monteith & Unsworth (1990) assume that for any angle β, both the intercepting area (A_β) and $N(\beta, \theta)$ are uniform for all azimuth angles θ. This simplifies the integral with respect to $d\theta$, which becomes 2π. Therefore I is calculated from:

$$I = 2\pi \int_0^{\frac{\pi}{2}} N(\beta) A_\beta \sin\beta d\beta \qquad (4.7)$$

which is integrated over the range β=0 *to* β= π/2. The only difference between this and Equation 3.24 in Monteith & Unsworth (1990) is that the projected area term for a flat disc ($\cos\beta$) is replaced by A_β, the projected (silhouette) area of the seedling in the plane normal to the direction of β.

This method was independently derived by Smolander & Stenberg (2001) who used it to calculate light interception by a shoot from a Scots pine. These authors obtained total seasonal downwelling PAR intercepted by a shoot ($\varphi_{p.i}$) by integrating:

$$\int_{\omega=0}^{\Omega} q(\omega) gf(\omega) SSA(\omega) d\omega \qquad (4.8)$$

where ω is a solid angle within a hemisphere above the shoot (sr), Ω is the total solid angle of the hemisphere (sr), $q(\omega)$ is the seasonal amount of PAR from the direction of ω (J m^{-2} sr^{-1}), $SSA(\omega)$ is the shoot silhouette area (m^2) on a plane normal to the direction ω,(equivalent to A_β in Equation 4.7) and $gf(\omega)$ is the gap fraction, the proportion of visible sky in the hemisphere above the shoot (the non-visible part of the sky is obscured by surrounding plant canopy).

Smolander & Stenberg (2001) specify ω in terms of elevation angle (ϕ) and azimuth angle (γ), so that $d\omega = \cos\phi d\phi d\gamma$. Substituting this term in Equation 4.8, and assuming an unobstructed radiant hemisphere ($gf(\omega) = 1$), then Equation 4.8 becomes:

$$\varphi_{p.i} = \int_{\omega=0}^{\Omega} q(\omega) SSA(\omega) \cos\varphi d\varphi d\gamma \qquad (4.9)$$

where $\phi_{p.i}$ = total seasonal intercepted downwelling PAR.

Confusion may arise from the use in this chapter of the same symbol (ϕ) to denote elevation angle and intercepted or absorbed PAR, but this is done to ensure consistency with the literature. To clearly identify the two different meanings for this symbol, absorbed and intercepted PAR will be denoted by $\varphi_{p.a}$ and $\varphi_{p.i}$ respectively. When used to denote an elevation angle, ϕ will not have a subscript.

Assuming that $q(\omega)$ and SSA(ω) are uniform for all azimuth angles γ and integrating with respect to $d\gamma$ gives:

$$\varphi_{p.i} = 2\pi \int_{\varphi} q(\varphi) SSA(\varphi) \cos\varphi d\varphi, \qquad (4.10)$$

which differs from Equation 4.7 only in that: 1) it includes the term cos ϕ rather than sin β, due to ϕ being the elevation angle from the horizontal (Equation 4.10) and β the zenith angle from the vertical (Equation 4.7); and 2) the equation is specified in terms of total intercepted seasonal PAR energy (J) rather than intercepted PAR flux (W).

Comparison of alternative methods for estimating $\varphi_{p.a}$ or $\varphi_{p.i}$

Theoretically, the net PAR integration method (method 1) is preferable, because the circular arrangement of sensors accounts for all PPFD incident to and emanating from the tree canopy i.e. not just the PAR intercepted by the canopy, but also PAR that is transmitted or reflected by the canopy. This transmitted or reflected PAR is measured as it leaves the surface of the sphere enclosing the tree crown, and thus is not counted as PAR absorbed by the tree canopy.

Both method 1 and method 2 also have the advantage of simplicity because intercepted or absorbed PAR is measured in real time and can be easily calculated from differences between sensor readings. In the case of method 1, the difference is in the PPFD measured entering and leaving the spherical surface described by the frame on which quantum sensors are mounted. In method 2, the difference is between PPFD measured by sensors above the seedling canopy, compared with that measured by sensors below the canopy. However, for measuring PAR interception/absorption by small seedlings, methods 1 and 2 are difficult to apply. This is because the shape and small size of the seedlings make it difficult to place a conventional quantum sensor beneath the canopy of the emerging seedling- a requirement of both methods. Method 3, despite its mathematical complexity and its dependence on the assumption that intercepted PAR is a realistic surrogate for absorbed PAR (i.e. $\varphi_{p.i} \approx \varphi_{p.a}$) has the advantage that it can be used for a single plant of any shape or size. Furthermore, Smolander & Stenberg (2001) contend that absorption of intercepted PAR is close to unity for conifer needles with only minor scatter, which implies that $\varphi_{p.i}$ will be a realistic estimate of $\varphi_{p.a}$. For this reason, method 3 was used to quantify intercepted PAR in this experiment.

4.1.3 Summary

The aim of this experiment was to test the RUE model, which states that seedling biomass growth is a quantifiable function of absorbed or intercepted PAR. This model can be specified in the form of Equation 2.4, (Section 2.3), with modifiers for environmental deficits ($f_{\theta,} f_{D,}$ f_T and f_N) set to 1. To test this model, seedling growth (NPP, measured as a change in total seedling dry biomass) and intercepted PAR ($\Sigma\varphi_{p.i}$) were measured under conditions where PPFD was controlled, and air temperature, plant available water and nutrients were both uniform and at optimal or near-optimal levels. Under such conditions, it was expected that seedling growth would be directly proportional to intercepted PAR.

The next section describes the methods used to 1) grow radiata pine seedlings under three different levels of PPFD in a growth chamber; 2) measure intercepted PAR and seedling NPP, and 3) calculate and compare seedling RUE at the three different PPFD levels .

4.2 Methods

4.2.1 Materials

Control-pollinated radiata pine seeds (seedlot no 99/174, supplied by Proseed Ltd, Amberley, New Zealand) were sown in November 2004 into 800 ml plastic pots filled with 50/50 (by volume) grade M perlite and sand. The growing medium was inoculated with mycorrhizal spores (*Rhizopogon rubescens*, collected 11 September 2003, Owhata Nursery, Rotorua, New Zealand). After germination, 120 radiata pine seedlings were transferred on 6 December 2004 to a controlled growth chamber (Contherm GR 48, Controlled Environments Limited, Winnipeg, Manitoba, Canada) and grown under controlled conditions for four months. The growth cabinet environment was monitored continuously over the duration of the experiment in general compliance with American Society of Agricultural Engineers standards for measuring and reporting environmental parameters from plant experiments in growth chambers (ASAE 2003).

Once seedlings were transferred to the controlled growth chamber, three levels of PPFD were imposed using horticultural shadecloth (Figure 4.3). Each PPFD level was imposed on two randomly chosen plots (each plot comprised 20 seedlings) so that the experiment comprised six plots in total, n= 120 seedlings. PPFD levels were 100% (no shadecloth), 50% and 25% of ambient PPFD in the growth chamber,which equated to nominal values of 500, 250 and 125 μmol m^{-2} s^{-1} respectively. Seedlings were subjected to PAR for 12 h d^{-1}, with 10 h d^{-1} of full darkness plus an additional 'ramp-up' and 'ramp-down' period of 1 h each morning and evening. Note that a PPFD of 500 μmol m^{-2} s^{-1} over a 12 h day plus a 2 h ramp-up and ramp-down equals a daily irradiance of 23.4 mol m^{-2} d^{-1}, similar to the figure of 23 mol m^{-2} d^{-1} which will saturate the photosynthetic system for many C_3 plants (Sager & McFarlane 1997). The 100% PPFD treatment therefore seemed likely to provide sufficient PAR for maximum or near-maximum seedling NPP.

Figure 4.3. Plot layout photograph.

Plots 1-3 are on the RHS of the photograph, (Plot 1 is nearest to the far wall and Plot 3 is closest to the camera); Plots 4-6 are on the LHS (Plot 6 is nearest to the far wall and Plot 4 is closest to the camera). Plots 1 and 3 (100% PPFD) have no shadecloth covering them.

Nominal daytime and nighttime air temperatures were a constant 17.5 ^{o}C and 12.5 ^{o}C respectively. Air temperatures were measured with one Hobo sensor (Onset Computer Corp., Bourne, Massachusets) located in each plot. These measurements revealed consistent differences in temperature between each pair of plots within a specific light treatment (Table 4.1). Differences in temperature may have been caused by the shadecloth frames used to impose the PPFD treatments, as these interrupted free air circulation within the growth chamber, causing local variations in ambient air temperature.

Table 4.1. Mean air temperatures (day and night) within plots.
Standard deviations (SD) are shown in brackets.

PPFD	Plot	Air Temperature (ºC)			
		Day		Night	
100%	1	16.3	(0.4)	10.8	(0.4)
100%	3	17.3	(0.8)	11.7	(0.8)
50%	4	17.6	(0.4)	11.2	(0.5)
50%	6	15.8	(1.0)	11.8	(0.8)
25%	2	19.4	(0.7)	12.1	(0.6)
25%	5	15.6	(0.3)	10.2	(0.4)

Relative humidity (*RH*) and CO_2 concentration within the chamber were not controlled but were monitored. *RH* was measured with two Hobo sensors (Onset Computer Corp., Bourne, Massachusets) located in Plot 1 (100% PPFD) and Plot 6 (50% PPFD). Mean daytime *RH* measured in Plot 1 and Plot 6 were 57% (SD 4.7%) and 59% (SD 7.3%) respectively. This is equivalent to a vapour pressure deficit (*VPD*) at 17.5 ºC of 0.8 kPa, a value greater than the threshold *VPD* of 0.5 kPa above which canopy conductance begins to decline in young radiata pine (Sheriff & Mattay 1995; Watt *et al.* 2003b). This suggests that the vapour pressure deficit modifier (f_D) was probably less than 1 during much of the experiment.

As far as possible, ambient CO_2 levels were measured continuously, using a Bruel and Kjaer multi-gas monitor 1302 (Bruel and Kjaer, Naerum, DK-2850, Denmark). However, this device was often unavailable so measurements of CO_2 were intermittent. From 9 March 2005 a Vaisala CO_2 probe (Vaisala Instruments, Helsinki, Finland) became fully available, and this was interfaced with a CR-10 data logger (Campbell Scientific Inc., Logan, Utah) to give continuous measurements of ambient CO_2 in the growth cabinet. CO_2 concentrations measured by the Vaisala probe averaged 401 μmol mol^{-1}. Most readings (93%) were in the range 350-450 μmol mol^{-1}, the remainder were in the range 450-550 μmol mol^{-1}. The readings in the lower range were frequently higher than the average atmospheric concentration (380 μmol mol^{-1}), possibly due to the growth chamber being located in a building. The readings in the higher range mostly occurred when people were working in the growth chamber for extended periods.

Air velocity in the chamber was measured on 17 December 2004. Air speed was measured above the growing tip of every seedling in the experiment (n=120). Air velocities were distributed in an inverse-J shaped distribution, with zero velocity (0 m s^{-1}) comprising 74% of all readings, and 0.3 m s^{-1}comprising a further 12.5%. The rest of the readings were between 0.4 to 1.0 m s^{-1}. Measured air velocities in the growth cabinet were highly variable and changeable, possibly due to interference of airflow by the shade frames.

Each seedling received 25 ml of a complete nutrient solution once a week (3 g Peters Excel CalMag high N (20N 2.2P 6.6K 5.8Ca 1.2Mg + trace elements) per litre of reverse osmosis water). ASAE (2003) recommend detailed recording of water quantities added to each pot or container, but this was not done because all seedlings were regularly watered to container capacity (as defined by Fonteno (1989)) every second day, to avoid any effect of moisture stress on growth. Visual inspections confirmed that even under100% light, pot media remained moist between applications of water. Similarly, the seedlings displayed no symptoms of nutrient limitation, and all had healthy foliage with needles of normal colour and length.

4.2.2 Measurements

The 120 seedlings in the experiment were divided into a main growth population and a calibration population. The main growth population comprised 10 randomly chosen seedlings per plot (n = 60) which were measured for *D*, *H* and *A* weekly from 7 March 2005 to 5 April 2005 (a period of 29 d). At the end of this period, all seedlings (n=60)) were destructively measured for biomass.

Of the remaining seedlings (n=60), a calibration population of eight seedlings per plot (n =48) was randomly selected for destructive measurement for biomass. Two seedlings per plot were excluded from this measurement because of mortality in some plots, which meant that only eight seedlings in those plots were available for measurement. For the

calibration population, measurements of silhouette area (*A*) and incident PPFD were also used to develop equations with which to calculate PAR intercepted by seedlings, using method 3 (Section 4.1.2).

Biomass

For the calibration population, two seedlings from each PPFD treatment were randomly selected for destructive measurement at intervals of ~10 d from 17 January 2005 until the conclusion of the experiment (5 April 2005). This resulted in measurement of 48 seedlings.

At the end of the experiment, as well as the final destructive measurement of two seedlings from each PPFD treatment in the calibration population, all seedlings in the main growth population (10 seedlings in each PPFD treatment (n=60)) were also destructively measured.

Seedling silhouette area (*A*), ground level diameter (*D*) and height to growing tip (*H*) of each seedling were measured before destructive measurement for biomass.
Seedling silhouette area (*A*) was measured by taking one digital photograph of the sample seedling. Photographs were taken using a Canon Powershot A300 digital camera, mounted on a custom-made easel. The metal arm on the photographic easel was adjusted to the required elevation angle (15 degrees above horizontal), and the seedling was placed on a platform directly in line with the camera's direction of view. The camera elevation of 15 degrees was chosen in order to capture differences in both height and diameter of the seedlings. A white cardboard sheet folded at right angles was fitted around the seedling to ensure maximum definition of the seedling against its background. A scale distance of 12 cm was marked on the white card adjacent to the seedling to provide a reference distance for digitally measuring the silhouette area of the seedling.

Photographs were digitally analysed using a beta version of programme QUANT (Vale *et al.* 2003). Each image was converted to a black silhouette outline figure by a thresholding process (Norgren *et al.* 1995). This process was subjective; although the "threshold"

could be specified numerically, no single threshold value gave consistent or realistic values for all seedlings on all measurement occasions. However, consistent results were obtained using threshold values that were set by visually checking silhouette outlines against the original photograph of the seedling.

By scanning the scale markers (of known distance apart (12cm)) into QUANT, the software then calculated the silhouette area of the seedling in the photograph in cm^2. For biomass measurements each seedling was dissected into three components: 1) the whole root system (cut off at "ground level"); 2) foliage; 3) the stem. Foliage included non-woody lateral shoots (there were no woody lateral shoots in these young seedlings). Roots, foliage and stem were fresh-weighed for each individual seedling. Samples were then aggregated by each component, then oven-dried at 65°C until repeat weighing at daily intervals gave identical results. This usually took 3-4 days.

The average ratio of total oven dry weight to total fresh weight for each biomass component (foliage, roots, stem) was then used to correct the individual seedling component fresh weights back to an oven dry weight (W). The calculated oven dry weights of foliage and stem were added to give a total above-ground biomass for each seedling (W_a). Adding W_a to root oven dry weight (W_r) gave the total W for each seedling. Stem biomass was a minor component of W_a (~ 15%) and was therefore not treated as a separate variable in the analysis.

PPFD and PAR Interception

PPFD in the chamber was measured continuously by a Li-Cor 190A sensor (Li-Cor Inc, Lincoln, Nebraska, USA)/Campbell CR 10 datalogger placed on a table between Plots 1 and Plot 6. Data from this sensor indicated only minor fluctuation in PPFD from the growth cabinet lights during the experiment (Mean daylight PPFD = 560 μmol m^{-2} s^{-1}, SD 16.8 μmol m^{-2} s^{-1}). Therefore to determine spatial variation in downwelling PPFD, only one measurement above the growing tip of each seedling was made on 18 February 2005, with this measurement assumed to be representative of PPFD levels during the

experiment. Measurements were made using Li-Cor 190A quantum sensor connected to a Li-Cor Li-188B Integrating quantum meter (Li-Cor Inc, Lincoln, Nebraska, USA) Spectral photon flux within the chamber was not measured. Instead, published data on the spectral distribution and energy equivalence for measured PPFD were used. This point will be covered in more detail later in this section.

For seedlings in the calibration population, incident PPFD (μmol m^{-2} s^{-1}) was also measured at elevation angles of 15, 45 and 75 degrees. These three measurements were repeated for four azimuth angles (0°, 90°, 180°, 270°) around the seedling.
These measurements of incident PPFD at varying zenith and azimuth angles showed that photon fluxes at elevation angles of 15, 45 and 75 degrees could be reliably predicted from a single measurement of vertically down-welling PPFD ($Q_{\phi = 90}$) above the seedling growing tip (Section 4.3.2). Therefore only vertically incident PPFD was measured for the main growth population, with PPFD at other angles of incidence estimated from regression equations of the form:

$$Q_{\phi} = a_{\phi} + b_{\phi} Q_{\phi = 90} \qquad (4.11)$$

where Q_{ϕ} = incident PPFD at elevation angle ϕ, $Q_{\phi = 90}$ = vertically down-welling PPFD ϕ = elevation angle of the direction in which the quantum sensor was aimed, a_{ϕ} and b_{ϕ} are coefficients which vary in value for each elevation angle ϕ.

To calculate intercepted downwelling PAR using method 3 described in Section 4.1.3, the incident PPFD (Q_{ϕ}) calculated using Equation 4.11 can be converted into an equivalent radiance (N) of a hemisphere above the seedling (Figure 4.2). Monteith & Unsworth (1990) state that for a flat area at the centre of an equatorial plane beneath a hemisphere with a uniform radiance N:

$$Q = \pi \int_{\beta=0}^{\frac{\pi}{2}} N \sin 2\beta d\beta \qquad (4.12)$$

where Q is the incident irradiance (W m^{-2}) on the flat area at the centre of the equatorial plane and N, β and $d\beta$ are defined in Equations 4.4, 4.5 and 4.6 (section 4.1.2). Integrating the right hand side of Equation 4.12 gives the value πN, so that Equation 4.12 simplifies to $Q = \pi N$, or $N = Q/\pi$. However, in this experiment Q was measured with a Li-Cor 190 sensor with a field of view of 160 degrees or 2.793 radians (Li-Cor Inc., 1991) rather than 180 degrees (π radians). Therefore, substituting 2.793/2 (=1.397) radians for $\pi/2$ in Equation 4.12, the PPFD measured by a Li-Cor 190 sensor (Q) beneath a uniform radiant surface of radiance N is:

$$Q = \int_{\beta=0}^{1.397} N \sin 2\beta d\beta \qquad (4.13)$$

which implies that $N = Q/3.047$ when Q is measured by a Li-Cor 190 sensor with a field of view of 160 degrees (2.793 radians).

Note that Monteith & Unsworth (1990) derived Equation 4.12 to calculate radiance in W m^{-2} sr^{-1} from irradiance in W m^{-2}. Q (W m^{-2}) must therefore be converted from measurements of incident PPFD in μmol m^{-2} s^{-1}. Although it is not strictly correct to do so (because the energy of the PAR depends on its spectral composition (Landsberg & Gower 1997, p64), conversion factors which reflect the spectral composition of PAR are used for this purpose. Light sources in this experiment were 20 × 400 W high pressure sodium horizontal bulbs and 20 × 400 W metal halide horizontal bulbs, evenly distributed within two separate barriered lofts which spanned the long axis of the chamber. Sager & McFarlane (1997, p3) state that the conversion factors (μmol s^{-1} to W) for high pressure sodium and metal halide lights are 0.201 and 0.218 respectively. Therefore a conversion factor of 0.21 was used to convert PPFD (μmol m^{-2} s^{-1}) measured in this experiment to Q (W m^{-2}).

Calculating PAR interception

For the calibration population, seedling silhouette area (A) was measured by taking digital photographs of the sample seedling, from the same elevation and azimuth angles from which incident PPFD was measured (φ = 15, 45 and 75 degrees elevation, θ = 0, 90, 180 and 270 degrees azimuth) . Photographs were taken using the same method used to measure A for biomass estimation. For each sampled seedling, 12 photographs were taken (three zenith angles × four azimuth directions).

Measurements of the calibration seedlings showed that the seedling silhouette area A calculated from one photograph taken from one azimuth direction (0°) at elevation angle φ = 15 degrees, was a reliable predictor of silhouette areas taken from other elevation and azimuth angles. Therefore weekly from 7 March to 5 April, each seedling in the main growth data population was digitally photographed once only from angle of φ = 15 degrees, and its silhouette area was measured using QANT. This single measurement of A taken from elevation angle φ = 15 degrees was used to predict A as viewed from φ = 45 and 75 degrees using Equation 4.17 (Section 4.3.2). Predicted radiance N and predicted values for A for elevation angles φ =15, 45 and 75 degrees were used to calculate intercepted PAR flux (in Watts) using Equation 4.7.

4.3 Results

This section follows the structure implied in the introduction to this chapter i.e.:
1) measurements of seedling NPP; 2) measurements of intercepted PAR; and
3) testing that their relationship is a constant one under the growth conditions of the experiment i.e. RUE (= NPP/ $\varphi_{p.i}$) does not vary between the three PPFD treatments. Measurement methods were also tested for accuracy and validity in this experiment, and the results of these tests are presented under the relevant headings (seedling NPP, intercepted PAR and seedling RUE).

As mentioned in Section 4.2.1 (Measurements), some measurements relate to the calibration seedlings, some to the seedlings in the main growth experiment, and some measurements were made of both. Results presented in this section will be identified in terms of which group of seedlings they relate to.

4.3.1 Seedling biomass prediction

Because seedlings in the calibration population were destructively sampled for biomass over an 11 week period of growth, as well as at three different PPFD levels, the data covered a wide range of seedling sizes. The data for the main growth population were more limited in their range since all seedlings were harvested at the same time at the end of the experiment (Table 4.2).

Table 4.2. Range of seedling sizes and total biomass for the calibration data set and the validation data set.

	Calibration data (n=48)		Validation data (n=60)	
Variable	Minimum	Maximum	Minimum	Maximum
D (mm)	1.3	4.7	2.0	4.8
H (mm)	53	185	85	210
A (cm^2)	5.3	70.4	16.2	89.6
W (g)	0.14	4.28	0.43	5.51

Calibration of seedling biomass prediction equations

Calibration of seedling biomass prediction equations was carried out using the calibration data set (n=48). For these seedlings, both total and above ground seedling biomass were highly correlated with all three measurement variables tested (silhouette area (A), D^2H and D^2). This is shown by Figures 4.4 (a), (b) and (c). The linear nature of the relationships between total W and the measurement variables suggests that they can be specified by Equation 4.1 i.e. $W = a + bX$.

However, when total W was plotted against A (Figure 4.4(a)), there was an apparent difference between the three PPFD treatments in the slope of the relationship of total W to A. In other words, for a given silhouette area A, seedlings grown in 100% PPFD were heavier than seedlings grown in 50% or 25% PPFD. This difference in slope between PPFD treatments was less pronounced when total W was plotted against D^2H (Figure 4.4(b)) or D^2 (Figure 4.4(c)).

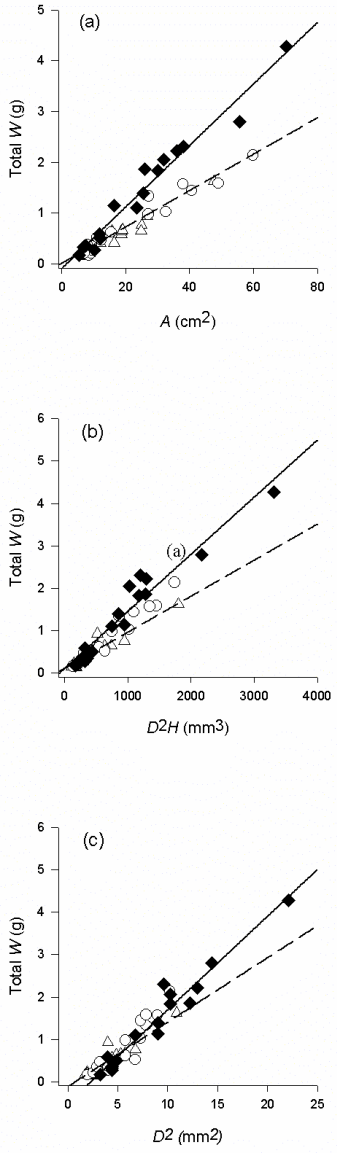

Figure 4.4. Total seedling W vs measurement variables.

♦=100% PPFD, ○ =50% PPFD, △=25% PPFD. n=48.
(a) measurement variable is *A*, ———— = trendline fitted to the data for PPFD = 100%, – – – – = trendline fitted to the data for PPFD = 25% and 50%;
(b) measurement variable is D^2H, ———— = trendline fitted to the data for PPFD = 100% and 50%, – – – – – = trendline fitted to the data for PPFD = 25%;
(c) measurement variable is D^2, ———— = trendline fitted to the data for PPFD = 100% and 50%, – – – – – = trendline fitted to the data for PPFD = 25%.

To examine the influence of PPFD treatments on the slope of the relationships between measurement variables and *W*, Equation 4.14 was specified as an analysis of covariance (Ancova) model where either *A, D*^{2}*H* or *D*^{2} was the continuous independent variable (covariate) and PPFD level was the factor variable, as follows :

$$\mu_{ij} = (\mu + \alpha_i) + (\beta + \gamma_i)x_{ij} \qquad (4.14)$$

where μ_{ij} is the expected value of *W* for an individual seedling; x_{ij} is the value of the independent variable (covariate) for an individual seedling; μ is the intercept and β is the slope of the relationship between *W* and the independent variable when PPFD =100%; and α_i and γ_i are the differences in intercept and slope, respectively, between 100% PPFD and either 50% PPFD (*i*=2) or 25% PPFD (*i*=3).

Equation 4.14 is plotted in Figures 4.4(a)-(c) as follows: the solid line is fitted to the data for 100% PPFD, whose parameters are specified by Equation 4.14 as $\mu_{ij} = (\mu) + (\beta)x_{ij}$. The broken line is specified by $\mu_{ij} = (\mu + \alpha_i) + (\beta + \gamma_i)x_{ij}$, i.e. where the intercepts and/or slopes for 50% and/or 25% PPFD treatments are significantly different from those for the 100% PPFD treatment. For Figure 4.4(a), the slopes but not the intercepts for the 50% and 25% PPFD treatments are both significantly different from the slope for the 100% PPFD treatment. For Figure 4.4(b), only the slope for the 25% PPFD treatment is significantly different from the slope for the 100% PPFD treatment. For Figure 4.4(c), both the intercept and slope for the 25% treatment are significantly different from the intercept and slope for the 100% PPFD treatment.

Equation 4.14 describes a "full" model with intercept and slope parameters for all three PPFD levels. A "reduced" model with one intercept and one slope parameter for all PPFD levels is specified by Equation 4.15:

$$\mu_{ij} = \mu + \beta x_{ij} . \qquad (4.15)$$

The "reduced" model assumes that PPFD levels do not influence the intercept or the slope of the relationship between W and the independent variable.

Because seedling measurements from the same plot may have been auto-correlated, Equations 4.14 and 4.15 were fitted to the experimental data using procedure "lme" in the R statistical package (R Development Core Team 2007). This procedure corrected estimates of parameters and their statistical significance for auto-correlation between seedlings from the same plot. Parameters were tested for statistical significance using the probability that they were not different from zero, using a two-tailed t- test. If this probability was less than 5%, the parameters were considered statistically significant. If the parameters α_i and γ_i (Equation 4.14) were statistically significant, the conclusion was that seedlings from different PPFD levels differed in their allometric relationships between W and the independent variable.

Table 4.3 shows that for the full model using A as the independent variable, PPFD levels did not have a significant effect on the intercept parameter, and the intercept parameter was not significantly different from 0. In contrast, the interaction between A and PPFD level was highly significant, with the slope of total W vs A for 50% and 25% PPFD differing by –0.025 and –0.026 respectively from the slope for 100% PPFD. These results are reflected in Figure 4.4(a), where the slope of the relationship between total W and A appears to be different for seedlings exposed to 100% PPFD, compared with those exposed to 50 and 25% PPFD.

Table 4.3. Parameter estimates for "full" Ancova models of total $W \sim A$, D^2H or D^2, with parameters for PPFD levels.
Parameters are defined in Equation 4.14. Models are depicted graphically in Figure 4.4.

Parameter		Symbol	Estimate	*t*-ratio	*p*
***W* ~ *A**PPFD**					
Constant		μ	–0.094	–1.35	0.184
PPFD	50%	α_2	0.103	1.05	0.369
	25%	α_3	0.050	0.49	0.659
A		β	0.061	27.1	<0.001
A * PPFD	50%	γ_2	–0.025	–7.49	<0.001
	25%	γ_3	–0.026	–5.95	<0.001
***W* ~ D^2H*PPFD**					
Constant		μ	0.111	1.34	0.187
PPFD	50%	α_2	–0.126	–1.03	0.379
	25%	α_3	0.004	0.04	0.972
D^2H		β	0.001	20.6	<0.001
D^2H * PPFD	50%	γ_2	–0.0001	–1.19	0.241
	25%	γ_3	–0.0005	–3.49	0.001
***W* ~ D^2 *PPFD**					
Constant		μ	–0.51	–4.41	<0.001
PPFD	50%	α_2	0.07	0.40	0.718
	25%	α_3	0.40	2.41	0.095
D^2		β	0.22	19.5	<0.001
D^2 * PPFD	50%	γ_2	0.005	0.23	0.821
	25%	γ_3	–0.07	–2.56	0.014

In contrast to the results using *A* as the independent variable, full models using D^2H or D^2 as independent variables showed the slope of the relationship between total *W* and D^2H or D^2 was no different for seedlings exposed to 100% PPFD, compared with those exposed to 50% PPFD ($p = 0.24$ and 0.82 for D^2H and D^2 respectively). However, the slope of the relationship for seedlings exposed to 100% PPFD was significantly different from the slope for seedlings exposed to 25% PPFD ($p \leq 0.001$ and $p = 0.014$ for D^2H and D^2 respectively).

Examination of the residual values for the full Ancova models (Equation 4.14) showed no evidence of bias, and variance appeared consistent across the range of predicted values. In contrast, reduced models (Equation 4.15) with A or D^2H as the independent variable showed a "fanning" residual pattern i.e. variances increased with larger predicted values. This "fanning" pattern seems to be due to the effect of PPFD levels and therefore can be eliminated by specifying a full model with different slope parameters for each PPFD level. However, residual plots for a reduced model using D^2 as independent variable appeared reasonably homogeneous across the range of values for D^2. This result is consistent with Figure 4.4(c), where the spread of data did not appear to change with increasing D^2.

Validation of Seedling Biomass Equations

Full and reduced models for above-ground and total W, derived from the calibration data set, were tested using the data for the main growth population. These data comprised final measurements of D, H, A and W for 20 seedlings in each of the three PPFD treatments (100%, 50% and 25% PPFD). The fit of the validation data to the full and reduced models was tested using the relative prediction error (RPE) where the W value that was predicted by the model was compared with the observed value of W as follows:

$$\text{RPE (\%)} = \frac{(\text{PredictedValue} - \text{Observed Value})}{\text{Observed Value}} \times \frac{100}{1} \qquad (4.16)$$

(Ter-Mikaelian & Parker 2000).

Table 4.4. Relative prediction error (RPE) means and standard deviations (SD) from validation data from the main growth population.
n=60

Model	Above-ground W_a		Total W	
	Mean RPE (%)	SD (%)	Mean RPE (%)	SD(%)
Full models				
$W \sim A$ * PPFD	10.5	13.8	6.8	16.2
$W \sim D^2H$ * PPFD	12.5	23.2	9.5	26.8
$W \sim D^2$ * PPFD	2.9	19.9	0.2	24.9
Reduced Models				
$W \sim A$	20.2	27.4	23.4	39.8
$W \sim D^2H$	17.7	26.9	21.9	37.3
$W \sim D^2$	5.1	20	8.7	30.8

Table 4.4 summarises the means and standard deviations of the relative prediction errors for the models when using the main growth population data as inputs. These results show the superiority of the full models using either A * PPFD (which was the most precise model, using the criterion of the standard deviation of the RPE) or D^2 * PPFD (which was the most accurate model, using the criterion of the RPE) to predict seedling biomass for the validation data set. For models using either D^2 or A, the reduced models (one parameter for slope and one parameter for intercept across all PPFD levels) were less accurate and precise (larger means and standard deviations for the RPE's) than the full models. The full model using D^2H *PPFD was less precise and accurate than full models using D^2*PPFD or A*PPFD, and the reduced model using D^2H was less precise and accurate than the reduced model using D^2.

These results are corroborated by plotting predicted W versus actual W for the main growth population data (Figure 4.5). The plots show that the predictions of full models using A*PPFD and D^2H*PPFD appeared to be more precise and less biased than those of the equivalent reduced models. The full and reduced models using D^2*PPFD and D^2 appeared similar in terms of precision and bias, but neither appeared as precise or unbiased as the full model using A*PPFD.

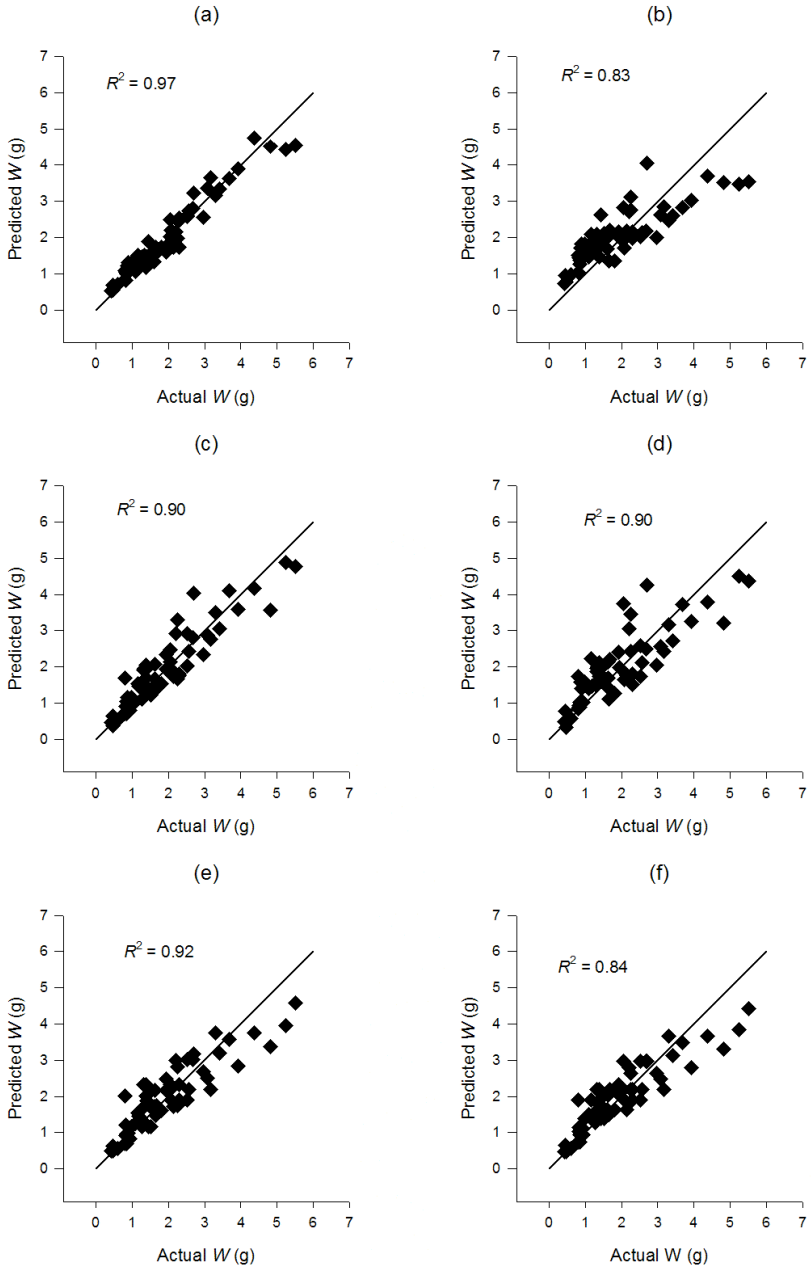

Figure 4.5. Predicted total seedling weights (W) vs actual W for the validation data set.

Predicted *W* was calculated using (a) *A*, full model; (b) *A*, reduced model; (c) D^2H, full model; (d) D^2H, reduced model; (e) D^2, full model; (f) D^2, reduced model. The solid line is $y = x$. n = 60.

Causes of variation in seedling biomass equations between PPFD levels

To examine the causes of differences between PPFD treatments in the relationship of total *W* to seedling silhouette area (*A*), analysis of covariance (Ancova) models were specified for:

1. The allometric allocation of growth to shoot (stem plus foliage DM) and root DM, using the model specified by Equation 4.14 i.e. $\mu_{ij} = (\mu + \alpha_i) + (\beta + \gamma_i)x_{ij}$, where μ_{ij} is the expected value of shoot DM (W_a) for an individual seedling; x_{ij} is the value of the independent variable (total DM, *W*) for an individual seedling; μ is the intercept and β is the slope of the relationship between *W* and the independent variable when PPFD =100%; and α_i and γ_i are the differences in intercept and slope, respectively, between 100% PPFD and either 50% PPFD (*i*=2) or 25% PPFD (*i*=3). Differences in shoot:root ratio for seedlings growing under different PPFD levels will be confirmed by statistically significant differences between α_i and γ_i for 100%, 50% and 25% PPFD.

2. The relationship of shoot DM (W_a) to seedling silhouette area, using Equation 4.14, where μ_{ij} is the expected value of shoot DM (W_a) for an individual seedling; x_{ij} is the value of the independent variable (seedling silhouette area, *A*) for an individual seedling; μ is the intercept and β is the slope of the relationship between W_a and the independent variable when PPFD =100%; and α_i and γ_i are the differences in intercept and slope, respectively, between 100% PPFD and either 50% PPFD (*i*=2) or 25% PPFD (*i*=3).
   The relationship of W_a to *A* depends on specific leaf area (*SLA*, = total seedling leaf area/total foliage dry mass (cm/g)) and spatial density of foliage (total seedling leaf area/total crown volume (cm^2/cm^3). A lower SLA and a higher foliage spatial density will result in a higher value of W_a for a given value of *A*.

The results of the Ancova models showed that 1) mean shoot biomass was a significantly higher fraction of total biomass for the PPFD =25% (0.714, p=0.014) and 50% (0.664, p= 0.031) treatments, compared with the PPFD = 100% treatment (0.595). Conversely, root biomass was therefore a smaller fraction of total biomass for both the 25% and 50% PPFD treatments, compared with the 100% PPFD treatment. This confirms that the shhot:root ratio differed between PPFD treatments. 2) Above-ground (shoot) biomass as a function of seedling silhouette area, was also significantly higher for the PPFD = 100% treatment (0.037) compared with the 50% PPFD (0.025, p<0.001) and 25% PPFD (0.024, p<0.001) treatments. The relative contributions of *SLA* and foliage spatial density to these differences could not be determined, as neither were measured in this study. However, it was clear that the between PPFD-treatment differences in the relationship of total W and seedling silhouette area (A) were associated with differences in both 1) allocation of growth to shoots and roots; and 2) the density of above-ground (shoot) biomass, (whether this arose from differences in spatial density of the foliage, *SLA* or both).

4.3.2 Estimation of PAR interception by seedlings

Variation in incident PPFD between seedlings

The shade structures caused variation in the incident PPFD within each of the six plots. Particularly for the seedlings at the edge of the plots receiving 25% PPFD, diffuse PAR incident at low elevations (which was not screened out by the shadecloth) meant that these edge seedlings experienced higher PPFD than intended.

Table 4.5 summarises variations in vertically incident PPFD for each of the three experimental light treatments, measured on 18 February 2005. The PPFD readings were made directly above the growing tip of all seedlings in the main growth data set (n=60), with the sensor pointing in a vertical direction.

Table 4.5. PPFD measurements of vertically downwelling PAR, above seedlings in the main growth population.

Plot	PPFD level	Nominal PPFD (μmol $m^{-2}s^{-1}$)	Actual PPFD (μmol m^{-2} s^{-1})		
			Mean	Minimum	Maximum
1	100%	500	493	431	530
2	25%	125	134	106	205
3	100%	500	503	460	533
4	50%	250	215	189	236
5	25%	125	96	80	132
6	50%	250	254	209	304

The maximum reading in the 25% PPFD treatment (205 μmol m^{-2} s^{-1}) was markedly higher than other PPFD values in this treatment, the next highest PPFD being 159 μmol m^{-2} s^{-1}. Incident PPFD for the 50% and particularly the 100% PPFD treatment was less variable.

Inspection of data from a Li-Cor 190A quantum sensor placed in the growth cabinet and whose output was continuously logged using a Campbell CR-10 data logger suggested that: 1) the PPFD emitted by the growth cabinet lights was quite stable, and therefore 2) the instantaneous PPFD values shown in Table 4.5 were a realistic measure of incident PPFD over the period of the experiment.

Variation in incident PPFD with angle of incidence

Measurements of PPFD (Q) incident to the calibration population seedlings at elevation angles (ϕ) of 15, 45 and 75 degrees, were highly correlated with a single vertical (ϕ = 90 degrees) measurement of PPFD made immediately above the growing tip of each seedling. Figure 4.6 shows consistent linear relationships between $Q_{\phi=90}$ and Q_{ϕ} at all three elevation angles. These linear relationships were maintained over the range of PPFD in the experiment.

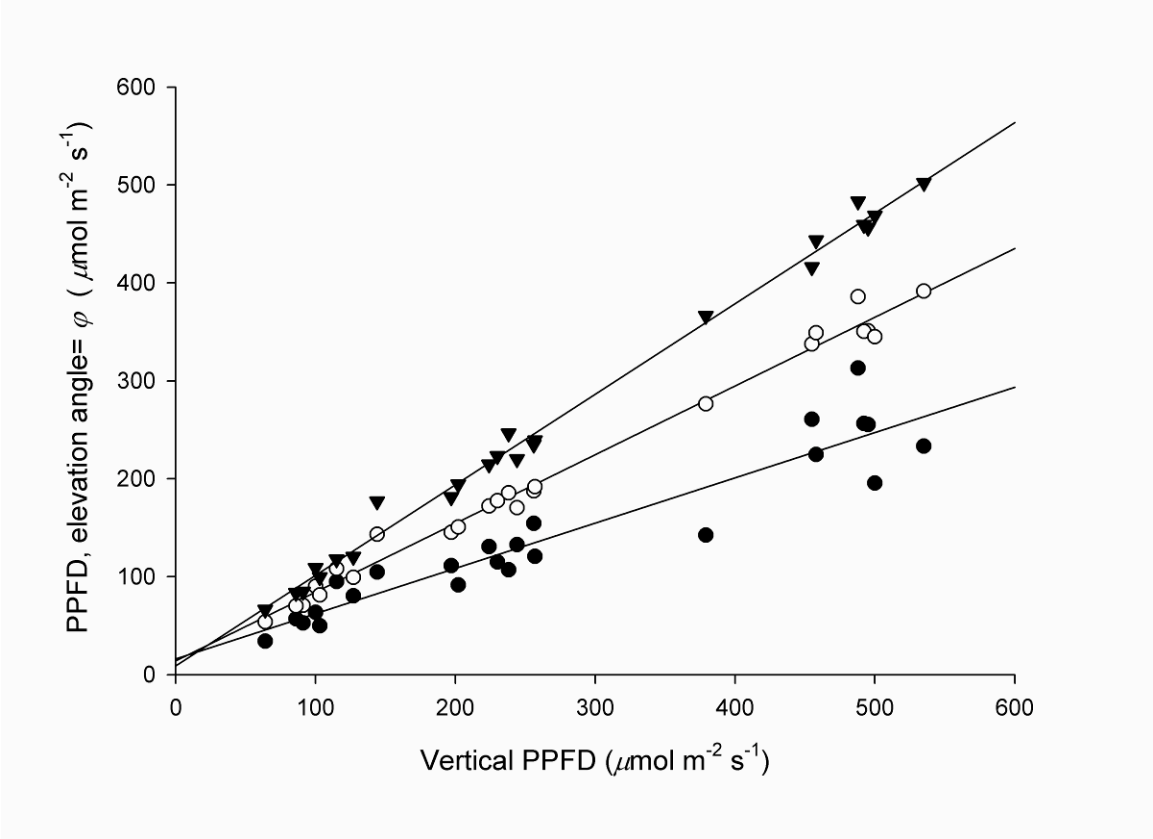

Figure 4.6. PPFD (measured at elevation angle of ϕ) vs PPFD measured in a vertical direction.

Data for elevation angles (φ) are plotted as ▼ = 75 degrees, ○ = 45 degrees, ● = 15 degrees. n = 60.

Because the slopes of the relationships in Figure 4.6 were markedly different between the three elevation angles, three linear regression models of the form $Q_\phi = a_\phi + b_\phi Q_{\phi=90}$ (Equation 4.11) were fitted separately with Q_ϕ as the dependent variable for ϕ = 15, 45 and 75 degrees. Model parameters are shown in Table 4.6.

Table 4.6. Regression parameters for the relationship between downwelling PPFD and PPFD incident at elevation angles 15, 45 and 75 degrees.
(Parameters are those defined in Equation 4.11).

Elevation angle ϕ	Intercept(a_ϕ)	Slope (b_ϕ)	R^2
15 degrees	16.1	0.462	0.891
45 degrees	14.0	0.702	0.989
75 degrees	8.9	0.925	0.994

Based on these results, the incident Q_ϕ at each elevation angle was estimated for the seedlings in the main growth experiment, using separate regression equations for each angle with $Q_{\phi=90}$ (measured in a vertically upwards direction above the seedling tip) as the independent variable.

Variation in projected seedling area with elevation angle.

If the radiance of a hemispheric surface surrounding a seedling can be measured at any specific solid angle ω, then the amount of PAR intercepted by the seedling can be worked out if the seedling's projected area (A) can be measured for the relevant elevation angle ϕ (refer Section 4.1.2 for a description of the theory underlying this method).

Measurements of the calibration population showed that the seedling silhouette area A calculated from one photograph taken from one azimuth direction at elevation angle ϕ = 15 degrees, was a reliable predictor of silhouette areas taken from other elevation and azimuth angles. Figures 4.7 (a) and (b) show the relationship between A measured from an angle ϕ= 15 degrees ($A_{\phi=15}$) versus A measured from 45 and 75 degrees ($A_{\phi=45}$ and $A_{\phi=75}$ respectively).

Although data from all three PPFD treatments show a good fit to a single regression line (R^2 = 0.975 and 0.958 for Figures 4.7 (a) and (b), respectively), the form and specific leaf area of radiata pine seedlings has already been shown to vary with light intensity (see Section 4.3.1). It might therefore be expected that the relationship between $A_{\phi=15}$ and $A_{\phi=45}$ or $A_{\phi=75}$ would vary between light treatments. To test this, a similar approach was taken to that used to analyse differences in allometric equations for biomass prediction (Section 4.3.1). Equation 4.17 was specified as two Ancova models (one for $A_{\phi=45}$ and one for $A_{\phi=75}$). For both models $A_{\phi=15}$ was the continuous independent variable (covariate) and PPFD level was the factor variable, as follows:

$$\mu_{ij} = (\mu + \alpha_i) + (\beta + \gamma_i)x_{ij} \qquad (4.17)$$

where μ_{ij} is the expected value of $A_{\phi=45}$ or $A_{\phi=75}$ for an individual seedling; x_{ij} is the value of the independent variable ($A_{\phi=15}$) for an individual seedling; μ is the intercept and β is the slope of the relationship between $A_{\phi=45}$ or $A_{\phi=75}$ and $A_{\phi=15}$ when PPFD =100%; and α_i and γ_i are the differences in intercept and slope, respectively, between 100% PPFD and either 50% PPFD (i=2) or 25% PPFD (i=3).

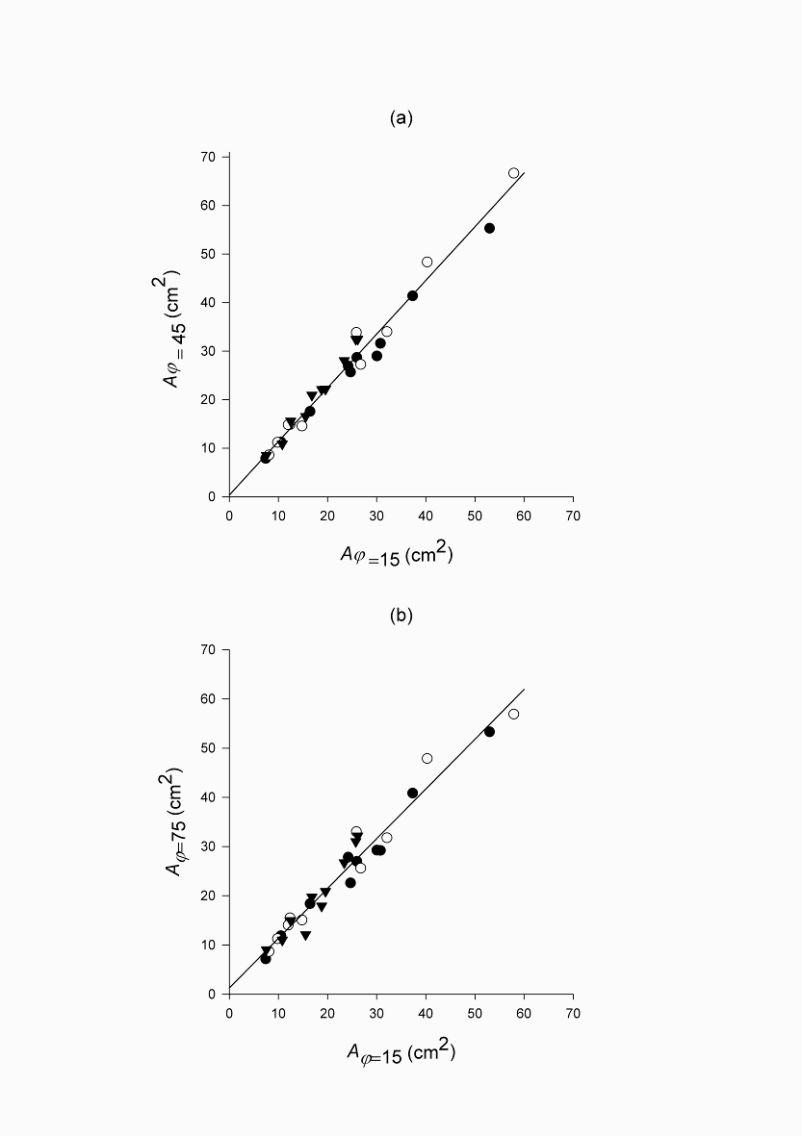

Figure 4.7. Seedling silhouette area (A) measured from (a) ϕ= 45; (b) ϕ= 75 degrees versus $A_{\phi=15}$.

▼ = 25% PPFD, ○ = 50% PPFD, ● = 100% PPFD.

Similarly to the estimation of allometric equations, a "reduced" model with one intercept and one slope parameter for all PPFD levels ($\mu_{ij} = \mu + \beta x_{ij}$, see Equation 4.15) can also be fitted to the data. The "reduced" model assumes that PPFD levels do not influence the intercept and slope of the relationship between $A_{\phi=45}$ or $A_{\phi=75}$ and the independent variable ($A_{\phi=15}$).

Equation 4.17 was fitted to the experimental data using procedure "lme" in the R statistical package (R Development Core Team 2007). This allowed individual seedling data rather than plot means to be used in the analysis. The linear model specified by Equation 4.17 seemed to fit the data well. However, the response of the two models (for ϕ =45 degrees or ϕ =75 degrees) to PPFD differed. For ϕ =75 degrees, the model parameters for the PPFD factor were not significant i.e. the relationship of projected area $A_{\phi=15}$ to $A_{\phi=75}$ was not affected by PPFD treatment. In contrast, for ϕ =45 degrees, the parameter values for the *PPFD* *$A_{\phi=15}$ interaction terms were both significantly different from zero (see Table 4.7). In other words, the slope of the relationship between $A_{\phi=15}$ and $A_{\phi=45}$ differed between PPFD treatments, with the slope being lowest for *PPFD* = 100% and highest for *PPFD* = 25%.

Table 4.7. Regression parameters for Equation 4.17 with t statistics and probabilities that the parameters are not significantly different from 0.

Parameter		Symbol	Estimate	*t*-ratio	*p*
ϕ =45 degrees					
Constant		μ	0.755	0.54	0.595
PPFD	50%	α_2	–1.469	–0.79	0.484
	25%	α_3	–2.778	–1.24	0.302
Slope		β	1.029	24.6	<0.001
$A_{\phi=15}$ * *PPFD*	50%	γ_2	0.144	2.67	0.014
	25%	γ_3	0.273	2.89	0.009
ϕ =75 degrees					
Constant		μ	1.45	0.67	0.509
PPFD	50%	α_2	0.02	0.01	0.995
	25%	α_3	–3.58	–1.06	0.368
Slope		β	0.97	16.1	<0.001
$A_{\phi=15}$ * *PPFD*	50%	γ_2	0.05	0.64	0.530
	25%	γ_3	0.26	1.88	0.074

The main effects of low PPFD (25%) on seedling morphology were reduced leaf area density and an increase in the height/diameter ratio. Note that:

1. Both these morphological effects were reflected in the relationship of $A_{\phi=15}$ to $A_{\phi=45}$ but not in the relationship of $A_{\phi=15}$ to $A_{\beta=75}$.

2. Although the interaction terms for $A_{\phi=15}$*$PPFD$ were significant in the Ancova model for $A_{\phi=45}$, the AIC (Akaike 1974)[2] values for the full and reduced Ancova models were not greatly different (137.6 and 141.8 respectively), suggesting that the reduced model is also "supportable" (*sensu* Burnham & Anderson (2001)).

For these two reasons, $A_{\phi=45}$ and $A_{\phi=75}$ for the main growth experiment population were predicted from measured $A_{\phi=15}$ using the reduced model ($A_{\phi=45}$ =0.275 + 1.111* $A_{\phi=15}$ and $A_{\phi=45}$ =1.269 + 1.012* $A_{\phi=15}$).

4.3.3 Intercepted PAR and seedling growth

This section presents results of seedling growth and intercepted PAR for the main growth population data set (n=60).

Intercepted PAR

The PAR intercepted by seedlings was calculated according to method 3 described in Section 4.1.3. This method requires as inputs: 1) A_ϕ, the silhouette area of the seedling when viewed from the elevation angle ϕ, and 2) N_ϕ, the radiance of the environment surrounding the seedling at elevation angle ϕ, averaged over the range of azimuth angles 0–2π.

[2] The AIC is a penalized log-likelihood criterion i.e. it calculates the likelihoods of alternative models fitted to the same data, but reduces the likelihood of each model in proportion to the number of parameters that it uses (Akaike, 1974; Burnham and Anderson, 2001). The lower (more negative) the AIC value, the greater the likelihood of the model.

For the main growth population, weekly measurements of seedling $A_{\phi=15}$ were used to calculate seedling projected areas for elevation angles ϕ = 45 and 75 degrees, using regression equations derived in Section 4.3.2. $A_{\phi=15}$ was measured weekly over the 29-day period 7 March to 5 April 2005. N_ϕ was calculated from a single measurement of vertically incident PPFD using Equations 4.11 and 4.13, (Section 4.2.1). $A_{\phi=15}$ and the calculated values for $A_{\phi=45}$ and $A_{\phi=75}$ were then multiplied by radiance at the relevant elevation angle (N_ϕ). The resulting interception values were then integrated using Equation 4.10 (Section 4.1.2).

The intercepted PAR flux (I) was in units of Watts (W). The energy of the intercepted PAR ($\varphi_{p,i}$) was calculated on a weekly basis by averaging the calculated I at the beginning and end of the week , and multiplying this by the number of seconds of illumination per week (7 d × 13 h d^{-1} × 3600 s h^{-1}). This gave the energy of the intercepted PAR in Joules (J). Note that the illumination time per day was approximated as 13 h i.e. 12 h d^{-1} of full illumination, plus 1 h d^{-1} of ramp-up and 1 h d^{-1} of ramp-down at the beginning and end of the illuminated period respectively. Table 4.8 summarises the plot mean, maximum and minimum energy of the intercepted PAR for Plots 1 to 6, estimated using this method.

Table 4.8. Total intercepted PAR energy estimates for the 29-day period, 7 March to 5 April 2005.

Mean and standard devotion (SD) are shown.

Plot	PPFD Treatment	Total intercepted PAR (MJ)	
		Mean	SD
1	100%	0.564	0.233
3	100%	0.880	0.197
4	50%	0.325	0.118
6	50%	0.287	0.082
2	25%	0.179	0.077
5	25%	0.103	0.036

Differences in intercepted PAR between plots were marked, even for plots with the same nominal light intensity. Possible reasons for this are discussed in the next section.

Seedling growth

For seedlings in the main growth population, initial seedling biomass at the beginning of the period for which intercepted PAR was calculated (7 March 2005) was determined from measurements of $A_{\phi=15}$, using regressions derived from destructive sampling of seedlings in the calibration data set over the duration of the experiment (Section 4.3.2). Final total biomass (*W*) of seedlings in the main growth population was measured destructively at the end of the experiment (5 April 2005). Seedling biomass increment (NPP) was calculated by subtracting the initial *W* from the final *W*. Table 4.9 summarises seedling biomass increment data over the period 7 March – 5 April 2005.

Table 4.9. Mean seedling *W* increments from 7 March to 5 April 2005, main growth data set.
Standard deviations (SD) are shown in brackets. n= 60.

PPFD Treatment	Plot	Final *W* (g)		*W* Increment (g)	
100%	1	2.57	(0.83)	1.35	(0.37)
100%	3	3.80	(1.06)	2.34	(0.82)
50%	4	1.68	(0.58)	0.86	(0.35)
50%	6	1.54	(0.50)	0.90	(0.39)
25%	2	1.34	(0.50)	0.65	(0.36)
25%	5	0.85	(0.39)	0.33	(0.23)

Table 4.9 shows that there was a positive seedling growth (*W* increment) response to PPFD, which is to be expected. However, there were also marked differences in growth within plots and between plots within light treatments. This was especially so for the 100% and 25% light levels, where the mean increment for one plot was nearly double that of the other plot.

All plants were well-watered and received a weekly application of a complete liquid fertiliser. Therefore differences between replicate plots are unlikely to arise from differences in water and nutrients available to the plants.

The most likely explanation for large differences in *W* increment between the two plots within each PPFD treatment was that there were marked differences in mean PPFD between the plots. Tables 4.4 and 4.8 show that the plots within each PPFD treatment

which had higher mean PPFD also had higher mean *W* increments. Differences in air temperature between plots may also have had an effect. However, although Table 4.1 shows that there were consistent differences in mean air temperature between plots, and comparison of data in Table 4.1 (air temperatures) and Table 4.9 (seedling *W* increments) suggests that seedlings in the warmer of each pair of plots with PPFD = 100 or 25% grew faster, there was no difference in increment between the warmer and colder plots with 50% PPFD. Temperature differences between plots may have interacted with PPFD differences to influence seedling *W* increment, with the warmer plots having higher mean PPFD levels for PPFD = 100 and 25%, but lower PPFD for the plots with 50% PPFD.

Within-plot differences in PPFD also occurred (Table 4.5), probably because seedlings at the edge of the plots intercepted diffuse PAR incident at low elevation angles (which was not screened out by the shadecloth) which meant that these edge seedlings experienced higher PPFD than seedlings in the centre of the plots.

These results show that it was not possible to achieve perfectly uniform PPFD and temperature treatments in this experiment, even in a controlled growth cabinet. Fortuitously, the randomized plot layout resulted in one plot from each PPFD treatment being located in the warmer and one plot in the cooler part of the controlled growth cabinet, so variations in temperature were not confounded with PPFD treatments.

Seedling growth versus PPFD

Figure 4.8(a) shows a great deal of scatter in the relationship between *W* increment plotted against mean vertically incident PPFD at the seedling growing tip. This suggests that incident PPFD alone cannot explain the difference in *W* increment between plots.

Obviously a higher PPFD will result in a larger cumulative intercepted PAR, but seedling size may also influence seedling growth in two ways:

1. The relative growth rate (RGR) concept embodies the idea that "a given amount of plant material is capable of producing a certain amount of new material" (van den Driessche and van den Driessche 1991). This concept implies that at least

some of the variation in NPP between seedlings is due to their initial seedling sizes, such that seedlings with larger initial *W* were the seedlings with higher NPP. To test this concept, RGR of the seedlings over the 29 d of the experiment was calculated using Equation 4.18 (van den Driessche and van den Driessche 1991):

$$\overline{R}_w = \frac{\ln W_2 - \ln W_1}{t_2 - t_1} \tag{4.18}$$

where $\overline{R}_w$ is the mean RGR over the time period $t_2 - t_1$, and W_1 and W_2 are plant DM weights at times t_1 and t_2 respectively. Figure 4.8(b) shows plot means for *RGR* versus PPFD for the growth measurement period (7 March to 5 April 2005). Although there is a relationship between *RGR* increment and PPFD, the two variables are not well-correlated. The RGR concept does not appear to fully explain differences in seedling NPP across the range of PPFD used in this experiment.

2. Seedling size also influences seedling growth through the above-ground seedling area (*A*), which is a measure of the area of foliage intercepting PAR—the other determinant of PAR intercepted by the seedling, along with ambient PPFD. The effect of seedling *A*, along with ambient PPFD, can be tested by relating seedling NPP (*W* increment during the growth measurement period) to PAR intercepted by the individual seedlings over the same period. The calculated values for intercepted PAR were reported in the previous section (Table 4.8 and accompanying text). Figure 4.8(c) shows seedling *W* increment versus cumulative intercepted PAR ($\Sigma\varphi_{p,i}$) for the growth measurement period (7 March to 5 April 2005). Although there is a consistent and reasonably linear relationship between *W* increment and cumulative intercepted PAR, closer inspection suggests that the slope of the relationship appears to differ between the PPFD treatments.

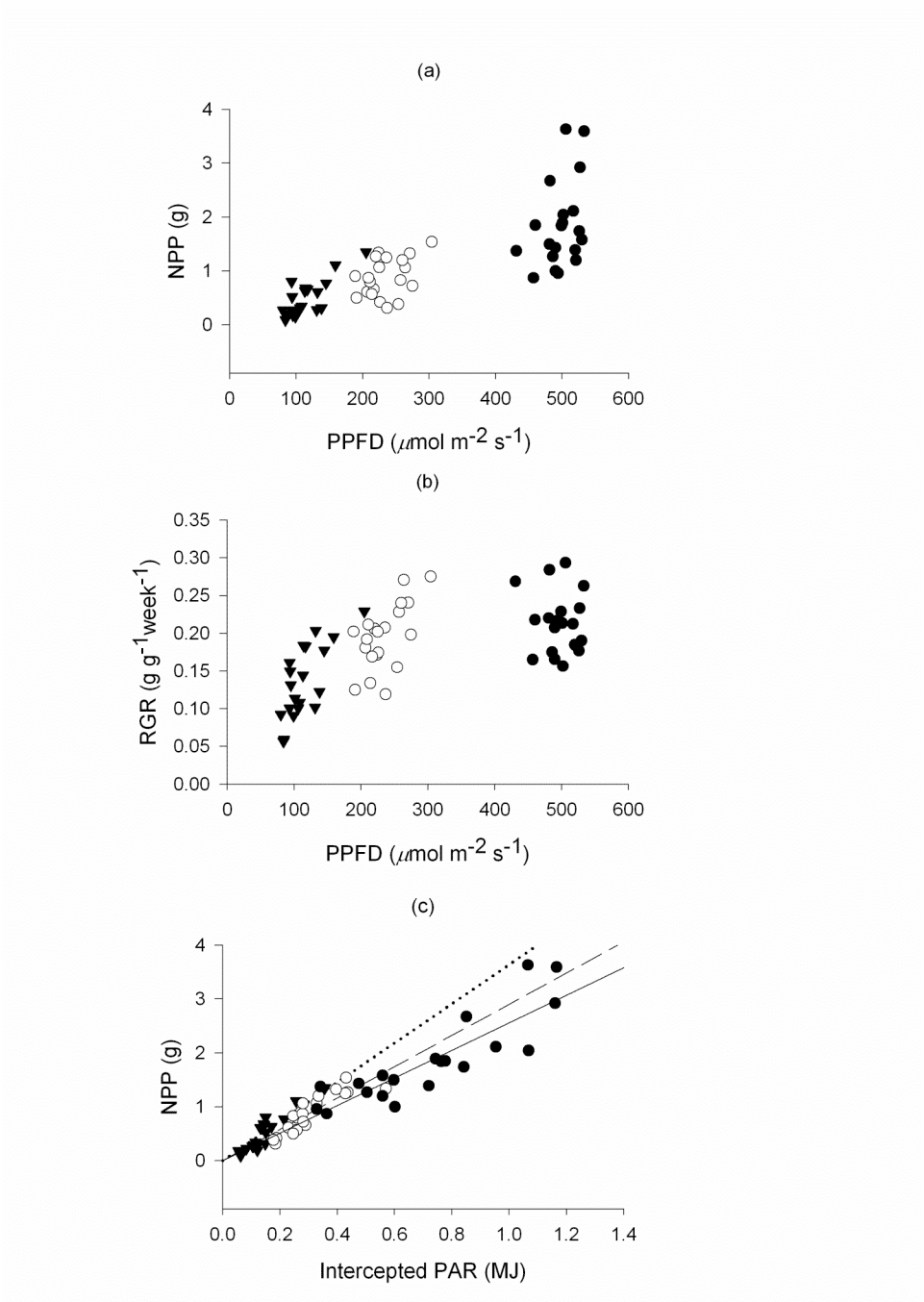

Figure 4.8. Seedling growth and PPFD.

(a) W increment (NPP) vs vertically-incident PPFD; (b) Relative growth rate (RGR) vs vertically-incident PPFD (c) W increment (NPP) vs cumulative intercepted PAR. □ = 25% PPFD, □ = 50% PPFD, □ = 100% PPFD. The dotted line in (c) is a trendline fitted to the 25% PPFD data, the dashed line is fitted to the 50% PPFD data, and the solid line is fitted to the 100% PPFD data. All trendlines are conditioned to pass through the origin.

Provided the intercept for the relationship between NPP and intercepted PAR ($\Sigma\varphi_{p.i}$) in Figure 4.8(c) is set to zero, the slope of the relationship is an estimator for the mean RUE for the main growth population (see Equation 2.2). If the slopes in Figure 4.8(c) are different between PPFD treatments, this suggests that RUE differs between the three PPFD treatments. Figure 4.9 shows the variation in individual seedling RUE's for the three PPFD treatments.

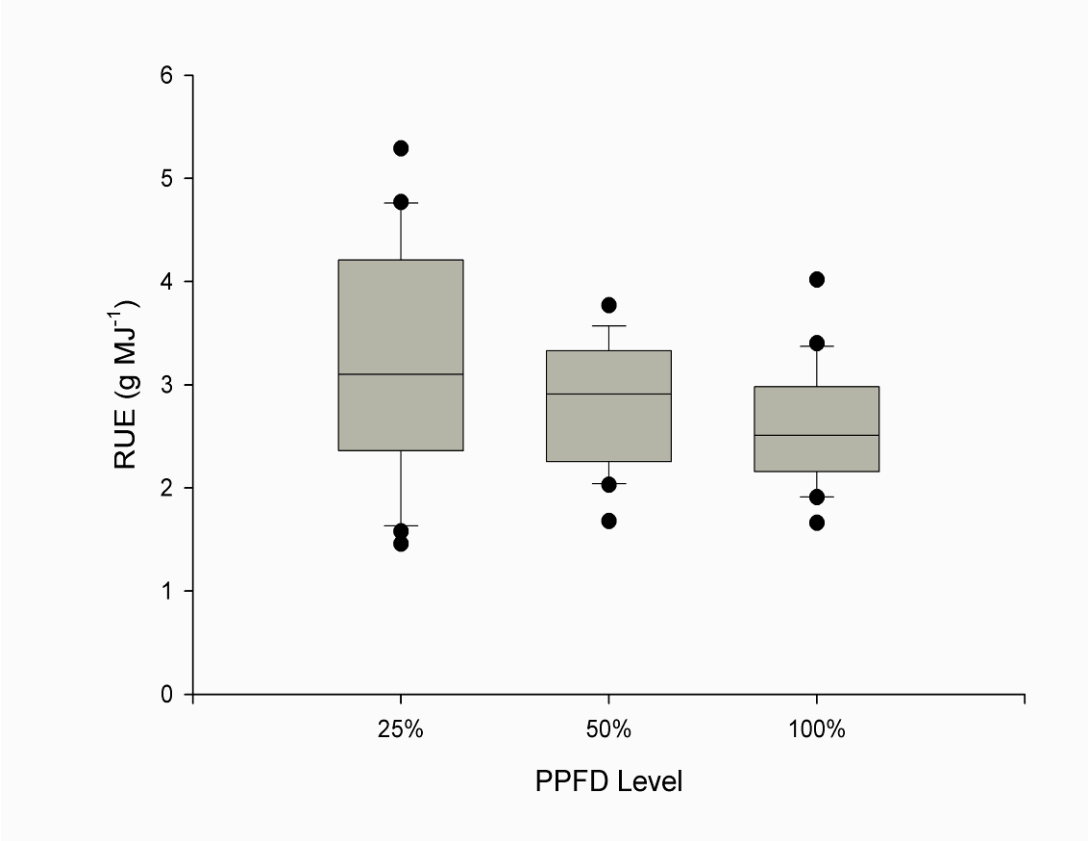

Figure 4.9. RUE vs PPFD levels.

For each PPFD level, the boxes = the 25% –75% percentile range, the mid-line = median value, the whiskers = 5%–95% percentile range of RUE values and ● = outlier data points.

Figure 4.9 also suggests that the RUE for the 100% PPFD treatment (mean =2.58 g MJ^{-1}) is somewhat lower than for the other two treatments (means = 3.22 and 2.82 g MJ^{-1} for the 25 and 50% treatments respectively), but this difference may not be statistically significant because of the variation in RUE within PPFD treatments. The statistical

significance of between-treatment differences in RUE was tested using a model of the form:

$$\mu_i = \mu + \alpha_i \tag{4.19}$$

where μ_i is the mean RUE for PPFD treatment i (i = 1 for 50% PPFD and i = 2 for 100% PPFD), μ is the mean RUE for the 25% PPFD treatment, and α_i is the parameter which estimates the differences between mean RUE for the 25% PPFD treatment (μ) and mean RUE for PPFD treatments (μ_i , where i = 1 or 2).

Since individual RUE values for seedlings within a plot were potentially auto-correlated, Equation 4.19 was fitted to the experimental data using procedure "lme" in the R statistical package (R Development Core Team 2007). Parameter values for Equation 4.18 were μ = 3.22 ($p < 0.001$), with α_i = –0.40 g MJ^{-1} (p = 0.224) and α_i = –0.64 g MJ^{-1} (p=0.092) for the 50% and 100% PPFD treatments respectively i.e. the RUE values for the 50% and 100% PPFD treatments are not significantly different from RUE values for the 25% PPFD treatments at the 95% confidence level, although the parameter for 100% PPFD is significant at the 10% confidence level. This result suggests that RUE is approximately constant across the range of PPFD values in the 25, 50 and 100% light treatments i.e. NPP increases linearly with increased $\varphi_{p,i}$; albeit that there is a slight but statistically non-significant tendency for RUE to decrease with increasing PPFD.

Environmental deficits were not expected to influence RUE because watering and fertilising treatments and ambient temperature in the growth cabinet were optimal or near optimal i.e. f_θ, f_T and f_N were all ≈ 1 . The exception was the vapour pressure deficit (*VPD*) which could not be maintained at the optimal level (<0.5 kPa). However, ambient *VPD* was reasonably uniform between plots as indicated by the *RH* and temperature data from Plots 1 and 6 reported in Section 4.2.1 (mean daytime *RH* in Plot 1 and Plot 6 = 57% (SD 4.7%) and 59% (SD 7.3%) respectively).

4.4 Discussion and Conclusions

4.4.1 Seedling biomass estimation

Variations in allometric relationships of seedlings due to PPFD

The results show that allometric models of seedling biomass were influenced by PPFD levels in the seedling's environment. There are four reasons why this may be so:

1. In general, conifer seedlings are reported to allocate proportionally more biomass above-ground when subject to shade (Khan *et al.* 2000; Robakowski *et al.* 2003; Kennedy *et al.* 2007). *D*, *H* and *A* are measurements of above-ground biomass components which, in the case of shaded seedlings, would therefore be expected to be a proportionally larger part of total *W* compared with seedlings growing under open conditions. However some authors report that the above-ground biomass/root biomass ratio in pine seedlings is insensitive to variations in light levels (Wetzel & Burgess 2001; Jose *et al.* 2003). In this study, the mean ratio of W_a to *W* was 0.71, 0.66 and 0.60 for the 25%, 50% and 100% PPFD treatments respectively i.e there is an apparently greater allocation of biomass above ground the more shaded 25% PPFD compared with the treatments with higher PPFD. This may contribute to the ratio of *D*, *H*, and *A* to total *W* differing between seedlings under low PPFD vs high PPFD.
2. Tree seedlings grown under higher PPFD tend to have leaves that are thicker and denser. This arises from structural differences between these 'sun' leaves compared with 'shade leaves' grown under low PPFD (Fitter & Hay 2002) and has been confirmed in studies of pine seedlings under varying levels of shade (Wetzel & Burgess 2001; de Chantal *et al.* 2003; Jose *et al.* 2003). Seedlings exposed to high levels of PPFD can therefore be expected to have a higher foliage *W* for a given silhouette area *A*. Foliar biomass is a significant part of seedling biomass, so differences in SLA due to different PPFD levels should lead to differences in the relationship of biomass to silhouette area (*A*).

   In addition to (2) above, the relationship of *W* to *A* may also vary with illumination due to the degree of self-shading by leaves. Self-shading is likely to be minimal in newly-germinated seedlings but may be a factor in older seedlings.

Where self-shading occurs, seedlings in the open may have a higher density of leaf surface area (and biomass) within the volume of the seedling crown than shaded seedlings, as there is a higher level of light penetrating past the external layers of foliage. Because A is an estimator of the volume of a seedling's crown (Ter-Mikaelian & Parker 2000), seedlings grown under high PPFD levels may have proportionally higher foliar biomass values for a given value of A.
In this study, above-ground biomass (W_a) was proportionally higher per unit of seedling silhouette area (A), for seedlings grown in the 100% PPFD treatments compared with seedlings from the 50% and 25% treatments (0.037, 0.025 and 0.024 respectively). It was not possible to determine whether this arose from higher foliage spatial density or lower SLA in the 100% PPFD seedlings.

3. In this study, the ratio of seedling height to seedling diameter (H/D) was also affected by PPFD treatment. This result is also reported frequently in the literature (e.g. Kennedy *et al.* (2007)). The mean H/D ratio for the 100% PPFD treatment was 36.1, compared with H/D ratios of 48.4 and 50.5 for 50% and 25% PPFD treatments respectively. This means that seedlings grown in shade may have reduced biomass, but the inclusion of H in the allometric parameter D^2H masks the consistency of the relationship between biomass and D^2 because reduced values for D^2 in shade are counteracted by relatively high values for H.

Reliability of model predictions

Testing of biomass prediction equations showed that either A or D^2 could be used as a reliable predictor of both above-ground and total W in radiata pine seedlings (see Table 4.4). However for the validation data set relative prediction errors for both were positive i.e. equations using A and D^2 as predictor variables tended to over-estimate W. Plots of predicted vs actual W (Figure 4.5) suggested that most of the models (the exception was the full model using A*PPFD) tended to slightly over-estimate W for smaller seedlings in the validation data set, and quite markedly underestimated W for the larger seedlings. Estimates of seedling biomass from seedling silhouette area (A) were more precise than estimates from D^2. Because of the influence of shade on seedling H/D ratios, use of D^2H

when seedlings are subject to a range of shade treatments could give misleading estimates of seedling biomass as described in paragraph 4 on the previous page.

Thus in a seedling growth experiment, initial and intermediate values of seedling W can be estimated from allometric equations using measurements of A and D^2. The final value for W can of course be measured by destructive sampling. For seedlings established on open sites with good weed control, shade levels will be low and variations in seedling allometric ratios should be less important. It may therefore be possible to use one general allometric equation across a range of sites. In contrast, it may not be possible to use a general allometric equation to estimate seedling biomass for seedlings established under partially shaded conditions e.g. beneath a forest canopy or where weed competition is vigorous. Instead, allometric parameters may need to be specified for each level of shade experienced by the seedlings.

4.4.2 Estimation of PAR interception and RUE

Estimation method and errors

If seedling NPP can be accurately measured then RUE can be calculated with confidence provided the absorbed PAR is also accurately measured. However, the method used in this experiment measured intercepted rather than absorbed PAR. Monteith & Unsworth (1990, pp 80-91) state that reflection and transmission of intercepted PAR is approximately 16% and 6% respectively in conifers. Therefore absorbed PAR should be approximately 80% of intercepted PAR for conifer seedlings. This is contradicted by Smolander & Stenberg (2001) who contend that absorption of PAR is close to unity for conifer needles with only minor scatter, and that realistic estimates of radiation absorbed by Scots pine needles can be made using a similar method to the one used in this study. Resolving this apparent contradiction was not possible within the time available for this study. Instead, all RUE estimates in this study are based on intercepted PAR and no attempt has been made to estimate RUE based on absorbed PAR.

Another potential source of error in this experiment is that only downwelling PAR was measured. However, because the seedlings were placed on tables, they were also able to intercept reflected (upwelling) light from tabletops, as well as from the floor and walls of the growth chamber. Particularly for the seedlings in the shaded PPFD treatments (25 and 50% PPFD), upwelling light may have been a significant part of the total PAR intercepted by the seedlings. This may account for the somewhat higher RUE for these treatments compared to the unshaded 100% PPFD treatment, because inclusion of upwelling light in the estimate for intercepted PAR would have meant a proportionately greater increase in total intercepted PAR for the shaded treatments. This in turn would have reduced the RUE for the shaded treatments by a proportionately greater amount.

There were two other identifiable sources of error in the method used to estimate intercepted PAR, although unlike those described above, they should not result in systematic over- or underestimates. They are:

1. Seedling projected area (A) for elevation angles $\beta = 45$ and 75 degrees, and incident PPFD for elevation angles $\beta = 15$, 45 and 75 degrees were estimated from regression equations (see Tables 4.5 and 4.6). Notwithstanding the good fit of these equations to the calibration data, direct measurement of A and PPFD would have been more accurate.
2. Measurement of seedling A relied on a subjective "thresholding" process when seedling photographs were digitally analyzed using programme QANT. However the good correlation of measured seedling A with W suggests that these measurements were reliable estimators for seedling biomass.

Comparison of RUE's with published data

The calculated RUE's for the main growth population in this experiment were approximately the same for all light treatments. This result accords with the empirical data and theoretical analysis reviewed in Section 2.5.4.

The results from this experiment do not conform to the general rule that for conifer species, RUE values tend to be low relative to broadleaf trees or agricultural crops (DeLucia *et al.* 2002). Mean RUE's of 2.6-3.2 g MJ^{-1} for the main growth population

compare favourably with reported values of 2.8 g MJ^{-1} for field crops (Russell *et al.* 1989, reported in Landsberg & Gower 1997). If the calculated RUE's are correct, then it may be that very young seedlings growing under ideal conditions are as productive as well-watered field crops. The generally low RUE's reported from conifers may therefore arise from the limitations of temperature, nutrition and soil water which apply to most conifer sites. In addition there is evidence that for a given species RUE may decline with age, so that values reported for older trees may not apply to young seedlings (Landsberg & Gower 1997).

Caution is needed even when making a comparison with other reported RUE values for young conifers. Landsberg & Gower (1997) state that reported values may not be commensurate because of differences in the way they are calculated, including: 1) for practical reasons some studies only measure above-ground dry biomass (W_a) not total dry biomass (W); 2) studies may use absorbed rather than intercepted PAR; 3) NPP may be expressed in terms of dry biomass or elemental C; 4) radiation may be expressed as PAR or as total solar radiation; 5) most studies do not account for reduction in maximum possible RUE due to suboptimal site conditions. In one study that is directly comparable with the present one, Cheaib *et al.* (2005) calculated the RUE of *Pinus pinaster* Aït seedlings. This study is comparable because: 1) RUE was calculated from the total (above- and below-ground) dry matter production of the seedlings vs total intercepted PAR; 2) seedlings were grown under optimum conditions in a growth chamber with controlled availability of light and soil P as the experimental treatments; and 3) seedlings were young, with the experiment conducted from ~ 30−120 days after initial sowing).

The RUE values from Cheaib *et al.* (2005) should be reasonably comparable with the results for the radiata pine seedlings in this study, which they were for the *P. pinaster* seedlings grown under high light (410-500 μmol m^{-2} s^{-1}). For these seedlings, RUE's were 2.8–3.8 g MJ^{-1} (compared with the mean RUE of 2.58 g MJ^{-1} for the radiata pine seedlings grown at ~ 500 μmol m^{-2} s^{-1}). However, for the *P. pinaster* seedlings grown under low light (120−180 μmol m^{-2} s^{-1}), RUE's were markedly higher (5.7–6.6 g MJ^{-1}, compared to the mean RUE of 3.22 g MJ^{-1} for the radiata seedlings grown at ~ 125 μmol

$m^{-2}\ s^{-1}$). It seems that the noticeably (but not significant statistically) higher RUE's observed for radiata pine seedlings at low light levels also occurred for *P.pinaster* seedlings in the study by Cheaib *et al.* (2005), only to a markedly greater degree. The very high values for RUE reported by Cheaib *et al.* (2005) at low PPFD's need further investigation.

Implications of seedling RUE values

The constancy of seedling RUE's over the range of PPFd treatments is consistent with work from earlier researchers which suggests that radiata pine seedlings can grow and persist in low light environments provided they are well-watered (Baker 1945; Moulds 1955). This suggests that even at low levels of PPFD (125 μmol $m^{-2}\ s^{-1}$) NPP of well-watered and fertilized seedlings is still positive, which in turn implies that reduced PPFD may not be the limiting factor for seedlings regenerating in gaps or under partial canopies. Some authors suggest that shade tolerance, the ability of seedlings to survive and grow under conditions of low PPFD, is the result of a complex of seedling characteristics interacting not just with light but with soil water (Sack 2004). This point will be explored in more detail in later chapters.

4.4.3 The Growth Chamber Environment

This experiment was designed to test for a consistent relationship between seedling NPP and intercepted PAR. It was intended to achieve this by placing the seedlings in a controlled environment where 1) air temperature, soil water, relative humidity and plant available nutrients were at similar levels for all seedlings and 2) seedlings were subject to one of three specific PPFD levels (approximately 125, 250 or 500 μmol $m^{-2}\ s^{-1}$).

In practice it was not possible to precisely control the seedling environment. In particular there were local differences between plots in air temperature and therefore in relative humidity. These differences may have resulted in differences in growth between plots subjected to the same nominal PPFD, although it was not possible to analytically demonstrate any effect of air temperature or relative humidity (Section 4.3.3).

There were also variations in incident PPFD between seedlings within plots. However, these could be accounted for by estimating individual intercepted PAR for each seedling. These individual estimates of intercepted PAR proved to be closely correlated to seedling NPP (Figure 4.8(c)).

Other attributes of the growth chamber environment varied but this variation was unlikely to be confounded with PPFD treatments. Ambient CO_2 levels were variable and overall were somewhat higher than normal atmospheric levels. Air speed was typically in the range 0 to 0.3 m s^{-1}, with localised eddies reaching 1m s^{-1}. However, there were no areas in the growth chamber where air speeds were consistently higher than average.

4.4.4 Conclusions

1. Using controlled growth chambers with seedlings grown in pots allows some control of the main "modifiers" of RUE (temperature, soil water, vapour pressure deficit, soil nutrients), and control of incident PPFD. There was enough variation in PPFD, temperature and relative humidity that these needed to be monitored for variation between and within plots. However, there was no evidence that uncontrolled variation in environmental conditions between plots led to biased estimates of seedling RUE and invalid comparisons between the three PPFD treatments.
2. Using PPFD levels ≤ 500 μmol m^{-2} s^{-1}, seedling NPP was linearly related to estimates of intercepted PAR ($\varphi_{p.i}$) i.e. RUE was approximately constant at all PPFD levels. This result was obtained in a growth cabinet with a reasonably constant daily regime for PPFD and temperature, and where temperature, soil water, vapour pressure deficit and plant available nutrients were at optimal or near-optimal levels.
3. RUE estimates were not entirely consistent with other estimates in the literature for conifer seedlings, but it is difficult to compare results from different studies due to variations in 1) the effect of "modifiers" i.e. temperature, soil water potential, water vapour deficit, plant available nutrients, plant age and 2) the way in which NPP is measured and reported. One comparable study of RUE for *Pinus*

pinaster seedlings reported similar RUE's at PPFD = 410−500 μmol m^{-2}, but markedly higher RUE's at lower PPFD's (120−180 μmol m^{-2} s^{-1}).

4. Seedling NPP can be measured with confidence using regression estimates with seedling A (in particular) or D^2 as predictor variables – although regression slope parameters will differ with light levels if A is the predictor variable.
5. The method used in the experiment to measure intercepted PAR ($\varphi_{p,i}$) has advantages, not least that it works with any shape of tree or seedling. However it has at least four potential sources of error. Some of these can be eliminated – for example, if this method is used in further experiments, upwelling PAR should also be included in the measured PAR incident on the seedling canopy. Also direct measurements of seedling projected area and incident PPFD could be made rather than using regression estimates. However frequent measurements of seedling silhouette area and PPFD from three elevation angles and four azimuth angles would be time-consuming.
6. Finally it is possible that the method used in this study, which estimates intercepted PAR, may therefore overestimate absorbed PAR. However, there is evidence that this over-estimate is negligible for conifer foliage (Smolander & Stenberg 2001). In this study, RUE will be estimated and reported on the basis of intercepted rather than absorbed PAR.

5 WATER DEFICITS AND SEEDLING RUE

5.1 Background

5.1.1 Conceptual model

The results from Chapter 4 show that NPP of newly-germinated radiata pine seedlings is linearly related to intercepted PAR ($\Sigma\varphi_{p.i}$) for PPFD = 125, 250 and 500 μmol m^{-2} s^{-1}. This result is consistent with assumptions underlying Equation 2.2 (NPP $= \acute{\varepsilon}\Sigma\varphi_{p.a}$, where $\acute{\varepsilon}$ is the radiation use efficiency (RUE) of a plant growing in the absence of deficits in soil water, ambient vapour pressure, temperature and nutrients). Where such deficits occur, RUE is reduced. This reduction is modelled in Equation 2.4 by multiplying $\acute{\varepsilon}$ by modifiers ($f_{\theta,}, f_D, f_T, f_N$) which each have a value between 1 (no deficit) and 0 (the deficit causes plant NPP to fall to 0).

Landsberg & Waring (1997) used Equation 2.4 as the basis for the hybrid tree growth model 3-PG (Physiological Principles to Predict Growth). The ability of 3-PG to model effects of environmental deficits on growth depends on the modifiers being general in nature i.e. they result in accurate predictions of RUE under all circumstances.
Correct specification and accurate estimation of these modifiers is therefore critical to successful modelling of tree growth with 3-PG. As stated by Landsberg & Gower (1997), "there is a clear need for rigorous research on the calculation of modifier values that are appropriate to the time scales used (for modelling)."
The results reported by Baker (1945), Moulds (1955) and in Chapter 4 of this study indicate that young radiata pine seedlings will grow even at quite low PPFD provided they are well watered. However, as noted by Barnes *et al.* (1998c, p197), an overstorey has important effects on a regenerating seedling other than those arising from reduced

PPFD, most importantly competition for available soil water. For a newly germinated seedling, available water is likely to be as critical to survival and growth as ambient PPFD.

This chapter describes an experimental investigation of the effect of reductions in available soil water on radiata seedling growth. This was achieved by calculating the RUE's of seedlings in an experiment where the only deficit was with respect to plant available water in the soil and comparing this with the RUE of seedlings growing in soil where there was no deficit in plant available water.

The soil water modifier (f_θ)

In 3-PG, Landsberg & Waring (1997) calculate the value of the soil water modifier from the soil moisture ratio (r_θ) where

$$r_\theta = \frac{\text{current soil water content + water balance}}{\text{available water}} \qquad (5.1)$$

Where the water balance is calculated from water inputs (rainfall, irrigation) minus water losses (evapotranspiration, drainage). The water balance is commonly expressed in millimetres of water but can also be expressed in terms of a volumetric ratio of water in the soil (v/v). However this formula seems to assume that all current soil water content is available water, which is not the case for most soil types. r_θ can more correctly be defined as follows:

$$r_\theta = \frac{\theta - \theta_{min}}{\theta_{max} - \theta_{min}} \qquad (5.2)$$

where θ = current soil water content (v/v), θ_{min} is the soil water content (v/v) at wilting point (soil matric potential (Ψ_{soil}) = –1.5 MPa) and θ_{max} is the soil water content at field

capacity ($\Psi_{soil} \approx -0.01$ MPa) (Townend *et al.* 2000). $\theta_{max} - \theta_{min}$ is defined as plant readily available water (PAW) (Townend *et al.* 2000).

The current soil water content (θ) will change over a time interval as follows:

$$\theta_{t+1} = \theta_t + \text{water balance} \qquad (5.3)$$

where θ_t is the value of θ at the beginning of the time interval and θ_{t+1} is the value of θ at the end of the time interval.

Plant growth response to r_θ

Sinclair (2005) contends that for a range of soil types, plant growth is at a maximum over a range of r_θ where $1 > r_\theta > 0.6$. However, once $r_\theta < 0.6$, plant growth declines linearly to the point where $r_\theta = 0$ i.e. where $\theta = \theta_{min}$ and $\Psi_{soil} \approx -1.5$ MPa.

The reduction in plant growth with decreasing r_θ arises because a plant must reduce its transpiration rate in order to maintain tissue turgor pressure when uptake of soil water is reduced (Fitter & Hay 2002, p151). Transpiration is reduced by reducing stomatal conductance (g_s), which is the ease with which water vapour passes from the leaf to the air surrounding the leaf. However this also decreases the conductance of the stomata to CO_2 which results in a reduced concentration of CO_2 within the leaf tissues; a decrease in the rate of photosynthesis therefore ensues, even though the amount of PAR absorbed by the plant has not changed.

For most soils, as r_θ declines from 0.5 to 0, Ψ_{soil} and soil hydraulic conductivity both reduce. The root uptake of soil water is inhibited and so too is the transpiration of the plant relative to a well-watered plant (Sinclair 2005). While this pattern is a general one, the upper and lower limits of PAW (in terms of θ (v/v)) and the onset of diminished hydraulic conductivity do depend on soil texture and structure. Landsberg & Waring (1997) propose that this variability can be modelled by the following function:

$$f_\theta = \frac{1}{1 + \left[(1 - r_\theta)/c_\theta\right]^{n_\theta}} \qquad (5.4)$$

where f_θ is the soil water modifier (taking a value between 0 and 1), c_θ = 0.7, 0.6, 0.5 and 0.4 for sand, sandy-loam, clay-loam and clay soils respectively; and n_θ = 9, 7, 5 and 3 for the same soil types. However they note that these values are indicative and are not based on experimental data. Figure 5.1 shows f_θ plotted against r_θ for the four abovementioned soil types.

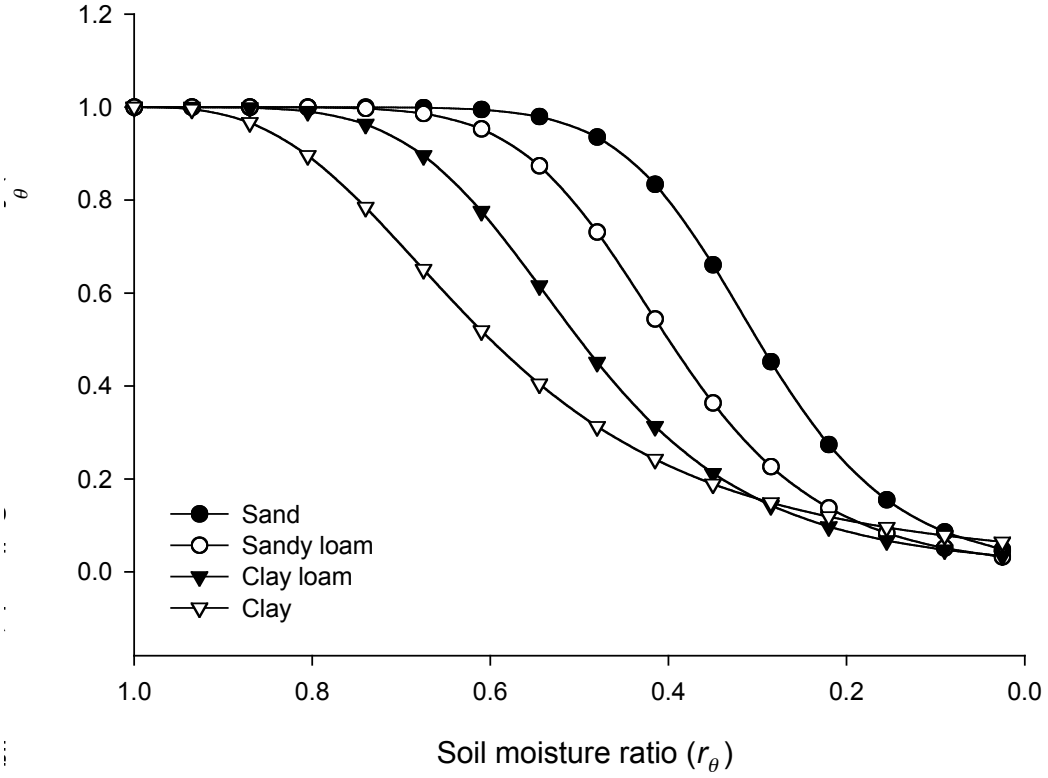

Figure 5.1. Relationship between the soil water modifier (f_θ) and the soil moisture ratio (r_θ) for four soil types.

Source: redrawn from Landsberg & Waring (1997).

Algebraically the differences in the curves for the different soil textures arise from the different values for the shape parameter (n_θ) and location parameter (c_θ) in Equation 5.4. Hydraulically, the difference in curves arises from the differences in Ψ_{soil} and soil

hydraulic conductivity between different soil textures at the same volumetric water content (Landsberg & Waring 1997). For example, a clay soil at $r_\theta = 0$ may have $\theta \approx 0.29$ (Sinclair 2005) , whereas a sandy soil at $r_\theta = 0$ may have $\theta \approx 0.07$.

5.1.2 Responses of radiata pine seedlings to water stress

Water stress frequently limits successful establishment and growth of planted radiata pine seedlings in Australia and New Zealand. For this reason, the effect of soil water deficits on photosynthesis and growth of radiata pine seedlings has been frequently studied (Heth & Kramer 1975; Kaufmann 1977; Nambiar *et al.* 1979; Attiwill *et al.* 1982; Sands *et al.* 1984; Squire *et al.* 1987; Squire *et al.* 1988; Richardson *et al.* 1996; Zou *et al.* 2000b; Watt *et al.* 2003a; Watt *et al.* 2003b). In most of these studies, the mechanistic links between soil water deficits, transpiration, stomatal conductance and transpiration are well characterised. However, there are no published studies of water stress effects on radiata pine seedling growth using a soil water modifier (f_θ) to calculate reductions in RUE.

Calculation of r_θ

To calculate r_θ, it is necessary to know θ, θ_{max} and θ_{min}. θ can be measured gravimetrically (w/w) where a soil sample is weighed, oven dried (105 ^{o}C) to constant weight and reweighed. The initial weight minus the final weight is the weight of water in the soil. This weight of water is divided by the final (oven-dry) soil weight to calculate the gravimetric θ (w/w). θ (w/w) can be converted to θ (v/v) by multiplying by ρ_b/ρ_w, where ρ_w is the density of water and ρ_b is the soil dry bulk density (Gardner *et al.* 2000). For soils in pots, soil volume can simply be calculated from the dimensions of the pot.

θ_{max} and θ_{min} are usually determined from a soil moisture characteristic curve (SMC) for the soil being investigated. A SMC plots θ (v/v) of a drying soil on the *y*-axis versus Ψ_{soil} on the *x*-axis (Townend *et al.* 2000, p96). The SMC is fitted to measurements of θ (v/v) made as a saturated soil sample ($\Psi_{soil} = 0$ MPa) is subjected to progressively greater suction. Suctions are imposed on the soil through a porous ceramic plate (or other porous

medium such as a fine sand), ensuring a continuous water column between the soil and a body of free water which is at a lower water potential than the water in the soil. For measurements between –10 kPa < Ψ_{soil} < 0 kPa, these lower pressure potentials can be achieved using a Buchner funnel and burette apparatus, with the soil in the Buchner funnel elevated above the free water in the burette in order to create a suction (Townend *et al.* 2000, p103-105). For Ψ_{soil} < –10 kPa, pressure gradients can be achieved using a vacuum pump and regulator (Townend *et al.* 2000, p105).

For most soils , the upper and lower θ values for plant available water (PAW) are determined by reading θ values from the soil moisture characteristic for $\Psi_{soil} \approx$ –10 kPa (this value varies between different countries and authors) and Ψ_{soil} = –1500 kPa, the conventionally assumed Ψ_{soil} values for field capacity and wilting point respectively (Townend *et al.* 2000, p128-130). However these assumptions may not hold for coarse textured soils such as sands and most artificial media used for growing plants in pots. These soils are made up of large relatively uniform particles with a high proportion of large macropores (Murray *et al.* 2002). This results in rapid drainage with most PAW held at matric potentials greater than –10kPa (Murray *et al.* 2002) and very little below this threshold. Artificial pot media (comprising peat, sand, vermiculite, perlite or mixtures of these) are used precisely because of these free-draining properties. Field soils in pots do not readily drain to field capacity, and plants may therefore suffer from water logging and lack of aeration (Passioura 2006). While use of sandy soil or free-draining artificial media is therefore desirable for pot culture, it is difficult to calculate f_θ (Equation 5.4) for these media because the upper limit of PAW is not the conventional –10kPa. Suggested upper limits for PAW include Ψ_{soil} = 0 kPa (Murray *et al.* 2002), Ψ_{soil} = –1 kPa (Fonteno 1989); or alternatively the θ (v/v) of soil which has been watered to saturation and allowed to drain overnight to a "drained upper limit" (Wahbi & Sinclair 2007) . All approaches are somewhat arbitrary. An upper limit of 0 kPa or –1 kPa ignores the reality that a proportion of water in saturated sands or artificial media will drain within a few minutes and will not be available for plant uptake; and setting θ as the water content (v/v) of a saturated pot which has been drained for 12 hours may not account for water that could be taken up by roots in that 12 hour period.

In this study a soilless substrate (50/50 (v/v) sand/grade M expanded perlite) was used to ensure adequate aeration and drainage for pot-grown radiata pine seedlings. This meant that the conventional upper limit to PAW of $\Psi_{soil} = -10$ kPa was not applicable. Therefore θ_{max} was estimated by repeated fitting of the estimated soil water modifier (f_θ) to the experimental data using a range of values for θ_{max}, and comparing the R^2 resulting from each θ_{max} value.

5.1.3 Summary

The aim of this experiment was to investigate the effect of reductions in available soil water on radiata seedling growth. To do this, growth and water use of young (< four months old) seedlings were measured under conditions where PPFD and PAW were controlled, and air temperature, and nutrients were at uniform, optimal or near-optimal levels. Under such conditions, it was expected that seedling growth would be directly proportional to absorbed PAR, but with the proportionality modified by f_θ, which would be calculated from measurements of soil θ. Soil θ was hypothesized to affect RUE through its mechanistic influence on stomatal conductance and therefore rate of photosynthesis.

The next section describes the methods used to: 1) measure seedling growth, absorbed PAR and RUE; 2) measure water in the growing media in which the seedlings were grown; 3) calculate a soil moisture modifier which would predict the reduction in seedling RUE due to a deficit in soil water; and 4) measure instantaneous photosynthetic rate and stomatal conductance of seedlings subject to varying deficits in PAW.

5.2 Methods

5.2.1 Growing methods

Sowing and germination

Open-pollinated radiata pine seeds (seedlot no 05/780B), supplied by Proseed Ltd, Amberley, New Zealand) were sown on 18 October 2007 into PB8 plastic bags filled

with 50/50 (v/v) grade M expanded perlite and sand[3]. Mean soil volume in each PB8 was 4452 ml (SD 174 ml). 2 g L^{-1} "Osmocote Exact" (15N 4P 7.5K 1.8Mg + trace elements) prills were mixed into the growing medium. A thin film of white plastic beads (~ 5 mm thickness) was spread over the surface of the growing medium, in order to minimise water loss from the pot by evaporation.

All seedlings had germinated by the end of November. After germination, the growing medium was inoculated on 6 December 2007 with mycorrhizal spores (*Rhizopogon rubescens*, collected 10 August 2006, Rotorua Nursery, Rotorua, New Zealand). Note that both the seedlot and the mycorrhizal inoculant are not the same as those used in the study described in Chapter 4. The germinated radiata pine seedlings were grown in a greenhouse, where they were watered regularly to container capacity (as defined by Fonteno (1989)).

Controlled growth cabinet

Seedlings were transferred on 3 December 2007 to a controlled growth chamber (Contherm PGV36, Controlled Environments Limited, Winnipeg, Manitoba, Canada). Seedlings were subjected to light for 12 h d^{-1}, including a 20 minute 'ramp-up' and 'ramp-down' period each morning and evening. Nominal PPFD during the experiment was 250 μmol m^{-2} s^{-1}, which over a 12 h day equals a daily irradiance of 10.8 mol m^{-2} d^{-1}. Air temperature and relative humidity (*RH*) were measured with one Hobo sensor (Onset Computer Corp., Bourne, Massachusets) located at seedling height (~30cm above the chamber floor) at the centre of the chamber. Nominal daytime and nighttime temperatures were a constant 17.5 ^{o}C and 12.5 ^{o}C, but actual air temperatures at seedling height were 19.0 °C (SD 1.3°C) and 12.9 °C (SD 1.5°C) respectively. Mean daytime *RH* was 76.5% (SD 8.1%) and mean night time *RH* was 92.5% (SD 7.3%). The mean daytime *RH* is equivalent to a vapour pressure deficit of 0.52 kPa at 19.0 °C, just over the

[3] In a paired treatment, seedlings were also grown in a sieved fine sandy loam. This treatment was abandoned due to the problems with drainage of field soils in pots mentioned in Section 5.1.

threshold of 0.5 kPa above which stomatal conductance begins to decline in young radiata pine (Sheriff & Mattay 1995; Watt *et al*. 2003b). This suggests that stomatal conductance and therefore photosynthesis were not limited by the vapour pressure deficit for most of the experiment. Ambient CO_2 levels in the growth cabinet were measured continuously, using a Vaisala CO_2 probe (Vaisala Instruments, Helsinki, Finland). Mean CO_2 concentration during the experiment was 414 μmol mol^{-1} (SD 33.7 μmol mol^{-1}). As discussed in Chapter 4, the readings in the higher range occurred when people were working in the growth cabinet for extended periods.

Air velocity in the chamber was measured on 5 February 2008. Air speed was measured above the growing tip of every seedling in the experiment (≈ 40 cm above floor level). Air velocities were all zero in the *x*-*y* (horizontal) plane. Readings in the vertical plane were between 0.3 to 0.5 m s^{-1} just above above the seedling growing tip, but were zero immediately above the pot surface. This is probably because of the ventilation system used by the PGV 36, where air is pumped upwards into the chamber via small holes in the chamber floor. The pot surface would therefore be sheltered from the air upwelling from the chamber floor by the bulk of the pot. There was little variation in air velocity between trees in the experiment.

Water and fertiliser treatments

Once transferred to the controlled growth chamber, seedlings were watered regularly to container capacity to ensure that no seedlings were subject to a deficit in plant available water. In addition to the slow release fertiliser in the growing medium, seedlings received a complete nutrient application once every 10 d with a fertiliser solution (Kristalon (18N 18P 18K + trace elements) 2 g L^{-1} H_2O, with 25 ml applied per tree).

On 28 December 2007, 15 randomly chosen seedlings were allocated to three row-plots (denoted as Plots 3, 5 and 6[4]) within the growth chamber. These seedlings will be referred to as the main measurement population. Within each row of five seedlings

[4] Row-plots 1, 2 and 4 were the abandoned treatments with seedlings grown in a fine sandy loam. However, the 15 seedlings in these pots were used to determine seedling silhouette area relationships (page 131).

(denoted as pots 1–5), one pot was randomly allocated to each of five watering treatments (200 ml, 140 ml, 100 ml, 60 ml and 20 ml of reverse osmosis water, applied at 5 d intervals). These rates were chosen because preliminary measurements indicated that well-watered pots were using 200 ml H_2O every five days. This figure included both evapotranspiration and drainage. The applied water treatments were therefore approximately 100%, 70%, 50%, 30% and 10% of pot water use respectively. These water applications continued at 5 d intervals over a 40 d period until 6 February 2008. During this 40 d period, seedling growth, PAR interception and water use were measured as described in the next section.

5.2.2 Measurements

Biomass and seedling silhouette area (A)

For the main measurement population in plots 3, 5 and 6 (n = 15), initial seedling biomass at the beginning of the growth measurement period (28 December 2007) was determined from measurements of seedling silhouette area ($A_{\phi=15}$) using the methods described in Section 4.2.2. To estimate the regression relationship between seedling W and A, 10 seedlings were randomly selected at the commencement of the 40 d measurement period from the 15 seedlings not used in the main experiment. Destructive measurement was used to determine their oven dry weight. Prior to destructive measurement, these seedlings were photographed using a digital camera from an elevation angle φ= 15 degrees, and seedling silhouette area (A) was calculated using digital image analysis software (see Section 4.2.2 for a detailed description of methods). All seedlings in the main measurement population (n = 15) were also measured for A using this method at day zero and subsequently every 10 d over the 40 d measurement period (28 December 2007 to 6 February 2008).

During the 40 d measurement period, one seedling in the main measurement population died from unknown causes. At the end of the experiment all remaining seedlings (n = 14) were also destructively measured for biomass. Seedling silhouette area (A) of each seedling was measured before destructive measurement. Methods for destructive

sampling are as described in Section 4.2.2, except that oven dry weight of biomass components were determined by oven drying and weighing each seedling individually, rather than by calculating them from the ratios of fresh weight to oven-dried weight for bulked samples.

After oven drying and weighing of biomass components, one bulked foliage sample for the seedlings in each applied water treatment (100%, 70%, 50%, 30% and 10% of pot water use) was analysed for foliar N levels. Before analysis samples were oven dried at 62°C overnight (residual moisture typically 5%) and ground to pass through a 1.0 mm screen. Foliar N was estimated by near infra-red spectroscopy (NIRS), with a calibration based on %N determined by Dumas combustion (Hill Laboratories, Hamilton, New Zealand pers. comm.).

PPFD in the growth chamber

PPFD in the chamber was measured continuously by a Li-Cor 190A sensor (Li-Cor Inc, Lincoln, Nebraska, USA) interfaced with a Hobo datalogger placed at 30 cm (≈ growing tip height for the seedlings) above the floor in the centre of the growth chamber. Data from this sensor indicated fluctuations in PPFD from the growth cabinet lights during the experiment (Mean daylight PPFD = 212.5 μmol m^{-2} s^{-1}, SD 66.1 μmol m^{-2} s^{-1}). These fluctuation occurred both on an hourly and daily basis.

Incident PAR on each seedling was estimated by measuring PPFD around the growing tip of each seedling on one occasion (18 January 2008). Measurements were made using a Li-Cor 190A quantum sensor connected to a Li-Cor Li-188B integrating quantum meter (Li-Cor Inc, Lincoln, Nebraska, USA). During these measurements, the mean incident PPFD measured by the Li-Cor 190A sensor at the centre of the growth cabinet was 222.5 μmol m^{-2} s^{-1} (SD 67.0 μmol m^{-2} s^{-1}), which was within 4% of the 40 d mean. Both downwelling (at positive elevation angles φ = 15, 45 and 75 degrees) and upwelling PPFD (at negative elevation angles φ = 15, 45 and 75 degrees) were measured. These measurements were repeated for four azimuth angles (β = 0°, 90°, 180°, 270°) around each seedling.

Spectral photon flux within the chamber was not measured. Instead, published data on the spectral distribution and energy equivalence for measured PPFD were used.
Light sources in the PGV36 controlled growth chamber comprised four incandescent banks and four fluorescent banks, as pairs of banks (one of each type). Sager & McFarlane (1997, p3) state that the conversion factors (μmol s^{-1} to W) for incandescent and fluorescent lights are 0.200 and 0.218 respectively. Therefore a conversion factor of 0.21 was used to convert PPFD (μmol m^{-2} s^{-1}) measured in this experiment to irradiance (W m^{-2}).

Calculating PAR interception

Measurements of the seedlings in Chapter 4 showed that the seedling silhouette area A calculated from one photograph taken from one azimuth direction (0°) at elevation angle φ = 15 degrees, was a reliable predictor of silhouette areas taken from other elevation and azimuth angles. This meant that $A_{\varphi=15}$ could be measured regularly using a single digital photograph of the seedling, as described in Section 4.2; this value for $A_{\varphi=15}$ could then be used to predict A as seen from other elevation angles, rather than laboriously measuring these silhouette areas from digital photographs.

Therefore, projected seedling areas at elevation angles φ = 15, 45 and 75 were estimated from measurements of seedling silhouette area (A) on 6 February 2008. Measurements were made of seedlings in the main experiment (n = 14), and also the surviving seedlings from the abandoned treatments where seedlings were grown in fine sandy loam (Plots 1, 2 and 4, n = 14). Measurements were made as follows:

1. Digital photographs were taken of each seedling and seedling projected area was measured using the same method used to measure A for biomass estimation. Photographs of the seedlings were taken from the same elevation and azimuth angles from which incident PPFD was measured (φ = 15, 45 and 75 degrees elevation, θ = 0, 90, 180 and 270 degrees azimuth). For each measured seedling, 12 photographs were taken (three zenith angles × four azimuth directions).

2. These measurements confirmed that the seedling silhouette area A calculated from one photograph taken from one azimuth direction at elevation angle ϕ = 15 degrees, was a good predictor of silhouette areas taken from other elevation angles (R^2 of 0.991 and 0.981 for linear regressions of $A_{\phi=15}$ vs $A_{\phi=45}$ and $A_{\phi=75}$ respectively). Therefore, $A_{\phi=45}$ and $A_{\phi=75}$ for the main growth experiment seedlings were predicted from measured $A_{\phi=15}$ using the regression models in Equation 5.5:

$$A_{\phi=45} = 1.083 * A_{\phi=15} \quad (5.5a)$$

$$A_{\phi=75} = 0.994 * A_{\phi=15} \quad (5.5b)$$

3. At 0, 10, 20 30 and 40 d during the experiment, each seedling in the main growth data population was digitally photographed once only from angle of φ = 15 degrees, and its silhouette area was measured using QANT. This single measurement of A taken from elevation angle φ = 15 degrees was used to predict A as viewed from φ = 45 and 75 degrees using Equations 5.5(a) and (b). A for seedlings at elevation angles –15, –45 and –75 degrees were assumed to be the same as the equivalent A values for 15, 45 and 75 degrees elevation respectively.

Measured PPFD and predicted values for A for elevation angles φ = ±15, ±45 and ±75 degrees were used to calculate intercepted PAR flux (in Watts) using Equation 4.10. Intercepted flux was summed for the 40 d measurement period using the methods described in Chapter 4, with one important difference−in Chapter 4, intercepted flux was only estimated for downwelling PAR (that is, intercepted PPFD summed over elevation angles 15, 45 and 75 degrees). In this study, intercepted upwelling PPFD (calculated for elevation angles –15, –45 and –75 degrees) was also included in the total.

Soil water content

Water content of each pot in the main measurement population was measured gravimetrically at day zero and at 5 d intervals over the 40 d measurement period. This was achieved by weighing pots on digital scales to the nearest gram. Gravimetric water

content in each pot was converted to volumetric water content by 1) calculating the filled volume of each PB 8 planting bag by measurement of external diameter (top and bottom) and filled height; 2) determination of oven dry bulk density of the soil from samples taken at the end of the 40 d measurement period; and 3) calculation of the oven dry weight of the soil for each pot from 1) and 2) above. The weight of water in the pot was obtained by subtracting the oven dry weight of sand from the pot weight, after allowing for the weight of the PB8, the plastic beads used as a surface mulch and estimated seedling fresh weight at time of measurement (which was negligible compared to the weight of sand and water in the pot). The weight of water in the pot was converted to a volume assuming a density of 1 g ml^{-1}.

After weighing, each pot received the prescribed volume of water appropriate to its watering treatment (200 ml, 140 ml, 100 ml, 60 ml or 20 ml). This added volume was added to the volumetric water content (estimated from the gravimetric water content using the method described above). Mean volumetric water content over the 5 d interval until the next weighing was assumed to be the mean of the water content after water was added, and the measured water content 5 d later (before watering).
Using the above method, a mean soil volumetric water content (θ) was calculated for each pot for each 5 d interval between day zero and d= 40.

Plant available water

The plant available water in each pot was calculated using 1) the mean soil volumetric water content (θ) values whose calculation was described in the previous section; and 2) a soil moisture characteristic (SMC) curve for the sand/grade M perlite mix (Figure 5.2), which enabled the calculation of an equivalent soil moisture suction (Ψ, kPa) for each value of θ. (Note: in this section, soil water potential (Ψ) will be expressed as a positive suction, rather than as a negative matric tension.) The SMC curve was fitted to data taken from three determinations made using a Buchner funnel apparatus (Townend *et al.* 2000) over a range of suctions from 0–100 cm (0–9.8 kPa). The fitted soil moisture characteristic curve shown in Figure 5.2 uses the function described by Buchan & Grewal (1990):

$$\Ø / \Ø_e = (\theta / \theta_s)^b \qquad \text{for } \Psi > \Psi_e \tag{5.6a}$$

$$\theta = \theta_s \qquad \text{for } 0 < \Psi < \Psi_e \tag{5.6b}$$

where Ψ is the soil moisture suction, θ is the soil moisture content (v/v), θ_s is the saturated water content (v/v) and Ψ_e is a value of suction below which $\theta = \theta_s$. Parameter values estimated by fitting this function to the draining soil moisture data for the sand/perlite mix were mean $\theta_s = 0.441$, $b = -1.79$ and $\Psi_e = 0.35$ kPa. The coefficient of determination (R^2) for the fitted relationship was = 0.983.

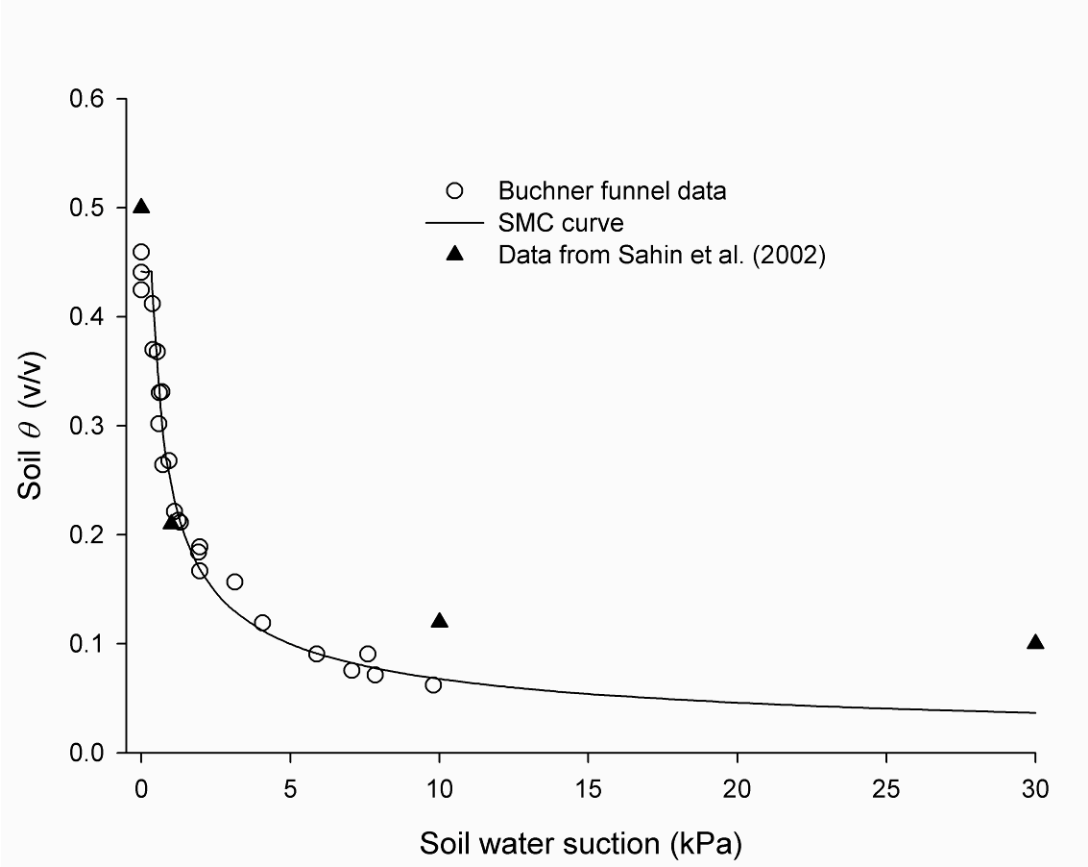

Figure 5.2. Soil moisture characteristic curve for sand/ perlite.

Data measured by Sahin *et al.* (2002) for a similar sand/perlite mix are shown for comparison.

In coarse textured soils such as the sand/grade M perlite mix used in this study, most of the water available to the seedlings is outside the range of Ψ conventionally assumed for calculating PAW (10–1500 kPa). Using the SMC curve with the parameter values stated above, θ was 0.068 at a soil water suction = 10 kPa and (estimating by extrapolation) θ_{min} (where Ψ =1500 kPa) was 0.004 (0.4%). Therefore the volumetric water content between soil saturation (θ_s = 0.441) down to soil water suction = 10 kPa is 85% of the soil water between θ_s and θ_{min}, with only 15% lying between soil water suctions = 10 kPa and θ_{min}.

As discussed in Section 5.1, the conventional upper limit of PAW of Ψ = 10 kPa probably does not apply to the sand/Grade M perlite mix. Therefore θ_{max} was estimated by repeated fitting of the estimated soil water modifier (f_θ) to the experimental data using a range of values for θ_{max}, and comparing the R^2 resulting from each θ_{max} value.

Seedling transpiration, photosynthesis and stomatal conductance

Stomatal conductance and net photosynthesis were measured on one occasion for each seedling between 24-30 January 2008, and for all seedlings in the 100%, 50% and 10% water use treatments on 1 February 2008. This resulted in 23 measurements. All measurements were made at least one hour after the 'daylight' phase commenced in the growth cabinet.

Measurements were made using a Li-Cor 6400 portable photosynthesis system (Li-Cor Inc., Lincoln, Nebraska), with a custom-built chamber interfaced to the sensor head. The design of this chamber is described in LI-COR Inc. (Undated). The Li-Cor 6400 is an "open" system (LI-COR Inc. 1992) which means that photosynthesis and transpiration measurements are based on measurements of CO_2 and water vapour concentration for air flowing into and out of the custom chamber. The chamber was made out of a plexiglass cylinder of 150 mm external diameter, with an approximate volume of 2 L (Figure 5.3). A custom chamber was required because 1) the soft young needles of the radiata pine seedlings were not suited for measurement using the conventional measurement cuvette on the Li-Cor 6400, and 2) the normal conifer chamber manufactured by Li-Cor for use on needle leaved plants (LI-COR Inc. 1992) is designed for measurement of assimilation

by foliage on lateral branches. As discussed in Chapter 4, the young radiata seedlings had few lateral shoots and these were typically short and non-woody.

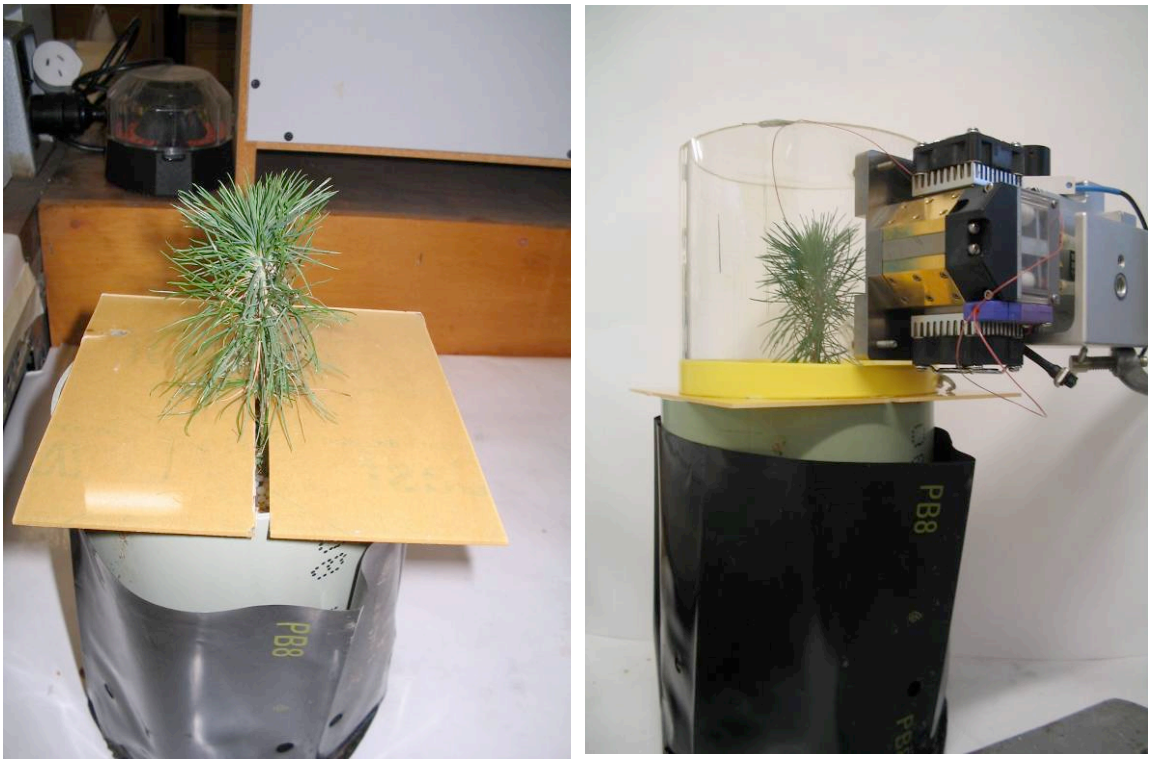

Figure 5.3. The custom chamber used to measure transpiration and net photosynthesis by radiata pine seedlings.

The left hand photograph shows the perspex mounting plate with a slot to allow the plate to be placed with the seedling stem at the centre of the plate. The right hand photograph shows the custom chamber mounted on the Li-Cor 6400 sensor head, and placed on top of the perpex mounting plate.

Use of a custom chamber required modifications to the default settings for the Li-Cor 6400, as follows:

1. The thermocouple sensor normally used to measure leaf temperature was instead located above the growing tip of the seedling in the chamber and used to measure air temperature (T_{air}). The temperature of the leaf surface (T_{leaf}) was not measured directly but estimated using a heat balance equation, as described in LI-COR Inc. (1992, Chapter 17).
2. For a conventional Li-Cor 6400 sensor head, incident PAR is normally generated by an LED light source mounted on the leaf chamber. For seedlings in the custom

chamber, incident PAR was from the growth chamber lights. PPFD was measured by a Li-Cor 190SA sensor mounted on the Li-Cor 6400 sensor head alongside the assimilation chamber.

3. For the conventional sensor head, a one-sided leaf area of 6 cm^2 is clamped within the cuvette where gas exchange is measured. In the custom assimilation chamber, the total leaf area of the seedling contributes to CO_2 and H_2O fluxes in the chamber. Whole seedling measurements of these fluxes must be corrected to a per m^2 leaf area basis in order to compare measurements between plants with different leaf areas, and to enable comparison of measurements with those reported by other authors. Total leaf area for each seedling was measured at time of destructive biomass measurement, as follows. After foliage had been weighed for fresh weight, a weighed subsample was spread over a piece of flat white rectangular cardboard. A digital photograph was taken of the foliage and its projected area measured using digital image analysis. A linear scale marked on the cardboard rectangle was used to calibrate the digital image software. The measured projected (one-sided) area of the subsample was multiplied by the ratio of weights of the total seedling foliage and the subsample weight, to calculate total seedling projected leaf area. A regression was used to fit an exponential relationship between total projected leaf area and the seedling silhouette area measured from an elevation angle φ = 15 degrees ($A_{\varphi = 15}$), as follows:

$$\text{Total projected leaf area} = 14.272e^{0.0354A_{\varphi = 15}} \quad (5.7)$$

Predicted total projected leaf area using this function was closely correlated with actual values, (R^2 = 0.903), and so it was used to predict projected needle area for a seedling from measurements of $A_{\varphi = 15}$ taken at 10 d intervals over the 40 d measurement period. Where necessary, $A_{\varphi = 15}$ values for days in between each 10 d measurement were estimated by linear interpolation. Finally, projected leaf area calculated by Equation 5.7 was corrected to total (all-sided) needle area by multiplying by π (Grace 1987).

Other settings for the Li-Cor 6400 used in this study are reported in Appendix 1. One key assumption is that the boundary layer conductance for conifer needle leaves is very high, due to the dissected nature of the foliage (Martin *et al.* 1999). For this study, boundary layer conductance was set to 8 mol m^{-2} s^{-1}. This means that important variables such as the CO_2 concentration and vapour pressure at the leaf surface (C_s and D_s respectively) can be assumed to be equal to the ambient CO_2 concentration and vapour pressure in the chamber (C_a and D_a respectively).

Measurement of seedling gas exchange parameters followed the following procedure:

1. The Li-Cor 6400 and custom chamber were tested for leaks and calibration of the measurements of CO_2 concentration, vapour pressure and air flow into the chamber.
2. While this was occurring, a thin flat perspex plate (170 mm × 170 mm) was mounted around the base of the seedling. A 5 mm wide slot cut from the margin of the plate to its centre allowed the plate to be slid horizontally over the soil surface until the seedling was located at the centre of the plate (Figure 5.3). The slot was then sealed with sellotape which leak testing had proved to be impermeable to CO_2.
3. The custom chamber was placed over the seedling such that its base sat flush on the perspex plate (Figure 5.3). The join between the chamber and the plate was sealed with a narrow bead of blu-tack (Bostik N.Z., Lower Hutt) which testing had shown to provide a leak-proof seal.

Air was passed through the chamber at a rate of 700 μmol s^{-1}. The CO_2 concentration of the incoming air was adjusted to 400 μmol mol^{-1}, and the vapour pressure deficit was set by adjusting the valve to the water vapour scrubbing cylinder through which the inlet air stream was passed. The seedlings proved to have transpiration rates on the limit of the Li-Cor 6400's capacity to remove water vapour by scrubbing, and the maximum vapour pressure deficit achieved was 0.9 kPA at 21.1 ^{o}C air temperature, equivalent to a relative humidity of 64%. Relative humidities within the chamber during measurement were typically > 70%. Seedlings typically took 5-10 minutes for transpiration and photosynthesis to equilibrate after being placed in the custom chamber, as air

temperatures and humidity within the chamber tended to be slightly higher than ambient values. Measurements were logged once the coefficients of variation (CV, %) for the difference between inlet and outlet CO_2 and water vapour concentrations were both < 0.1%. Data were logged on at least three occasions over the ensuing five minutes and an average of these was used for subsequent analysis.

5.3 Results

This section follows the structure implied in the introduction to this chapter i.e.: 1) measurements of seedling NPP (increase in total seedling oven dry weight) and intercepted PAR, and calculation of seedling RUE; 2) measurements of plant available water in the soil where the seedlings were growing and calculation of a soil water modifier (f_θ) ; 3) testing of the soil water modifier as a means of explaining variation in seedling RUE in terms of variation in plant available water and 4) examination of the evidence for the mechanistic explanation of how reduced RUE is caused by deficits in plant available water.

5.3.1 Seedling biomass and NPP

This section presents results of seedling growth and NPP for the main growth population data set (n=14).

Initial seedling biomass at the beginning of the growth measurement period (28 December 2007) was determined from measurements of seedling silhouette area ($A_{\phi=15}$) using the methods described in Chapter 4. A linear regression was fitted to measurements of total seedling oven dry weight (W) and $A_{\phi=15}$ for 10 seedlings destructively sampled on 28 December 2007. This yielded the following function:

$$W = 0.0088 + 0.0299\, A_{\phi=15}, \qquad (5.8)$$

Predicted W using this function was closely correlated with actual values ($R^2 = 0.983$), therefore initial W for the seedlings in the main experiment was calculated using this relationship. Final total biomass (W) of seedlings in the main growth population was

measured destructively at the end of the experiment (6 February 2008). The increment in seedling oven dry weight (ΔW = final W –initial W) was calculated by subtracting the initial W from the final W. This increment was the seedling NPP (net primary production) over the 40 d period. Table 5.1 shows the individual NPP values for each seedling. Foliar nitrogen levels for the seedlings in the main growth population at time of destructive harvest were all in excess of 1.7%, which is the level considered to provide no restriction to seedling growth (Sheriff & Mattay 1995). Mean foliar N was 3.0%, (SD 0.2%).

Table 5.1. Total intercepted PAR, NPP and RUE estimates for 28 December 2008 to 6 February 2008.
Data are for the main growth population (n = 14). Pot numbers are given in the format "plot no/seedling no".

Pot number	Applied Water (% of maximum water use)	Intercepted PAR (MJ)	NPP (g)	RUE (g MJ^{-1})
3/3	10	1.13	2.66	2.35
5/2	10	0.86	1.81	2.10
6/2	10	0.72	1.43	1.98
3/1	30	0.93	2.38	2.55
6/1	30	0.89	1.73	1.93
3/4	50	0.86	2.06	2.39
5/3	50	1.18	2.58	2.19
6/4	50	0.87	2.22	2.56
3/5	70	1.22	2.97	2.43
5/5	70	0.90	2.11	2.34
6/5	70	0.76	1.78	2.34
3/2	100	0.80	2.07	2.57
5/1	100	1.15	2.94	2.56
6/3	100	0.93	2.33	2.49

5.3.2 PAR interception and seedling growth

Incident PPFD

Incident PAR on each seedling was estimated by measuring PPFD around the growing tip of each seedling on one occasion (18 January 2008). Both downwelling (positive

elevation angle) and upwelling PPFD (negative elevation angle) were measured. PPFD's for each elevation angle were calculated from the average of the PPFD readings taken at each of four azimuth angles (0, 90, 180 and 270 degrees) around the seedling. PPFD (irradiance) was converted to radiance of a theoretical spherical surface surrounding each seedling using the methods described in Chapter 4.

Intercepted PAR

The PAR intercepted by seedlings was calculated according to method 3 described in Section 4.1.2. This method requires as inputs: 1) A_ϕ, the silhouette area of the seedling when viewed from the elevation angle ϕ; and 2) N_ϕ, the radiance of a spherical surface around the seedling at elevation angle ϕ, averaged over the range of azimuth angles 0–2π. Measurements of seedling $A_{\phi=15}$ were used to calculate seedling projected areas for elevation angles ϕ = 45 and 75 degrees, using Equations 5.5 (a) and (b), reported in Section 5.2.2. $A_{\phi=15}$ was measured every 10 d over the 40-day period 28 December 2007 to 6 February 2008. $A_{\phi=15}$ and the calculated values for $A_{\phi=45}$ and $A_{\phi=75}$ (and the equivalent areas for negative elevation angles) were then multiplied by radiance at the relevant elevation angle (N_ϕ). N_ϕ was calculated from PPFD measurements made on 18 January as described in Section 5.2.2. The resulting interception values were then integrated using Equation 4.10, Section 4.1.2.

The calculated intercepted PAR flux (I) was in units of Watts (W). The energy of the intercepted PAR ($\varphi_{p.i)}$ was calculated on a 10 d basis by averaging the calculated I at the beginning and end of the 10 d period , and multiplying this by the number of seconds of illumination per measurement period (10 d × 12 h d^{-1} × 3600 s h^{-1}). This gave the energy of the intercepted PAR in Joules (J) based on an illumination time per day of 12 h. Table 5.1 shows the total intercepted PAR (MJ) estimated using this method for all trees, along with the total NPP (g dry weight) values (Section 5.3.1) and RUE (g MJ^{-1}).

5.3.3 Soil water

Figure 5.4 shows mean soil θ (v/v) values for all seedlings (n=14) over the four 10 d intervals in the 40 d measurement period. The mean for each 10d period was calculated as the unweighted mean of the two 5 d mean θ whose calculation was described in Section 5.2.2. For the first 10 d period, θ was quite uniform for all pots (mean = 0.275, SD = 0.021). The 100% water use pots maintained a reasonably constant θ value throughout the experiment (initial mean θ for 0–10 d = 0.285, SD = 0.016 and final mean θ = 0.282, SD = 0.017). As expected, the 10% water use pots dried down over 40 d to θ values which were about half of the initial values (mean θ at 40 d = 0.153, SD = 0.007).

However the intermediate treatments showed greater variation in the rate at which pots dried down. In particular, Pot 3/1 (30% water use) used relatively little water, with initial mean (0–10 d) θ = 0.291 and mean θ = 0.249 for 30-40 d. This meant that θ values for Pot 3/1 were similar to those for the well watered pots (70% and 100% water use) throughout the 40 d measurement period. This may have been due to measurement error but as will be shown later, seedling growth and RUE for Pot 3/1 were similar to seedlings in the well-watered pots, suggesting that the high θ values for this pot were correct.

Pots in the 50% and 70 % water use treatments were also variable in the rate at which they dried down, although not to the same degree as the pots in the 30% treatment. Figure 5.5 shows the effect of this variation. There is scatter in the plot of RUE versus water use treatment. The implications of this lack of correlation between water use treatment (evapotranspiration plus drainage) and RUE are discussed in Section 5.3.4.

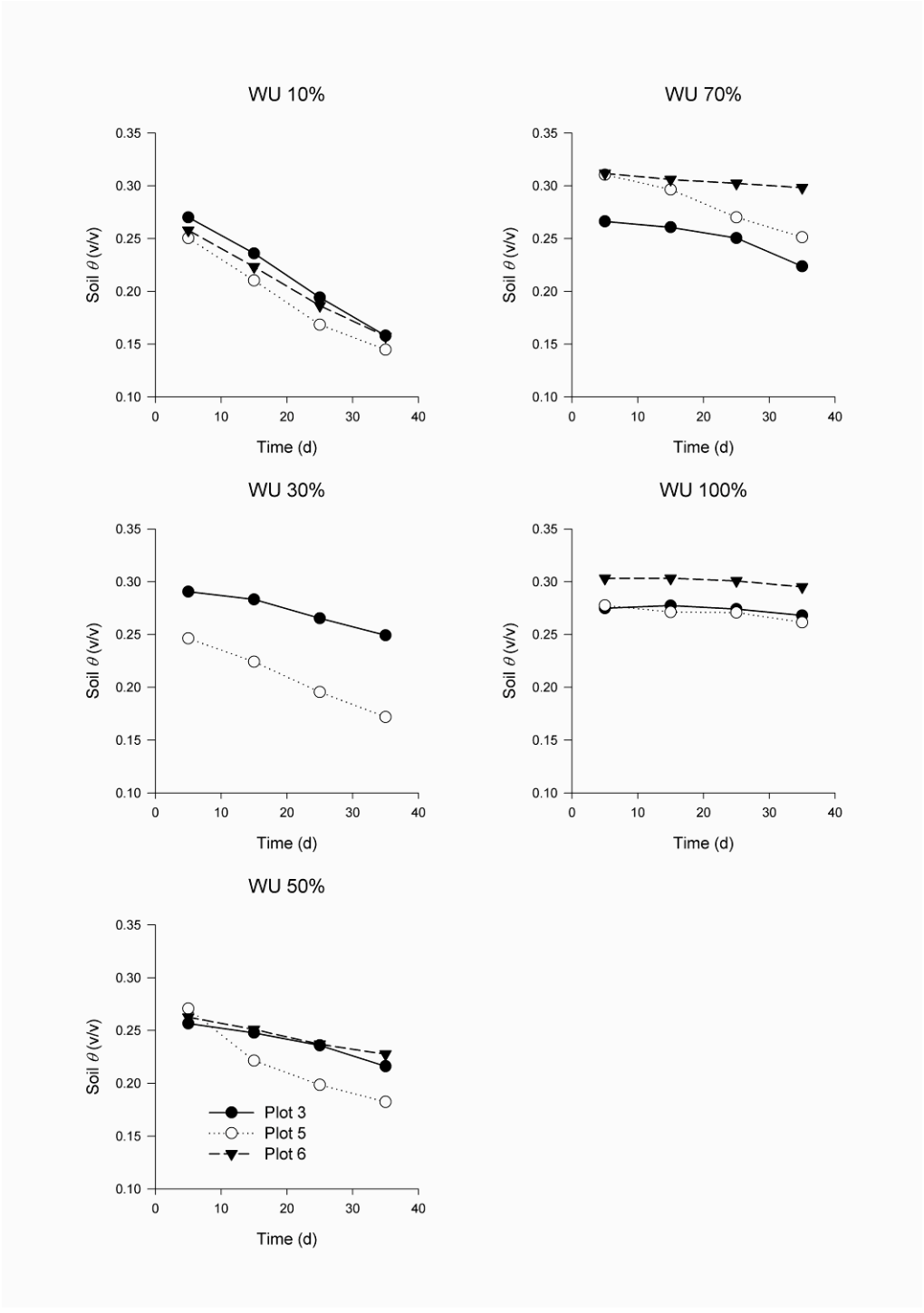

Figure 5.4. Mean soil θ in each pot for successive 10 d periods.

Data are plotted for each water use treatment (WU) applied to the main growth population. n=14.

5.3.4 Radiation use efficiency and soil water

Table 5.2 summarises mean RUE (g MJ^{-1}) for all five water use treatments, calculated from NPP /total intercepted PAR for the 40 d measurement period. NPP was the change in total dry biomass (ΔW) over the 40 d period. Calculation of total intercepted radiation is described in Section 5.3.2. The mean RUE value for well-watered seedlings (2.54 g MJ^{-1}) is very similar to the RUE's reported for well-watered seedlings under a range of PPFD in Chapter 4 (2.6–3.2 g MJ^{-1}).

Table 5.2. Mean RUE for seedlings for 28 December 2008 to 6 February 2008
SD = standard deviation.

Water use treatment (%)	Mean RUE (g MJ^{-1})	SD (g MJ^{-1})
10	2.14	0.189
30	2.24	0.346
50	2.38	0.185
70	2.37	0.050
100	2.54	0.041

Although Table 5.2 shows a reasonably consistent increase in mean RUE in relation to water use treatment, there was considerable scatter in the individual RUE vs water use data as shown by Figure 5.5(a). This appears to be caused by the variation in soil θ values within water use treatments mentioned in the previous section. To allow for this, RUE's were plotted against mean θ (average of measured θ over 40 d) for individual pots, which allowed a clearer relationship to emerge (Figure 5.5(b)).

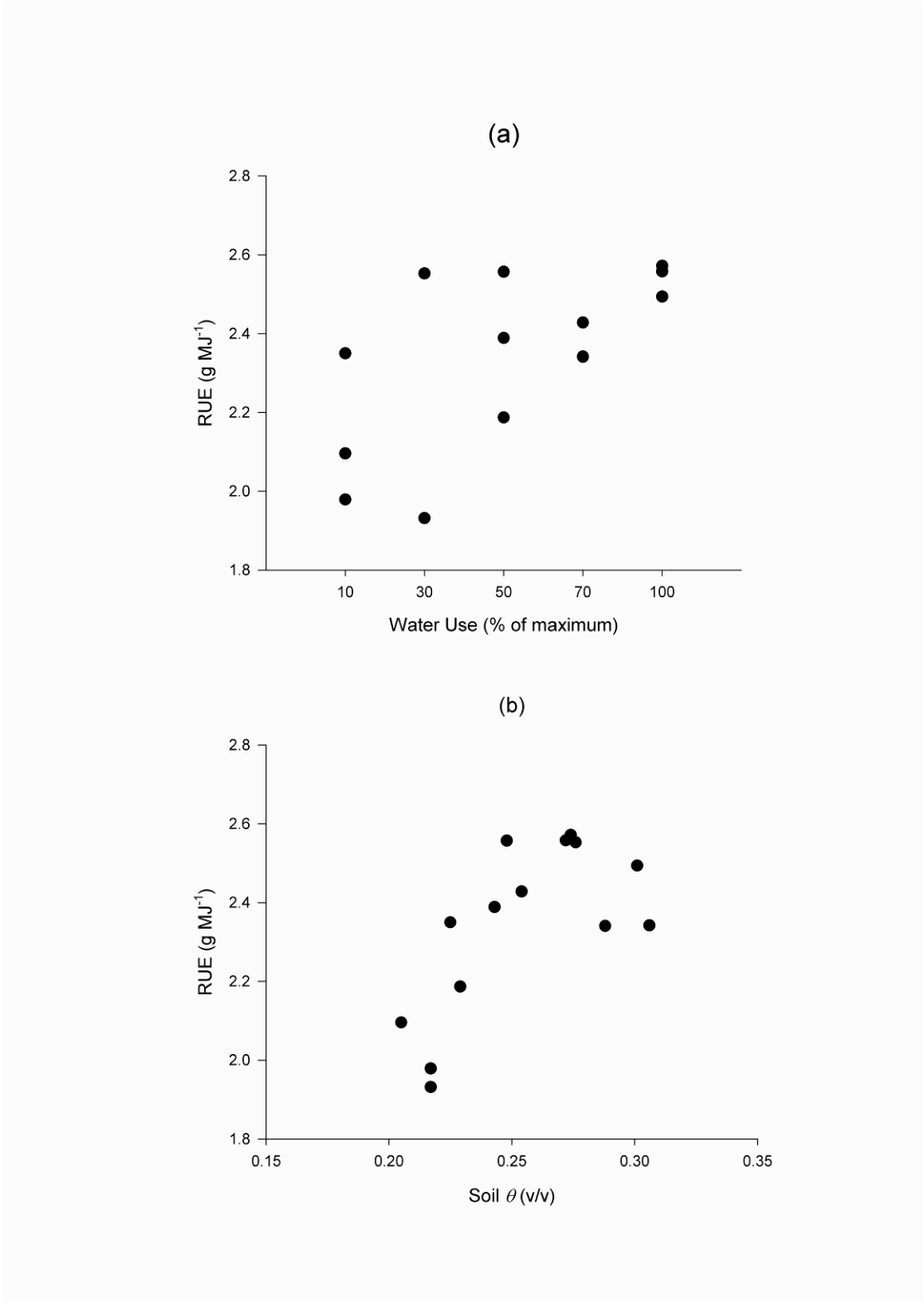

Figure 5.5. Seedling mean RUE's (40d) vs (a) Water use treatment; (b) Soil θ. All data are means for the 40 d measurement period.

Figure 5.5(b) is consistent with the model proposed by Landsberg & Waring (1997). For $\theta > 0.25$, RUE is more or less constant with a mean value ≈ 2.5 g MJ^{-1}. For $\theta < 0.25$, RUE begins to decline towards 0, although this trend would be clearer if lower θ values (in the range = 0.1 – 0.2) had been achieved during the experiment. Note that the maximum θ (40 d mean) achieved in this experiment was ≈ 0.30, even for well watered treatments. This is approximately 0.14 (v/v) less than the saturated value for the sand/grade M perlite mix (0.441 (v/v), Figure 5.2).

5.3.5 RUE and the soil water modifier

For soilless substrates such as the sand/grade M perlite mix used in this experiment, calculation of f_θ using Equation 5.4 is made difficult by uncertainty regarding θ_{max}, the upper limit for PAW. To show the sensitivity of f_θ to θ_{max}, a simple linear regression model was fitted to values of f_θ calculated using a range of assumed θ_{max} values. This regression equation was of the form:

$$\text{RUE} = a + b\, f_\theta \qquad (5.9)$$

where a is the RUE when $f_\theta = 0$, and $a + b$ is the maximum RUE for well watered plants, where $f_\theta = 1$. To fit the regression, a and b were constrained to the values of 0 and 2.5 respectively, and the best-fitting model was obtained by varying the c_θ and n_θ parameters used to calculate f_θ in Equation 5.4. The best fitting model was determined using the coefficient of variation (R^2) between actual RUE and the predicted RUE calculated using Equation 5.4. Results are shown in Table 5.3.

Table 5.3. Parameter values and R^2 for Equation 5.4 with different assumed values for θ_{max}.

θ_{max}	a	b	n_θ	r_θ	R^2
0.35	–0.019	2.500	6.108	0.555	0.664
0.40	–0.006	2.500	7.370	0.619	0.665
0.44	0.005	2.500	8.206	0.660	0.663

Although only three scenarios are shown, they illustrate two key points:

1. Provided n_θ and r_θ are allowed to vary, model R^2 is relatively insensitive to the assumed value for θ_{max}.
2. Assuming that $\theta_{max} = 0.35$ resulted in n_θ and c_θ values similar to those suggested by Landsberg & Waring (1997) for clay loams (≈ 6 and 0.5 respectively), whereas θ_{max} values of 0.4 and 0.44 meant that n_θ and c_θ took values suggested for sandy loams (≈ 7 and 0.6). Comparison of moisture characteristic data for a range of soil textures (Townend *et al.* 2000) suggests that the drainage and plant water availability characteristics of sand/perlite mixes more closely resemble those of sands and sandy loams than those of clay loams.

Therefore, in order to model RUE vs f_θ, a θ_{max} value of 0.4 was assumed because 1) it resulted in values for n_θ and c_θ more in keeping with a coarse porous soil texture than a θ_{max} value of 0.35; and 2) it seems more realistic to assume that θ_{max} is somewhat less than the θ value when the soil is saturated (0.44). Figure 5.6 (a) and (b) show RUE versus (a) r_θ and (b) f_θ calculated using the parameters for the $\theta_{max} = 0.4$ scenario.

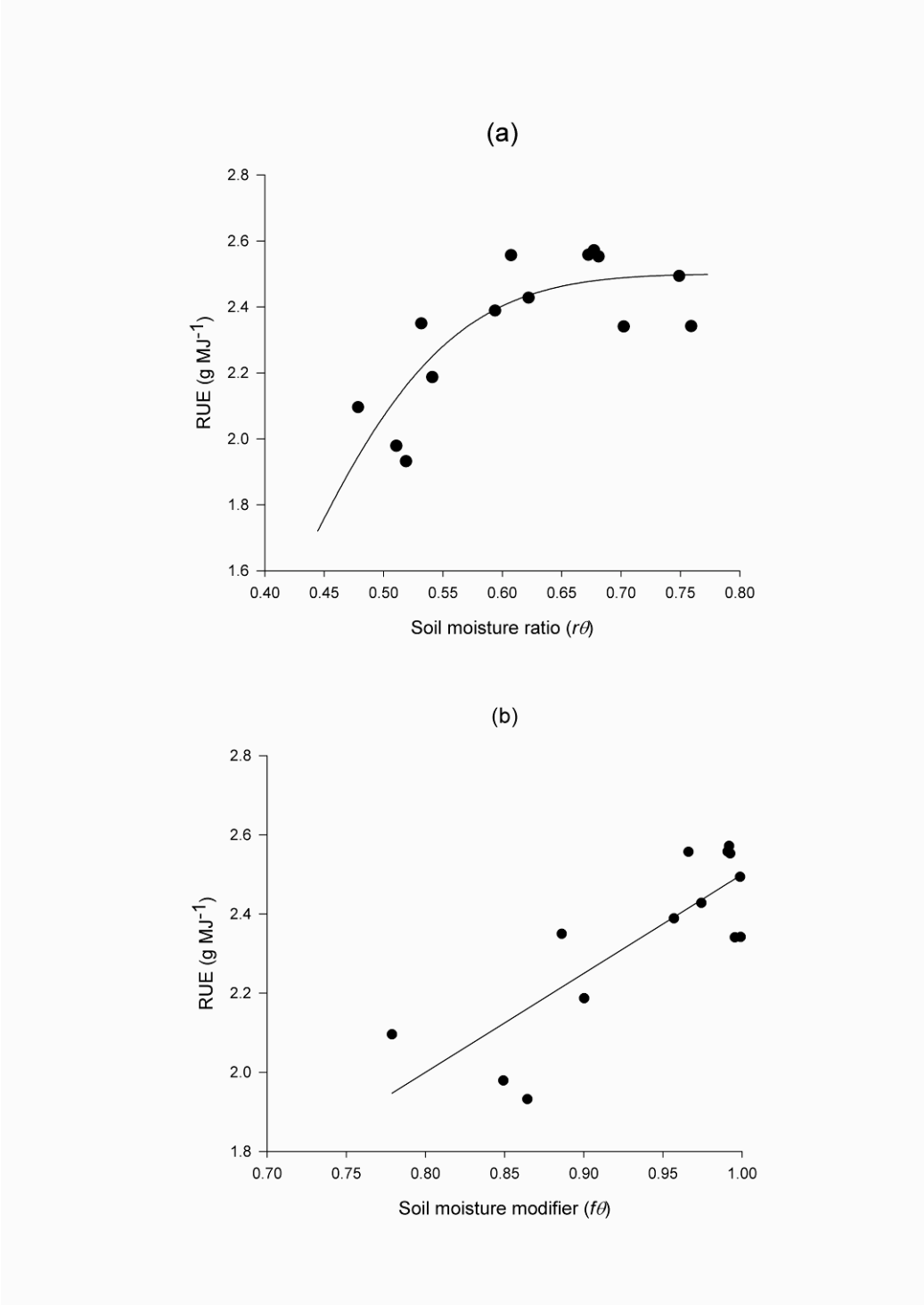

Figure 5.6. RUE (40 d mean) for the main growth population vs (a) soil water ratio; (b) soil moisture modifier.

The solid line is predicted RUE using Equation 5.4., with $\theta_{max} = 0.4$ and n_θ and $c_\theta \approx 7.37$ and 0.619). n =14.

The data in Figure 5(b) shows a reasonable linear fit of f_θ to the observed RUE data, given the limitations discussed above – a small number of data (n = 14), a limited range for the independent variable (f_θ) and uncertainty about the value of θ_{max}.

5.3.6 RUE, plant available water and water use

The physiological mechanisms underpinning the relationship between PAW and RUE are discussed in Section 5.1. These mechanisms were investigated using measurements of seedling assimilation and transpiration made using a modified assimilation chamber interfaced with a LI-Cor 6400, as described in Section 5.2.2. Results are shown in Table 5.4. Also shown in Table 5.4 are soil θ values at the time of measurement. The assimilation chamber environment was similar for all measurements; mean T_{air} was 20.2 °C (SD = 0.32 °C), vapour pressure deficit was 0.64 kPa (SD = 0.13 kPa) and ambient PPFD was 255.8 μmol m^{-2} s^{-1} (SD=30.3 μmol m^{-2} s^{-1}). Note that all transpiration, photosynthesis and stomatal conductance values in this section are expressed per square metre of seedling leaf area, where seedling leaf area is calculated as described in Section 5.2.2.

Figure 5.7 shows transpiration rates (mmol H_2O m^{-2} s^{-1}) versus (a) the estimated soil r_θ at time of measurement and (b) the equivalent soil water modifier (f_θ), calculated using Equation 5.4 with $\theta_{max} = 0.4$ and n_θ and $c_\theta \approx 6.854$ and 0.594. Note that transpiration increases non-linearly with r_θ even when $r_\theta > 0.65$, in contrast to RUE which reached a plateau at that point (Figure 5.6(a)). Using f_θ as the independent variable appears to linearise the relationship between transpiration and soil plant available water.
In general the correlations between the x and y variables in Figure 5.7 are quite close (R^2 = 0.843 and 0.804 for Figures 5.7 (a) and (b) respectively, excluding the data for the seedling in pot 5/1). Both data for pot 5/1 (25 January and 1 February) appear anomalous. The antecedent measurements for these data have been checked and appear to be free from any obvious errors, so the apparent anomalies may well be genuine. The

RUE vs f_θ relationship for this seedling is consistent with other seedlings (Figure 5.6(b)), so the anomaly was not reflected in the growth of the seedling over 40 d.

Table 5.4. Gas exchange measurements of seedlings (transpiration, stomatal conductance and photosynthesis).
A_p = net photosynthesis, g_s = stomatal conductance, Et = transpiration, θ = soil water content (v/v).

Pot	Date	Water use (%)	A_p (μmol m^{-2} s^{-1})	g_s (mol m^{-2} s^{-1})	Et (mmol m^{-2} s^{-1})	θ
3/3	28-Jan	10	0.440	0.014	0.098	0.172
3/3	1-Feb	10	1.037	0.017	0.117	0.159
5/2	25-Jan	10	0.679	0.016	0.114	0.162
5/2	1-Feb	10	0.687	0.010	0.073	0.147
6/2	24-Jan	10	0.873	0.017	0.114	0.180
6/2	1-Feb	10	0.490	0.010	0.064	0.159
3/1	29-Jan	30	0.512	0.028	0.210	0.255
6/1	29-Jan	30	1.483	0.028	0.201	0.181
6/4	28-Jan	50	1.040	0.034	0.234	0.231
3/4	1-Feb	50	0.756	0.031	0.208	0.228
5/3	21-Jan	50	0.875	0.028	0.166	0.197
5/3	1-Feb	50	1.044	0.034	0.198	0.192
6/4	24-Jan	50	0.598	0.032	0.187	0.236
6/4	1-Feb	50	1.273	0.026	0.240	0.240
3/5	23-Jan	70	0.648	0.029	0.218	0.224
5/5	29-Jan	70	1.736	0.047	0.298	0.259
6/5	30-Jan	70	1.661	0.056	0.355	0.297
3/2	28-Jan	100	1.312	0.051	0.279	0.286
3/2	1-Feb	100	1.689	0.038	0.274	0.293
5/1	25-Jan	100	0.899	0.028	0.152	0.275
5/1	1-Feb	100	0.744	0.026	0.114	0.288
6/3	24-Jan	100	1.597	0.040	0.271	0.305
6/3	1-Feb	100	1.663	0.051	0.278	0.322

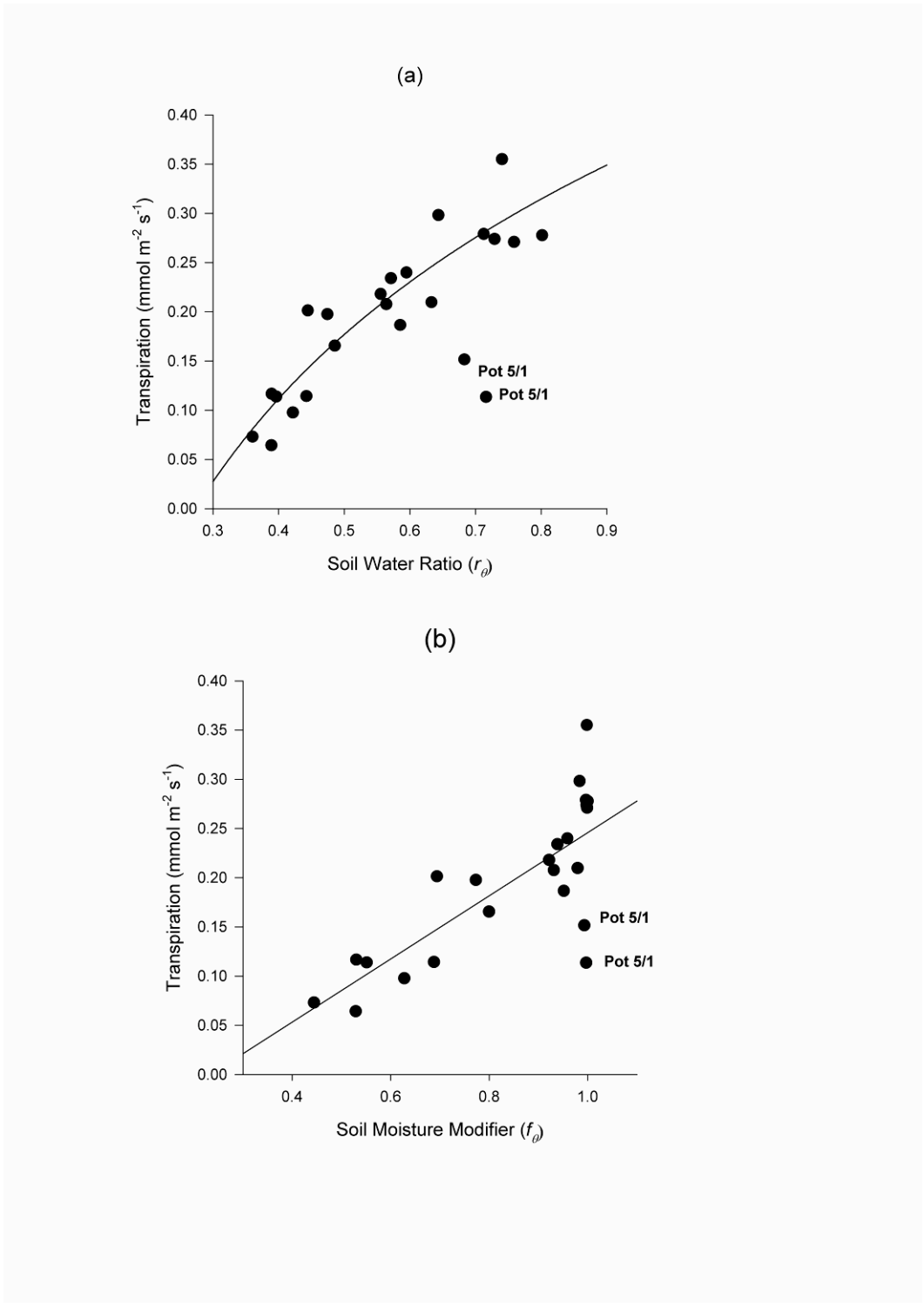

Figure 5.7. Transpiration vs plant available water, expressed as (a) r_θ; (b) f_θ.

f_θ was calculated assuming $\theta_{max} = 0.4$ and n_θ and $c_\theta \approx 7.37$ and 0.619.

Transpiration rates are a function of stomatal conductance, interacting with the vapour pressure deficit from the leaf surface to the surrounding air (D_l) and CO_2 concentration at the leaf surface (Leuning 1995). Assuming that the air within the leaf is saturated, D_l in turn is a function of leaf temperature and the vapour pressure deficit of the surrounding air. These were quite uniform within the assimilation chamber and so the variation in transpiration and stomatal conductance data shown in Table 5.4 should be largely due to variation in plant available water in the soil, which acts on stomatal conductance via the water potential of the leaf tissues as discussed in Section 5.1. This relationship is illustrated by Figure 5.8, which shows the relationship between the fractional water content of the seedling (weight of water in a seedling/ total fresh weight of the seedling) versus the measured r_θ on 6 February when the seedlings were harvested for biomass.

Once again the data exhibit a non-linear pattern, with fractional water content for well-watered seedlings on a plateau (≈ 0.8) but declining to < 0.75 for seedlings experiencing a water deficit. In other words, seedlings were able to maintain high leaf turgor (and therefore stomatal conductance and photosynthesis) until the soil moisture ratio (r_θ) reached ≈ 0.5. This threshold was consistent with the relationship between RUE and r_θ (Figure 5.6(a)).

The relationship between stomatal conductance (g_s) and soil θ was examined by plotting g_s vs soil r_θ and f_θ (calculated from estimated values of θ for the same time that the conductance was measured) (Figure 5.9(a) and (b)).

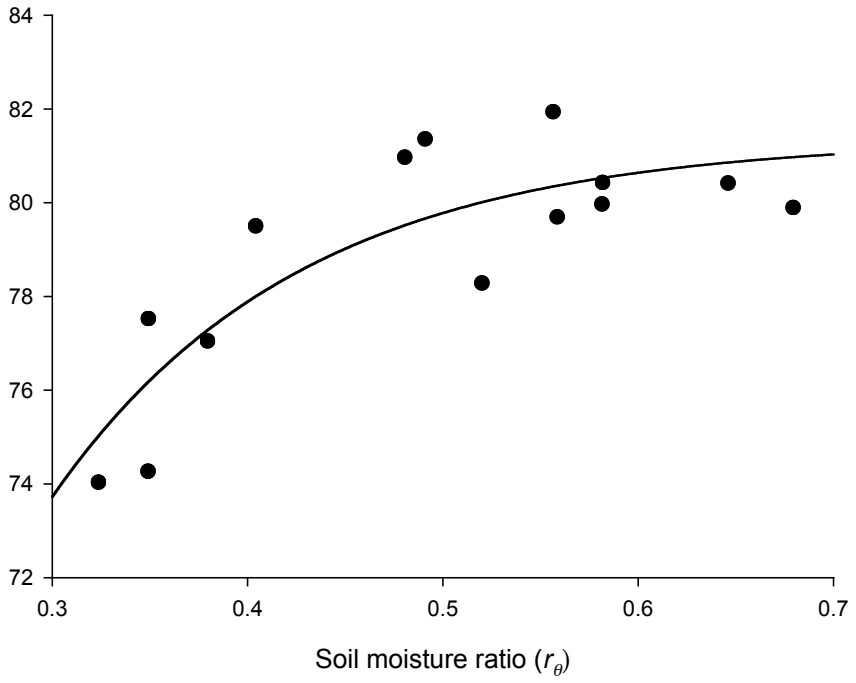

Figure 5.8. Plant water content vs plant available water, expressed as the soil moisture ratio (r_θ).

The solid line is a best-fit trendline drawn to illustrate the asymptotic relationship between the *y* and *x* variables.

There is a clear non-linear relationship between g_s and soil r_θ ($R^2 = 0.794$) as shown by Figure 5.9, although there is no evidence of an asymptotic plateau in conductance when $r_\theta > 0.5$, in contrast to the plateau in plant water content in Figure 5.8. This result is in contrast to that reported by Watt *et al.* (2003b) for well-watered one year old radiata pine seedlings, where stomatal conductance declined linearly from a maximum of 0.28 mmol m^{-2} s^{-1} only when θ became less than a threshold value ($\theta = 0.23$[5]).

[5] Note that the maximum leaf conductance reported by Watt *et al.* (2003b) isconsiderably higher than the values measured in this study. This is because 1) Watt *et al.* (2003b) calculated g_s on a one-sided leaf area basis and 2) the seedlings that they measured were exposed to saturating PPFD ($\approx$ 1000 μmol m^{-2} s^{-1}) compared with an ambient PPFD in the assimilation chamber $\approx$ 250 μmol m^{-2} s^{-1}.

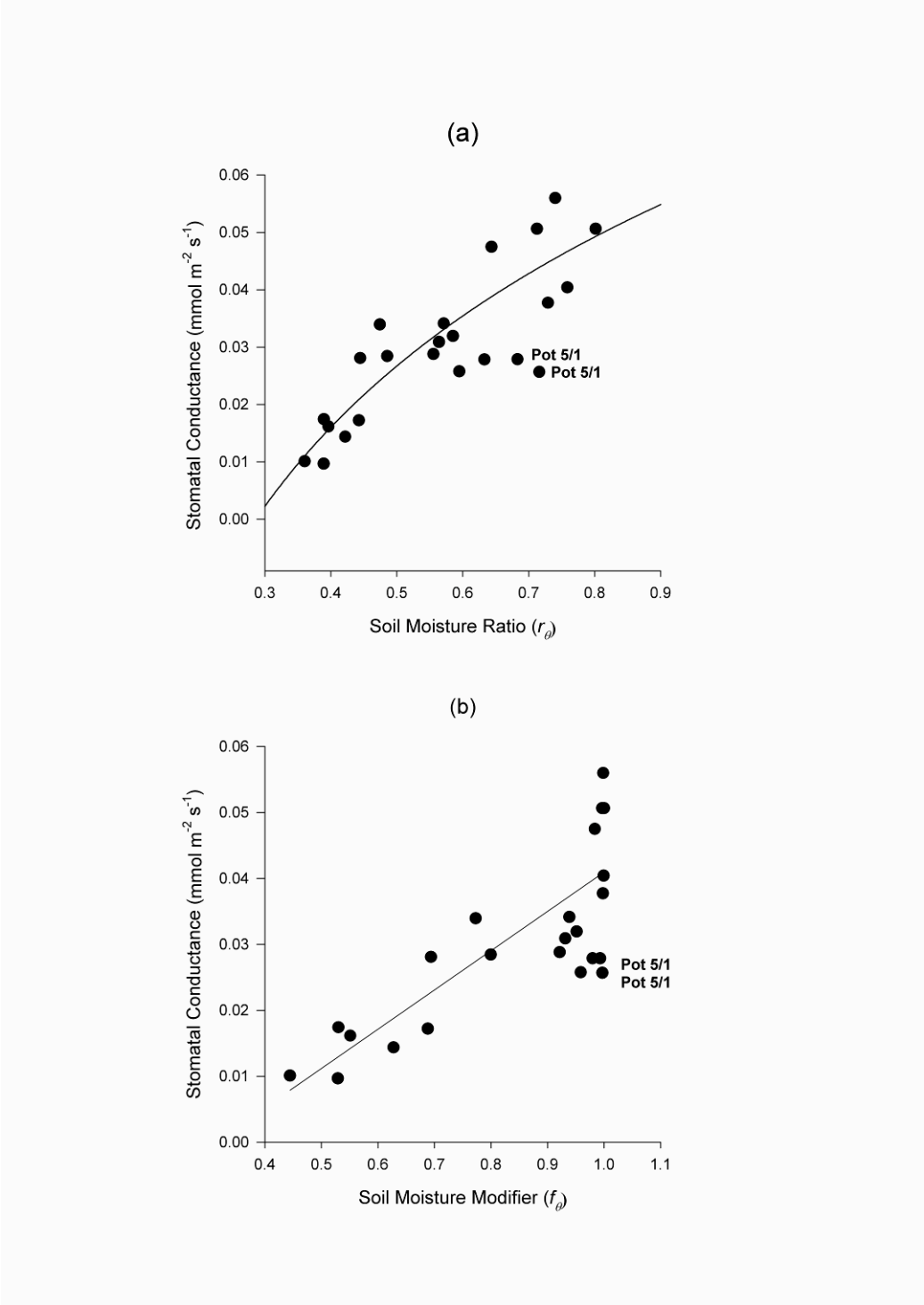

Figure 5.9. Stomatal conductance vs soil water content, shown as (a) r_θ ; (b) f_θ.

f_θ was calculated assuming $\theta_{max} = 0.4$ and n_θ and $c_\theta \approx 7.37$ and 0.619.
The solid lines are a best fit logarithmic (a) and linear (b) trendlines drawn to illustrate the relationship between the *x*-*y* variables. See Table 5.4 for data.

It also meant that linearising the relationship with soil θ using the soil moisture modifier f_θ did not improve the R^2 value (0.701) compared with the relationship with r_θ.

There was insufficient range in ambient PPFD and vapour pressure deficit in this experiment, to be able to model the relationship between stomatal conductance, vapour pressure deficit, photosynthesis and ambient CO_2 concentration specified by models such that of Leuning (1995). However, given the quite uniform PPFD and vapour pressure deficit when gas exchange measurements were taken, it might be expected that stomatal conductance was closely related to photosynthesis. Figure 5.10(a) shows that the relationship between stomatal conductance and instantaneous photosynthesis, while positive, is not a close one ($R^2 = 0.57$). Instantaneous photosynthesis was also normalised for CO_2 concentration at the leaf surface (C_s) by expressing it as a ratio (A_p/C_s, mmol m^{-2} s^{-1}) but this resulted in no improvement in the R^2 value (0.55) of the relationship with stomatal conductance (Figure 5.10(b)).

This lack of close correspondence between instantaneous photosynthesis and stomatal conductance is also reflected in an even weaker correlation shown in Figure 5.11 between instantaneous photosynthesis and soil water status (specified by the soil water modifier f_θ). For the instantaneous photosynthesis data shown in Figure 5.11(a), $R^2 = 0.21$ and for the corrected instantaneous photosynthesis data shown in Figure 5.11(b), $R^2 = 0.18$.

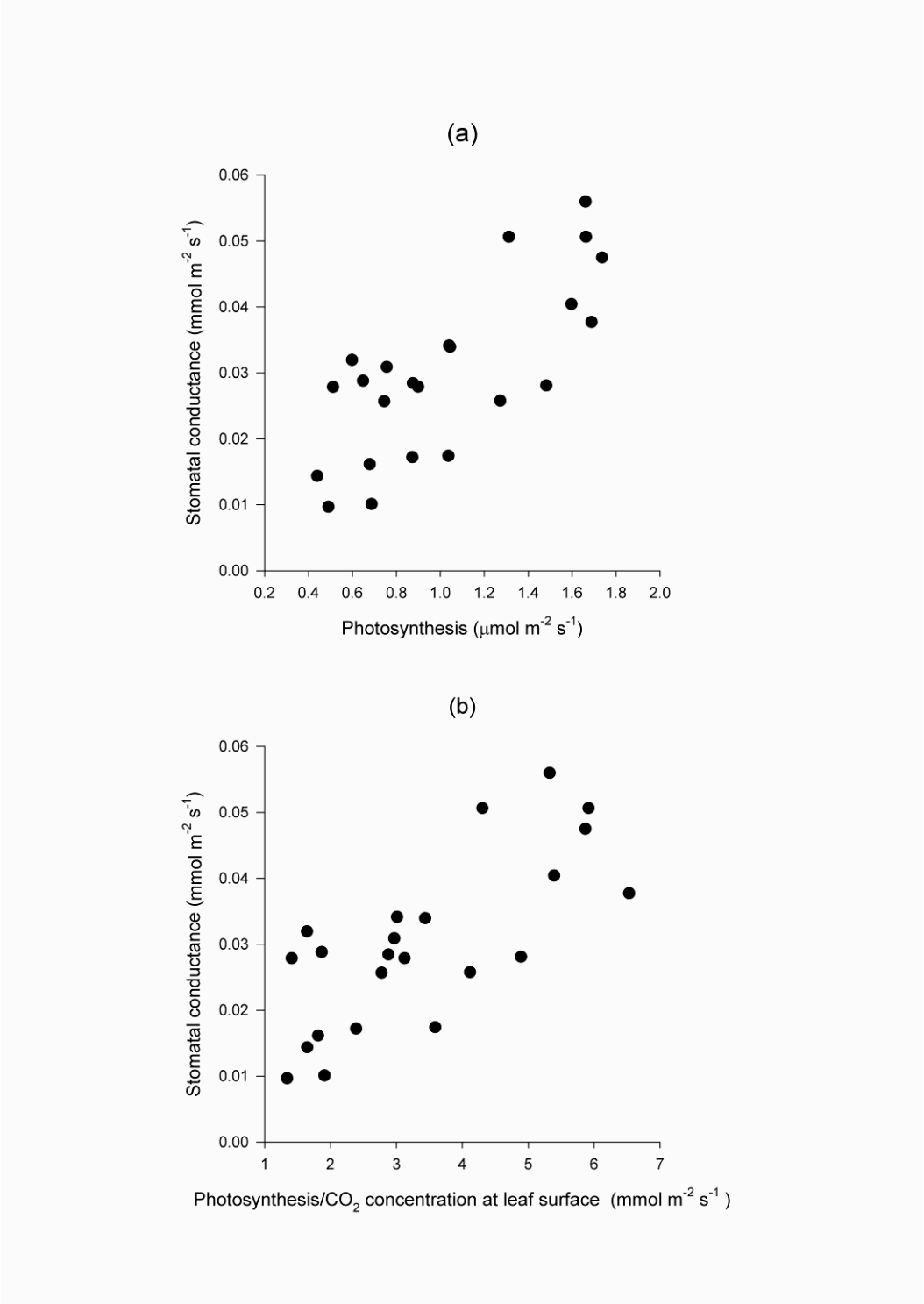

Figure 5.10. Stomatal conductance vs (a) net photosynthesis; (b) net photosynthesis normalized for for CO_2 concentration at the leaf surface (C_s).

See Table 5.4 for data.

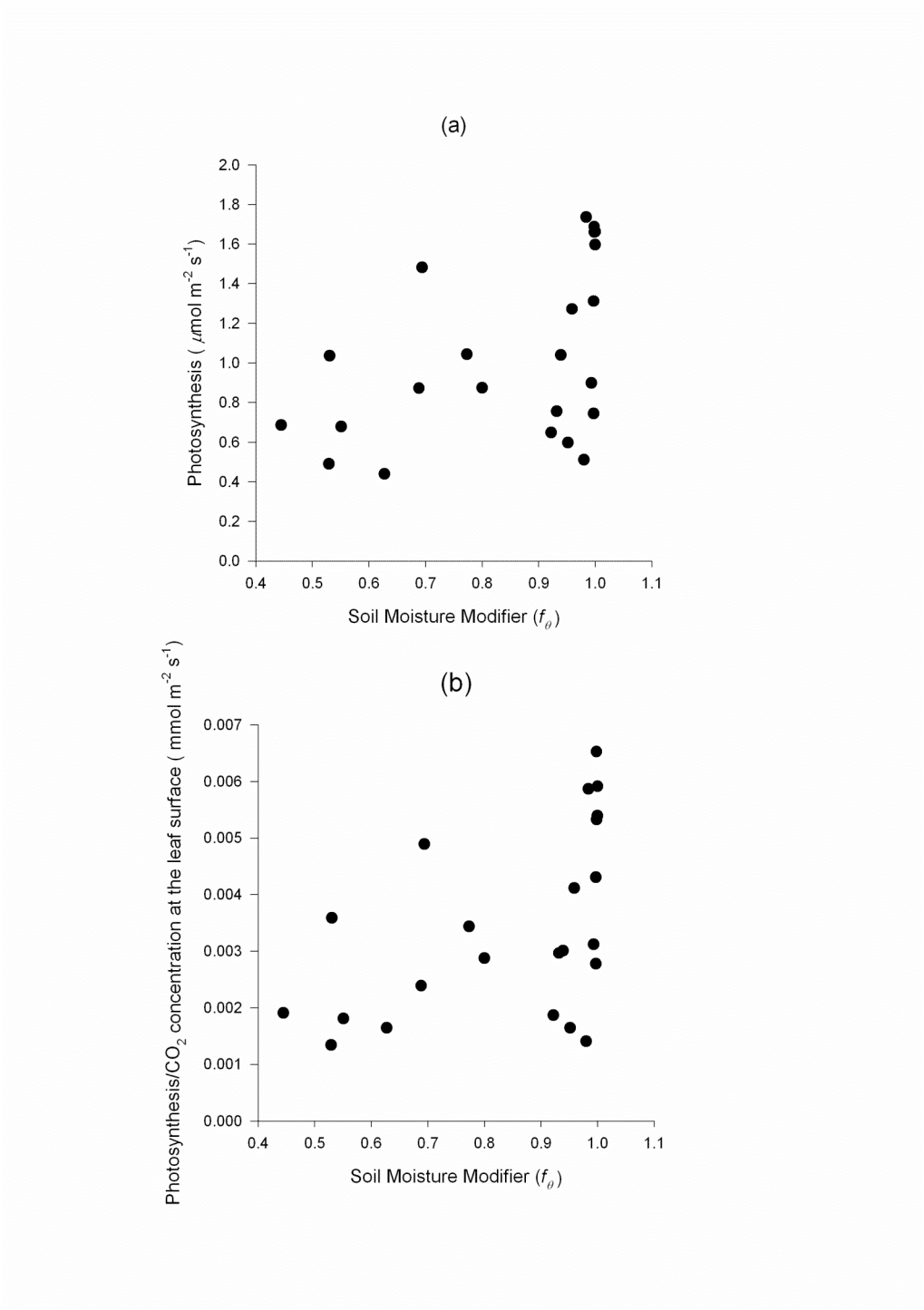

Figure 5.11. (a) Net photosynthesis vs soil water content (f_θ); (b) net photosynthesis normalized for CO_2 concentration at the leaf surface (C_s) vs soil water content (f_θ)

f_θ was calculated assuming $\theta_{max} = 0.4$ and n_θ and $c_\theta \approx 7.37$ and 0.619. See Table 5.4 for data.

5.4 Discussion and Conclusions

The objective of the study described in this chapter was to investigate the effect of deficits in soil plant available water (PAW) on radiata pine seedling RUE. This was done by relating mean seedling RUE measured over a 40 d period, to the mean value of a calculated soil water modifier (f_θ) for the same period.

The mechanistic explanation for the expected relationship between RUE and f_θ was that reduced PAW would cause reduced stomatal conductance of the seedlings in order to reduce tranpirational water loss from seedling tissues. Reduced stomatal conductance would in turn lead to reduced CO_2 flux into the seedling foliage and therefore reduced photosynthesis. This mechanistic explanation was investigated by measuring seedling gas exchange (water vapour and CO_2) in a custom assimilation chamber.
Each of these aspects will be discussed in more detail in the following sections.

5.4.1 Estimation of seedling biomass, PAR interception and RUE

Measurement of seedling biomass, PAR interception and RUE used the methods successfully developed in Chapter 4. The relationship of seedling dry biomass (W) to seedling silhouette area (A) had an R^2 of 0.983 and was used to predict initial W of seedlings at the beginning of the 40 d measurement period. Final W was measured by destructive sampling.

Intercepted PAR was measured using estimated radiance of a sphere surrounding each seedling multiplied by the projected area of the seedling normal to the incident PAR.

Radiance was in turn calculated from measurements of PPFD in the same direction made using a cosine-corrected quantum sensor. While this method is theoretically sound, measurements of PPFD are time-consuming and so were only made once during the 40 d measurement period. These instantaneous measurements were assumed to be representative of radiance for the whole 40 d, usually a safe assumption in a controlled growth cabinet. In this experiment, measurements of PPFD within the cabinet showed temporal variability (mean daylight PPFD = 212.5 μmol m^{-2} s^{-1}, SD 66.1 μmol m^{-2} s^{-1},

coefficient of variation = 31%) which casts doubt on this assumption. Notwithstanding, mean PPFD when the instantaneous measurements were made was 222.5 μmol m^{-2} s^{-1} (SD 67.0 μmol m^{-2} s^{-1}). This is within 4% of the 40 d mean, so the instantaneous measurements are taken as representative of an admittedly variable PAR regime within the cabinet. There is some reassurance that this is a reasonable assumption, in that 1) the calculated RUE's for the well watered seedlings were very similar to those for well-watered seedlings reported in the previous chapter and 2) the calculated RUE's showed a statistically significant relationship with measured PAW.

5.4.2 Effects of soil water deficits on RUE and seedling water use

The relationship between RUE and deficits in soil PAW was shown clearly in the results (Figure 5.6). The use of f_θ transformed an asymptotic relationship between RUE and the soil moisture ratio r_θ into a linear one (Figure 5.6). A simple linear regression fitted to the linearised data yielded an $R^2 = 0.665$, despite limitations in the data (n=14, and f_θ only ranging from 0.78–1.00).

The availability of water for plant uptake will differ between soils with the same value for r_θ but with different textures. A theoretical advantage of using the soil water modifier f_θ is that it normalizes the relationship between the soil moisture ratio r_θ and RUE for the effects of soil texture, so that a particular f_θ value specifies the same deficit in PAW for all soil types. It was originally intended to test this by also imposing the same water use treatments (100, 70, 50, 30 and 10%) on seedlings growing in a fine sandy loam as part of the experiment. This would have allowed 1) estimation of n_θ and c_θ parameters for a different soil texture and 2) testing of the power of the resulting f_θ to explain variation in seedling RUE. However, for the reasons described by Passioura (2006), drainage from the fine sandy loam in PB8 containers was not satisfactory and this part of the experiment was abandoned.

One other limitation in this study was that seedlings were grown at a uniform PPFD (≈ 212 micromol m^{-2} s^{-1}) and under conditions where daytime vapour pressure deficit did not vary widely (mean *RH* 76.5%, SD 8.1%). The applicability of the results from this

experiment at other PPFD and/or vapour pressure deficits was therefore not tested, nor was the underlying assumption in Equation 2.4 that the effects of the soil moisture modifier on RUE are independent of those of the other modifiers.

5.4.3 Effects of soil water deficits on seedling water use and photosynthesis

The relationships between seedling gas exchange and the soil moisture ratio (r_θ) and/or soil moisture modifier (f_θ) were consistent with the mechanistic explanation of the link between RUE and deficits in PAW (Figures 5.7 and 5.9). This supports the assumption that modelled relationships between RUE and PAW deficits can be explained in terms of physiological processes such as gas exchange. Because measurements were made towards the end of the 40 d measurement period, some pots had dried down to $r_\theta < 0.4$, so that effects of water deficits on seedling gas exchange could be shown over a wider range of PAW ($r_\theta = 0.389–0.801$).

One caveat to all the gas exchange data is that they were measured directly on a whole plant basis. Measurements were then corrected to a per m^2 basis using an estimate of total seedling leaf area, which in turn was calculated using a regression equation (Equation 5.7) fitted to data from destructively measured seedlings. Although the seedling projected leaf areas were quite closely correlated with seedling silhouette area (A), estimates of total leaf area using this procedure would have an associated sampling error as well as the measurement error in determining seedling silhouette area. These errors would lead to errors in estimating seedling gas exchange rates (expressed on a leaf area basis), additional to any measurement error in the readings made using the Li-Cor 6400.

With the exception of the measurements for pot 5/1, both stomatal conductance and transpiration rates of seedlings were well correlated with r_θ, although the relationship was curvilinear in both cases. A logarithmic transformation of r_θ allowed a simple linear regression to be fitted to the relationships with both transpiration (Et) and stomatal conductance (g_s) ($R^2 = 0.843$ and 0.794 respectively). However, the logarithmic rather than asymptotic relationship between Et or g_s and r_θ meant that transformation of r_θ to f_θ using Equation 5.4 resulted in lower R^2 values of 0.804 and 0.701 respectively, compared

with the simple logarithmic transformation. The asymptotic plateau in the 40 d mean seedling RUE observed once r_θ was > 0.6 (Figure 5.6(a)), was not paralleled by a plateau in the instantaneous measured rates of g_s and Et. This suggests that for r_θ > 0.6, stomatal conductance increased above the level required to maintain sufficient gas exchange for maximum photosynthesis.

Reduced stomatal conductance with decreasing r_θ was expected to result in reduced photosynthesis and therefore lower seedling RUE, although the relationship between g_s and net photosynthesis is not a simple cause-effect one, with photosynthetic demand for CO_2 "feeding forward" to influence g_s independently of the effects of any soil water deficit, and the leaf to air vapour pressure deficit (D_l) and C_s/C_i ratio also having a bearing (Leuning 1995). There were insufficient data to model these interactions between g_s, net photosynthesis and D_l; a simple *x*-*y* plot of g_s vs net photosynthesis showed an expected positive relationship (Figure 5.10), but the relatively low R^2 (0.575) reflects the lack of data over a sufficiently wide range of values for net photosynthesis. The lack of a close correlation between A_p and g_s may also have arisen from other causes such as: 1) minor variation in D_l and r_θ , but also 2) the uncoupling between g_s and soil r_θ when r_θ was > 0.6, discussed in the preceding paragraph.

5.4.4 Conclusions

1. Methods used to estimate seedling growth, light interception and RUE that were developed in the previous chapter were validated by the results of this study, in that seedling RUE estimates appeared to be realistic, and were consistent with results for well-watered seedlings from the previous experiment.
2. Specification of deficits in plant available water (PAW) experienced by seedlings in terms of a soil moisture modifier (f_θ), resulted in a reasonably close (R^2 = 0.665) linear correlation with mean seedling RUE over a 40 d period. This lends tentative support to the soil moisture modifier proposed by Landsberg & Waring (1997). However, it was not possible to test the ability of the soil moisture modifier to normalize the effects of PAW deficits between different soil types.

Nor was the soil moisture modifier tested for its ability to predict reductions in RUE at PPFD higher or lower than ~ 250 μmol m^{-2} s^{-1}.

3. Measurements of seedling gas exchange in a custom chamber supported the accepted mechanistic explanation of how PAW deficits affect seedling RUE and growth– through reductions in stomatal conductance and CO_2 exchange between the atmosphere and the leaf, which in turn limit photosynthesis. However, it was not possible to test the effects on gas exchange of varying PAR (which also controls photosynthetic rate) or the leaf to air vapour pressure deficit.

6 GENERAL DISCUSSION

Chapter 2 described a conceptual model of regeneration which had four aspects: 1) production and dispersal of seeds, 2) their storage in seed banks until conditions are favourable for germination, followed by 3) germination and 4) the establishment of seedlings on the forest floor. This study has focussed on the latter two aspects of regeneration i.e. seed germination and seedling establishment.

The overall objective of this study was to model aspects of radiata pine regeneration using hybrid models which describe the influence of the environment on germination and initial seedling growth of radiata pine. This chapter reviews how much progress this study has made, and identifies further steps that should be taken towards more complete achievement of this objective.

6.1 Modelling the germination of radiata pine.

The study described in Chapter 3 resulted in a general model of seed germination which made quite accurate predictions over the full range of controlled seedbed conditions under which germination was likely to occur. The model was particularly accurate at suboptimal temperatures, but also made reasonable predictions about germination at supra-optimal temperatures. In the process of developing the model, a mechanistic explanation for the decline in germination rates at supra-optimal temperatures was developed (Section 3.4.6), based on earlier models proposed by Alvarado & Bradford (2002) and Rowse & Finch-Savage (2003). This mechanistic explanation was that the decline in germination rate was not driven just by temperature, but by accumulated hydrothermal time above the base temperature for germination (T_o). This in turn raised the base soil water potential (Ψ_b) towards 0, so that the reduction in germination rate arose from a reduced accumulation of hydro-time, rather than from thermal denaturation of enzymes facilitating germination – the conventional explanation for non-linear

accumulation of thermal time at supra-optimal temperatures for plant development (Bonhomme 2000; Trudgill *et al.* 2005).

The hydrothermal time model was not tested for its predictive accuracy under variable seedbed conditions, and this would be the logical next step in modelling radiata pine seed germination. While the hydrothermal germination model should also apply under fluctuating T and Ψ, there has been varying success in predicting seed germination with hydrothermal models under such conditions (Finch-Savage *et al.* 2000; Taylor *et al.* 2004; Finch-Savage *et al.* 2005b). This may limit the usefulness of the models in predicting germination of seeds sown in seedbeds in the field, where T and Ψ fluctuate both diurnally and over longer time intervals.

As discussed by Finch-Savage *et al.* (2005b), a particularly important challenge is measuring the rate of dehydration and re-imbibition of seeds caused by fluctuating soil moisture. Fluctuations in seedbed temperature may be less critical, because a small object like a seed will rapidly equilibrate with the temperature of the surrounding soil, whereas dehydration and re-imbibition will impose a lag in the response of seed germination rate to soil moisture.

If a hydrothermal time model could be successfully developed for radiata pine under fluctuating conditions, this would lead to the next component in the conceptual model of germination–characterising the seed bed. As discussed in Chapter 2, radiata pine has serotinous cones, which means that natural seed dispersal is typically onto the surface of a seedbed created by fire. Seed is unlikely to be buried and so must be adapted to germination in the most variable part of the seedbed, near the surface. Even when germinated in cultivated nursery beds, the recommended sowing depth for radiata pine is two centimetres (Minko 1986) at which level soil T and Ψ are likely to be highly variable unless Ψ is managed by irrigation or other means.

Therefore, successfully characterizing the seedbed for radiata pine means describing soil T and Ψ values which will fluctuate widely on a diurnal basis, as well as with the rapid

drying that occurs on the soil surface between rainfall or irrigation events. This can be achieved by direct measurements, but there are mathematical models which predict variations in T and Ψ with depth in the soil profile, based on soil characteristics and environmental factors which control the heat and water balance of the soil (Groot & King 1993; Finch-Savage *et al.* 2005a). Once again, models have the advantage of generality in that they allow extrapolation of results from field experiments or other measured data to all sites where radiata pine is regenerated. Therefore a logical development of this study would be screening of published predictive models of soil T and Ψ, followed by validation with measurement data. This would allow predictions of the likelihood of germination success for any particular site, at any particular time (specified in terms of spatial or temporal variation in soil T and Ψ). Descriptions of seed production and dispersal, and seed banking could be integrated into the overall model by using them to define where and when radiata pine seed would be dispersed, and in what quantities, with the germination model then being used to predict the proportion of seeds that germinate and the rate at which they would do so.

For example, in the simplest case where seed is precision-sown into a nursery seedbed, the timing of sowing and the number and location of the seeds are known precisely. In this case, accurate measurements or predictions of soil temperature and soil water potential should lead to accurate predictions of seed germination. For natural regeneration where seed dispersal is triggered by wildfire or extremely high summertime air temperatures, and where a proportion of seed will be lost to predation, predictions of germination success will have a stochastic element. Nonetheless, it should be possible to predict the likelihood of germination success for the range of positions where seed lands after dispersal; on the soil surface, on litter or on a humus layer, partially or fully buried, and in different positions within the newly created gap which may range in size from that created by a single treefall to that created by a catastrophic forest-replacing wildfire or clearfell harvesting.

6.2 Modelling the initial growth of a radiata pine seedling.

Testing the assumptions of the RUE model

The conceptual model of initial seedling growth used in this study is specified by Equation 2.4. Central to this conceptual model are three assumptions:

1. Maximum RUE (RUE in the absence of deficits in environmental factors) for the seedlings would be uniform across all levels of PPFD.
2. Deficits in environmental factors controlling seedling NPP can be specified in the form of modifiers. Multiplying these by RUE would simulate the reduction in photosynthetic efficiency caused by the deficits.
3. The effects of the modifiers on RUE are multiplicative but independent of each other, so that the value of a modifier is determined only by the values of the environmental variables used to calculate the modifier.

Assumption 1 was supported by the results of the study described in Chapter 4. For the three PPFD treatments (25, 50 and 100% PPFD), RUE was reasonably constant albeit with a noticeably (but statistically non-significant) higher mean RUE for PPFD= 25% compared with the two other PPFD treatments in the experiment.

Within the limits of the study described in Chapter 5, the results gave tentative support to assumption 2. Soil water deficits were imposed using five different watering treatments (100, 70, 50, 30 and 10% of maximum seedling water use). For these treatments, PAW (as specified by the soil moisture modifier f_θ) was quite closely correlated with seedling RUE and with the mechanistic processes which are affected by PAW deficits (transpiration and stomatal conductance). In summary, the studies described in Chapters 4 and 5 had results that were consistent with assumptions 1 and 2, and this suggests that RUE models are potentially a very good way to study the regeneration niche of forest seedlings. In particular, the consistency of seedling RUE across a range of PPFD's is encouraging because in contrast to agronomic or pastoral crops, forest seedlings are often regenerated in forest gaps or in the shade of canopies of mature trees or competing weeds. Hence models of seedling growth must be able to predict the effect of variations

in absorbed or intercepted PAR on seedling growth, as well as the deficits in temperature, nutrients, soil water and atmospheric vapour pressure that may be encountered by crops or pastures.

However, this study was not able to test assumption 3, i.e. the independence of the modifiers in their effects on RUE. In the study described in Chapter 5, all other environmental factors (vapour pressure deficit, soil nutrients, temperature) were applied uniformly across all watering treatments and so interactions of f_θ with other modifiers were not tested.

In a study of 14 temperate forest species in the United Kingdom Sack (2004) found that effects of drought on the relative growth rate (RGR) of one year old seedlings was independent of two shade treatments (3% and 30% of full daylight irradiance), suggesting that the soil water modifier could be used to modify RUE at any PPFD level. This result (independence of shade and drought effects on seedling growth) was consistent with other studies of drought × shade interactions on seedling growth (Sack 2004). However, the drought × shade interaction or any other interaction of PPFD and environmental deficits on seedling growth is seldom explored using RUE as the response variable.

One published study that did explore the interaction between RUE and environmental factors was Cheaib *et al.* (2005), which investigated the effect of phosphorus (P) nutrition on seedling RUE for *Pinus pinaster* Aït. and concluded that there was an interaction, such that the slope of the regression equation for NPP vs $\varphi_{p.i}$ (=RUE) was different for seedlings subjected to low PPFD compared to the slope for those subjected to high PPFD. Cheaib *et al.* (2005) suggested that this was due to an interaction with P availability– seedlings at low PPFD were not P limited (due to low NPP) and so the slope of the NPP vs $\varphi_{p.i}$ line was equal to the maximum seedling RUE, whereas the faster growing seedlings were limited by P and so the slope of the NPP vs $\varphi_{p.i}$ line (and therefore seedling RUE) was lower. This highlights one possible limitation of Equation 2.4, where modifier functions may not be independent of the rate of growth of the seedling, because larger faster-growing plants will have greater demand for plant growth factors. This

problem could be avoided by dynamically modelling the levels of nutrients in the soil, and changing their values in the model as depletion occurs–similar to the way in which soil water depletion by faster growing seedlings will be reflected in dynamic changes in the value of f_θ. Regarding the soil nutrient modifier, it should be noted that this modifier is not well specified in 3-PG, and that in the opinion of Mason *et al.* (2007) research into fertility modifiers for different sites is an urgent need.

6.2.1 Estimating the soil water modifier

The soil moisture modifier (f_θ) was estimated using the function proposed by Landsberg & Waring (1997), where f_θ is an sigmoidal function of the soil moisture ratio r_θ. Experimental results (Section 5.3.5) gave only tentative support to the use of f_θ to estimate the effects of soil water deficits on RUE. Apart from the specific difficulties encountered in this study with estimation of f_θ (due to the difficulty in estimating θ_{max} for the sand/perlite mix), the other caveat regarding the use of f_θ is a lack of empirical support for the parameters n_θ and c_θ which specify the effect of soil texture on the relationship between f_θ and r_θ (Landsberg & Waring 1997).

Landsberg & Gower (1997) proposed that an alternative to estimation of f_θ from the soil water ratio was to equate f_θ to the plant water stress integral (PWSI), an integral of measured leaf water potentials proposed by Myers (1988). As with any plant measurement variable used to characterize soil water deficit, this has the advantage that there is no need to measure or assume any soil variables. The plant integrates the effects of soil water potential, hydraulic conductivity and available water volume into its rate of water uptake, which interacts with evapotranspiration from its leaf surfaces to determine leaf water potential.

The disadvantage of PWSI is that leaf water potentials, whether measured by pressure bomb or other apparatus, are relatively time-consuming to measure. Medrano *et al.* (2002) proposed that stomatal conductance could be an alternative measure of water stress in plants, if normalized to remove the effects of variables not related to plant water stress (specified as turgor pressure deficits in the plant tissues). The advantage of

stomatal conductance is that it can be quite rapidly determined for seedlings using gas exchange measurement apparatus such as the Li-Cor 6400, or using porometers specifically designed to measure conductance such as the Li-Cor 1600-M (Mena-Petite *et al.* 2003; L'Hirondelle *et al.* 2007).

A potential way to normalize stomatal conductance could be the Leuning (1995) model discussed in Section 5.4.3. Stomatal conductance of a well watered plant can be related to plant photosynthetic rate A_p, leaf to air vapour pressure deficit D_l and CO_2 concentration at the leaf surface C_s. If this relationship can be specified for radiata pine seedlings, then the maximal stomatal conductance (for a well-watered plant) can be estimated from measured leaf photosynthesis, leaf to air vapour pressure deficit and CO_2 concentration at the leaf surface. The ratio of actual to estimated maximum stomatal conductance would be a suitable measure of plant water stress directly related to the reduction in A_p and therefore RUE arising from a deficit in plant available water.

6.2.2 Estimating other modifiers

The easiest way to estimate modifier values is with experiments in controlled growth cabinets where deficits in one environmental variable can be imposed on seedlings while others are maintained at non-deficit levels. Intercepted or absorbed PAR is also easy to estimate in a controlled environment, as temporal and/or spatial variation in PPFD is minimized. If there is enough room in the cabinet, deficits in more than one environmental variable can be imposed using a split-plot or factorial design, although with a smaller chamber (such as the PGV 36 used in the study described in Chapter 5) there is limited scope for such designs, or for use of shade structures to test for interactions between the effect of the environmental deficit and different levels of PPFD.

Some environmental variables (plant available water, nutrients, PPFD) are relatively easy to manage and therefore impose as designed treatments in environments other than controlled growth cabinets (e.g. greenhouses, shadehouses or field experiments).

However controlled air temperature and vapour pressure deficit are difficult to impose as long-term treatments in such uncontrolled or less-controlled environments. The alternative is to measure the effects of these on leaf gas exchange in cuvettes or assimilation chambers, and use these "instantaneous" measurements to estimate values of modifiers for RUE. Ratios of instantaneous measures of net photosynthesis to incident PPFD can be used as estimators of RUE (Mena-Petite *et al.* 2003; Kruger & Volin 2006) This was attempted in Chapter 5, but it was not possible to vary PPFD, vapour pressure deficit or temperature within the assimilation chamber with a sufficient degree of control or over a wide enough range to generate suitable data for modelling.

6.2.3 Acclimation and variation in RUE with seedling ontogeny and age

At the beginning of this section (6.2), three underlying assumptions of the RUE model were stated and discussed. Two other assumptions underlying this study were not mentioned:

1. Maximum seedling RUE is assumed to be constant throughout the measurement period and independent of seedling ontogeny. Faster growing seedlings not subject to environmental deficits will be larger, and initiate development of branches and secondary needles earlier than seedlings subject to deficits. In order to estimate modifier values such as f_θ in this study, it was assumed that this faster development does not affect seedling RUE.
2. Effects of the modifiers on RUE over a measurement period are assumed to be independent of any previous deficits experienced by the seedling. But plants respond to environmental deficits by acclimation, where they make allometric or physiological adjustments that enable them to maintain photosynthesis and growth despite limitations in essential factors such as light or water. Acclimation responses to variations in temperature for photosynthesis, respiration and growth have been reported for radiata pine seedlings (Rook 1969; M. Turnbull pers. comm.). Conversely, imposed stresses can reduce seedling resilience, so that seedling growth does not recover to maximum levels when the stress is removed. For example, Wood & Brittain (1973) and Squire *et al.* (1988) reported that

radiata pine seedlings subject to soil water deficits did not recover to their previous growth rate when re-watered. These results imply that the effects of deficits on RUE will vary, depending on the deficits previously experienced by the seedling and the resulting degree of acclimation and/or loss of resilience.

6.3 Limitations of the study and future research

This study has demonstrated that existing hybrid models (the hydrothermal time germination model and the 3-PG growth model) can be adapted to model germination and growth of radiata pine under controlled environmental conditions. However, it did not investigate the performance of these models under variable conditions within controlled environments or under field conditions.

In addition the seedling model studies (Chapters 4 and 5) did not:

1. Test the soil moisture modifier over the full range of soil moisture ratios and over more than one soil texture.
2. Succeed with using instantaneous gas exchange measurements to fully characterize the links between seedling net photosynthesis, PPFD, vapour pressure deficit and plant available water.
3. Investigate the effects of environmental factors other than light or water.

Clearly, these deficiencies leave plenty of scope for further studies. Given the importance of light, water and temperature factors to germination and seedling growth, research priorities are as follows:

Seed germination and emergence

1. Investigate whether hydrothermal models can be applied to predict seed germination under variable temperature and water potentials in controlled environments.

2. Review existing literature (and/or simulation models) which quantify variations in seedbed temperature and moisture under field conditions, including forest sites.
3. Assuming success with modelling germination under variable seedbed conditions, the final step would be to develop field experiments to investigate the linkage between soil temperature and moisture and seed germination and emergence, for seeds in various positions within the soil profile.

Seedling growth

1. Develop methods to grow seedlings in a range of soil textures under controlled conditions, and parameterize the soil moisture modifier function (Equation 5. 4) for the range of soil textures from sand to clay.
2. Develop and improve methods for whole-seedling gas exchange measurement, so as to explore the use of instantaneous net photosynthesis and PPFD measurements to estimate RUE, particularly as affected by variations in air temperature and vapour pressure deficit.
3. In order to estimate RUE based on cumulative NPP and intercepted PAR in the field, PAR interception by a seedling has to be quantified under varying conditions of direct radiation flux density and beam angle, and flux density of indirect radiation. This variation occurs both diurnally and from day to day and season to season. Modelling approaches similar to those used by Smolander & Stenberg (2001) may be needed, where direct radiation beam angle and global radiation levels are estimated from standard functions, modified by local factors such as cloudiness and PAR interception by overstorey trees or competing weeds.

6.4 Summary

1. Existing hybrid models (the hydrothermal time germination model and the 3-PG growth model) can be adapted to model germination and growth of radiata pine under controlled environmental conditions.
2. Hydrothermal time models of germination accurately describe radiata pine seed germination under constant conditions of water potential and temperature. Adjustments to base water potentials (Ψ_b) of germinating seeds was proposed as a mechanism whereby seed population "hedged their bets" when encountering less than ideal germination conditions. These adjustments took the form of a slow linear upwards shift in Ψ_b in response to accumulated hydro-time (the hydro-time index) at sub-optimal temperatures (Section 3.4.2); and a rapid asymptotic upwards shift in Ψ_b in response to a supra-optimal hydrothermal time index (*SOHTI*) at supra-optimal temperatures (Section 3.4.6). These adjustments meant that a proportion of the seed population would not germinate under less than ideal conditions, acting as a reserve population in case of mortality by the seeds that did germinate.
3. RUE of young germinated radiata pine seedlings growing in a controlled growth cabinet was reasonably uniform over a range of constant applied PPFD, $\approx$ 125, 250 and 500 μmol m^{-2} s^{-1} (Section 4.3.3).
4. Seedling biomass (W) was most precisely and accurately estimated using a regression equation to predict biomass from seedling silhouette area (A). Seedlings growing in the lower PPFD treatments made allometric adjustments (such as a larger height/ diameter ratio), so that the linear regressions had different parameter values than the regressions for the seedlings in the highest (500 μmol m^{-2} s^{-1}) treatment (Section 4.3.1).
5. RUE was estimated from cumulative NPP (= ΔW), and intercepted PAR which was estimated using measurements of PPFD and seedling projected areas at elevation angles of ±15, ±45 and ±75 degrees. This method yielded estimates of

RUE over 28 d (Chapter 4) and 40 d (Chapter 5) periods that seem consistent with theory and published results.

6. Predicting RUE of seedlings subjected to water stress (Chapter 5) using a calculated soil water modifier (f_θ) was successful within a limited range of soil water stress conditions. The limited range of these conditions means that support for the use of the soil water modifier to predict seedling growth must be tentative at this stage.
7. This study represents first steps towards a hybrid model of radiata pine regeneration under field conditions, which was proposed in Section 2.3.1 as an alternative to empirical models such as the "gap" model of forest regeneration. The study has been successful enough in demonstrating the validity of two hybrid models for predicting germination and young seedling growth. Nonetheless it has been a "methods" study, and the further research proposed in Section 6.3 will be needed before the models can be confidently used to model regeneration in "real-world" forests.

7 ACKNOWLEDGEMENTS

This PhD was supervised by Dr Peter Jarvis, Associate Professor Graeme Buchan and Associate Professor Euan Mason (School of Forestry, University of Canterbury). I am deeply grateful for their advice, encouragement and assistance, without which I could not have completed this study. Thanks also go to Dr Jenny Grace (Scion) and Dr Matthew Turnbull (University of Canterbury) who were external supervisors for this study. Finally, I would like to acknowledge the role of Dr Glenn Stewart, who supervised my thesis before a change in research direction necessitated a change in supervisor.

I am also deeply grateful to my wife Rosemary who has lovingly and patiently endured the role of a postgraduate's partner for the last six years, and provided the necessary balanced outlook when I was severely lacking in that quality. Members of my family all lent a hand, but special thanks to Rosemary, Lauren and Johanna for technical assistance, data entry and typing.

This study has benefited from discussions with and assistance from the following colleagues: Richard Sedcole and Richard Duncan (statistics); David Whitehead (physiological modelling); Bill Finch-Savage and Kath Phelps (hydrothermal models); Mike Watt (modelling); Sam Carrick (data sensing and soil moisture characteristic measurements); Murray Davis (mycorrhizal inoculum); and Horacio Bown (measurements). Derrick Moot, Annamaria Mills, Hamish Brown and Andrew Fletcher dispensed useful advice on how to survive a PhD.

Lincoln University is blessed with capable and enthusiastic technical staff. Particular thanks go to Neil Smith (soil moisture measurement and datalogging)), Stephen Stilwell (who helped with just about everything technical) and Lissy Kajer, who did much of the day to day work in the germination experiments. I would also like to acknowledge the contribution to this study of the following people: Keith Pollock (experimental set-up,

data logging, light measurement); Brent Richards (pots, media, propagation); Lewis Jennings and Alastair Galbraith (electronic data sensing and data logging), Stu Larsen (data sensing and controlled growth cabinets), Don Heffer (equipment fabrication) Barbara Brunton and Adrienne Goldsack (seed incubators and germination methods), Alan Wise (thermocouples) and Amanda Clifford (stores and administration).

Financial and material support was provided by Proseed NZ Ltd and the Robert C. Bruce Trust. Funding for travel in connection with this study was provided by the Lincoln University Foundation. Most importantly, Lincoln University allowed me to work part-time on this study while a member of the teaching staff, and a Lincoln University scholarship allowed me to complete this study on a full-time basis in 2007-2008.

Finally, a big thank you to the colleagues and friends with whom I have worked and socialised during my time at Lincoln University. To study and teach here with such a great bunch of people has been one of the best experiences of my life.

8 REFERENCES

Akaike H. 1974. A new look at the statistical model identification. *IEEE Transactions on Automatic Control* **AC-19**: 716-723.

Allen PS, Meyer SE, Khan MA. 2000. Hydrothermal time as a tool in comparative germination studies. In: M. Black, K. J. Bradford, J. Vasquez-Ramos eds. *Seed Biology: Advances and Applications.* Oxford, U.K.: CAB International, 401-410.

Alvarado V, Bradford KJ. 2002. A hydrothermal time model explains the cardinal temperatures for seed germination. *Plant, Cell and the Environment* **25**: 1061-1069.

Anon. 1997. To stratify or not to stratify radiata seed-research update. In. *Tree Seed News (published by PROSEED NZ Ltd)*. 2.

ASAE. 2003. Guidelines for measuring and reporting environmental parameters for plant experiments in growth chambers (ANSI/ASAE EP411.4 MAR02). *ASAE Standards 2003*. St. Joseph, Missouri: American Society of Agricultural Engineers, 708-713.

Attiwill PM, Squire RO, Neales TF. 1982. Photosynthesis and transpiration of *Pinus radiata* D.Don under plantation conditions in Southern Australia. II. First -year seedlings and 5-year old trees on aeolian sands at Rennick (South-western Victoria). *Australian Journal of Plant Physiology* **9**: 761-771.

Baker FS. 1945. Effects of shade upon coniferous seedlings grown in nutrient solution. *Journal of Forestry* **43**: 428-435.

Baker FS. 1949. A revised tolerance table. *Journal of Forestry* **47**: 179-181.

Bannister MH. 1973. The Origins of Radiata Pine in Cultivation. In: *What's New in Forest Research*. Rotorua, New Zealand: Forest Research Institute. 4.

Barnes BV, Zak DR, Denton SR, Spurr SH. 1998a. *Forest Ecology*. New York: John Wiley & Sons.

Barnes BV, Zak DR, Denton SR, Spurr SH. 1998b. Forest tree variation. Chapter 4. *Forest Ecology*. New York: Wiley, 63-93.

Barnes BV, Zak DR, Denton SR, Spurr SH. 1998c. Light. Chapter 8. *Forest Ecology*. New York: John Wiley & Sons, 182-205.

Barnes BV, Zak DR, Denton SR, Spurr SH. 1998d. Regeneration ecology. Chapter 5. *Forest Ecology*. New York: Wiley, 94-121.

Bewley JD, Black MD. 1983. *Physiology and Biochemistry of Seeds in Relation to Germination. Volume 1; Development, Germination and Growth*. New York: Springer Verlag.

Bonhomme R. 2000. Bases and limits to using "degree.day" units. *European Journal of Agronomy* **13**: 1-10.

Bradford KJ. 1995. Water relations in seed germination. In: J. Kigel, G. Galili eds. *Seed Development and Germination*. New York, U.S.A: Marcel Dekker, 351-396.

Bradford KJ. 2002. Applications of hydrothermal time to quantifying and modeling seed germination and dormancy. *Weed Science* **50**: 248-260.

Bradford KJ, Somasco OA. 1994. Water relations of lettuce seed thermoinhibition.1. Priming and endosperm effects on base water potential. *Seed Science Research* **4**: 1-10.

Buchan GD, Grewal KS. 1990. The power-function model for the soil moisture characteristic. *Journal of Soil Science* **41**: 111-117.

Burnham KP, Anderson DR. 2001. Kullback-Leibler information as a basis for strong inference in information studies. *Wildlife Research* **28**: 111-119.

Cheaib A, Mollier A, Thunot S, Lambrot C, Pellerin S, Loustau D. 2005. Interactive effects of phosphorus and light availability on early growth of maritime pine seedlings. *Annals of Forest Science* **62**: 575-583.

Coley PD, Bryant JP, Chapin FS. 1985. Resource availability and plant anti-herbivore defense. *Science* **230**: 895-899.

Coops NC, Waring RH, Landsberg JJ. 1998. Assessing forest productivity in Australia and New Zealand using a physiologically-based model driven with averaged monthly weather data and satellite-derived estimates of canopy photosynthetic capacity. *Forest Ecology and Management* **104**: 113-127.

Covell S, Ellis RH, Roberts EH, Summerfield RJ. 1986. The influence of temperature on seed germination rate in grain legumes. *J. Exp. Bot.* **37**: 705-715.

Crawley MJ. 2002. *Statistical Computing: an Introduction to Data Analysis Using S-Plus*

Chichester, U.K.: Wiley.

Dahal P, Bradford KJ. 1994. Hydrothermal time analysis of tomato seed germination at suboptimal temperature and reduced water potential. *Seed Science* **4**: 71-80.

Dallman PR. 1998. *Plant Life in the World's Mediterranean Climates: California, Chile, South Africa, Australia, and the Mediterranean Basin*. Berkeley and Los Angeles: University of California Press.

Daskalakou EN, Thanos CA. 2004. Postfire regeneration of Aleppo pine-the temporal pattern of seedling recruitment. *Plant Ecology* **171**: 81-89.

de Chantal M, Leinonen K, Kuuluvainen T, Cescatti A. 2003. Early response of *Pinus sylvestris* and *Picea abies* seedlings to an experimental canopy gap in a boreal spruce forest. *Forest Ecology and Management* **176**: 321-336.

DeLucia EH, George K, Hamilton JG. 2002. Radiation-use efficiency of a forest exposed to elevated concentrations of atmospheric carbon dioxide. *Tree Physiology* **22**: 1003-1010.

Dewar RC, Medlyn B E, McMurtrie, R E. 1998. A mechanistic analysis of light and carbon use efficiencies. *Plant, Cell & Environment* **21**: 573-588.

Driessche P vd, Driessche R vd. 1991. Growth analysis (Chapter 3). In: R. van den Driessche ed. *Mineral Nutrition of Conifer Seedlings*. Boca Raton, Florida: CRC Press, 61-84.

Dzierzon H, Mason EG. 2006. Towards a nationwide growth and yield model for radiata pine plantations in New Zealand. *Canadian Journal of Forest Research* **36**: 2533-2543.

Elsacker Pv, Keppens H, Impens I. 1983. A simple photographical method for analyzing the radiation interception by an individual tree. *Agricultural Meteorology* **29**: 285-298.

Ellis RH, Covell S, Roberts EH, Summerfield RJ. 1986 The influence of temperature on seed germination rate in grain legumes: II. Intraspecific variation in chickpea (Cicer arietinum L.) at constant temperatures. *J. Exp. Bot.* **37**: 1503-1515.

Farmer RE. 1997. *Seed Ecophysiology of Temperate and Boreal Zone Forest Trees*. Delray Beach, Florida: St. Lucie Press.

Farquhar GD, von Caemmerer S, Berry JA. 1980. A biochemical model of photosynthetic CO2 assimilation in leaves of C3 species. *Planta* **149**: 78-90.

Fenton GR. 1951. Regeneration of *Pinus radiata* D.Don following fire. *New Zealand Forest Service Research Notes* **1**: 1-10.

Fielding JM. 1947. *The Seeding and Natural Regeneration of Monterey Pine in South Australia. Bulletin No. 29*. Canberra, Australia: Forestry and Timber Bureau.

Finch-Savage W, Rowse HR, Whalley R. 2005a. Simulation of seed germination and seedling emergence.Beta version. http://www2.warwick.ac.uk/fac/sci/hri2/research/seedscience/simulation/

Finch-Savage WE. 2004. Chapter 2. The use of population-based threshold models to describe and predict the effects of seedbed environment on germination and seedling emergence of crops. In: R. L. Benech-Arnold, R. A. Sanchez eds. *Handbook of Seed Physiology. Applications to Agriculture*. Binghamton, New York: The Haworth Reference Press, 51-95.

Finch-Savage WE, Phelps K, Peach L, Steckel JRA. 2000. Use of threshold germination models under variable field conditions. In: M. Black, K. J. Bradford, J. Vasquez-Ramos eds. *Seed Biology: Advances and Applications.* Oxford, U.K.: CAB International, 489-497.

Finch-Savage WE, Rowse HR, Dent KC. 2005b. Development of combined imbibition and hydrothermal threshold models to simulate maize (*Zea mays*) and chickpea (*Cicer arietinum*) seed germination in variable environments. *New Phytologist* **165**: 825-838.

Fitter AH, Hay RKM. 2002. *Environmental Physiology of Plants*. London U.K.: Academic Press.

Fonteno WC. 1989. An approach to modelling air and water status of horticultural substrates. *Acta Horticulturae* **238**: 67-74.

Forcella F, Benech Arnold RL, Sanchez R, Ghersa CM. 2000. Modeling seedling emergence. *Field Crops Research* **67**: 123-139.

Forde MB. 1966. Pinus radiata in California. *New Zealand Journal of Forestry* **11**: 20-42.

Gardner CM, Robinson D, Blyth K, Cooper JD. 2000. Soil water content. In: K. A. Smith, C. E. Mullins eds. *Soil and Environmental Analysis; Physical Methods*. New York: Marcel Dekker.

Gianinetti A, Cohn MA. 2007. Seed dormancy in red rice. XII: Population-based analysis of dry-afterripening with a hydrotime model. *Seed Science Research* **17**: 253-271.

Grace JC. 1987. Theoretical ratio between "one-sided" and total leaf surface area for pine needles. *New Zealand Journal of Forestry Science* **17**: 292-296.

Grace JC, Jarvis PG, Norman JM. 1987. Modelling the interception of solar radiant energy in intensively managed stands. *New Zealand Journal of Forestry Science* **17**: 193-209.

Gray AN, Spies TA. 1997. Microsite controls on tree seedling establishment in conifer forest canopy gaps. *Ecology* **78**: 2458-2473.
Green SR. 1993. Radiation balance, transpiration and photosynthesis of an isolated tree. *Agricultural and Forest Meteorology* **64**: 201-221.
Groot A, King KM. 1993. Modeling the physical environment of tree seedlings on forest clearcuts. *Agricultural and Forest Meteorology* **64**: 161-185.
Grubb PJ. 1977. The maintenance of species-richness in plant communities; the importance of the regneration niche. *Biological Reviews* **52**: 107-145.
Grundy AC, Phelps K, Reader RJ, Burston S. 2000. Modelling the germination of *Stellaria media* using the concept of hydrothermal time. *New Phytologist* **148**: 433-444.
Gummerson RJ. 1986. The effect of constant temperatures and osmotic potentials on germination of sugar beet. *Journal of Experimental Botany* **37**: 729-741.
Hardegree SP, Emmerich WE. 1990. Effect of polyethylene glycol exclusion on the water potential of solution-saturated filter paper. *Plant Physiology* **92**: 462-466.
Heth D, Kramer PJ. 1975. Drought tolerance of pine seedlings under various climatic conditions. *Forest Science* **21**: 72-82.
Hutchinson FE. 1957. Concluding remarks. *Cold Spring Harbour Symposia on Quantitative Biology* **22**: 415-427.
ISTA. 2003. *International Rules for Seed Testing. Adopted at the Extraordinary Meeting 2002, Santa Cruz Bolivia to Become Effective on 1st January 2003*. Bassersdorf, Switzerland: International Seed Testing Association.
Jose S, Merritt S, Ramsey CL. 2003. Growth, nutrition, photosynthesis and transpiration responses of longleaf pine seedlings to light, water and nitrogen. *Forest Ecology and Management* **180**: 335-344.
Kao C, Rowan KS. 1970. Biochemical changes in seed of *Pinus radiata* during stratification. *Journal of Experimental Botany* **21**: 869-873.
Kaufmann MR. 1977. Soil temperature and drought effects on growth of Monterey pine. *Forest Science* **23**: 317-325.
Kebreab E, Murdoch AJ. 1999. Modelling the effects of water stress and temperature on germination rate of *Orobanche aegyptiaca* seeds. *Journal of Experimental Botany* **334**: 655-664.
Kennedy S, Black K, O'Reilly C, Ni Dhubain A. 2007. The impact of shade on morphology, growth and biomass allocation in *Picea sitchensis*, *Larix X eurolepis* and *Thuja plicata*. *New Forests* **33**.
Khan SR, Rose R, Haase DL, Sabin TE. 2000. Effects of shade on morphology, chlorophyll concentration, and chlorophyll fluorescence of four Pacific Northwest conifer species. *New Forests* **19**: 171-186.
Kirschbaum MUF. 1999. CenW, a forest growth model with linked carbon, energy, nutrient and water cycles. *Ecological Modelling* **118**: 17-59.
Korzukhin MD, Ter-Mikaelian M, Wagner RG. 1996. Process versus empirical models: which approach for forest ecosystem management? *Canadian Journal of Forest Research* **26**: 879-887.
Kruger EL, Volin JC. 2006. Re-examining the empirical relation between plant growth and leaf photosynthesis. *Functional Plant Biology* **33**: 421-429.

Kusmintardjo, Coolbear P, Firth A. 1991. Pre-sowing treatments for the improvement of germination in *Pinus radiata*. In: P. Coolbear, C. A. Cornford, K. M. Pollock eds. *Seed Symposium-Seed Development and Germination. Special Publication No. 9*. Tauranga: Agronomy Society of New Zealand. Christchurch., 103-104.

L'Hirondelle SJ, Simpson DG, Binder WD. 2007. Chlorophyll fluorescence, root growth potential and stomatal conductance as estimates of field performance potential in conifer seedlings. *New Forests* **34**: 235-251.

Landsberg JJ, Gower ST. 1997. *Applications of Physiological Ecology to Forest Management*. San Diego, California: Academic Press.

Landsberg JJ, Waring RH. 1997. A generalised model of forest productivity using simplified concepts of radiation-use efficiency, carbon balance and partitioning. *Forest Ecology and Management* **95**: 209-228.

Lavery PB, Mead DJ. 1998. *Pinus radiata*: a narrow endemic takes on the world. In: D. M. Richardson ed. *Ecology and Biogeography of Pinus*. Cambridge, United Kingdom: Cambridge University Press, Chapter 21. pp 432-449.

Leuning R. 1995. A critical appraisal of a combined stomatal-photosynthesis model for C3 plants. *Plant, Cell and the Environment* **18**: 339-355.

LI-COR Inc. 1992. *LAI-2000 Plant Canopy Analyser Instruction Manual*. Lincoln, Nebraska: Li-COR Inc.

LI-COR Inc. Undated. *Application Note No 3. Interfacing Custom Chambers to the LI-6400 Sensor Head*. Lincoln, Nebraska: LI-COR Inc.

Martin TA, Hinckley TM, Meinzer FC, Sprugel DG. 1999. Boundary layer conductance, leaf temperature and transpiration of *Abies amabilis* branches. *Tree Physiology* **19**: 435-443.

Mason EG. 2004. Effects of soil cultivation, fertilisation, initial seedling diameter and plant handling on the development of maturing *Pinus radiata* D. Don on Kaingaroa gravelly sand in the Central North Island of New Zealand. *Bosque (Valdivia)* **25**: 43-55.

Mason EG, Rose RW, Rosner LS. 2007. Time vs. light: a potentially useable light sum hybrid model to represent the growth of Douglas-fir subject to varying levels of competition. *Canadian Journal of Forest Research* **37**: 795-805.

McMurtrie RE, Landsberg JJ. 1992. Using a simulation model to evaluate the effects of water and nutrients on the growth and carbon partitioning of *Pinus radiata*. *Forest Ecology and Management* **52**: 243-260.

McNaughton KG, Green SR, Black TA, Tynan BR, Edwards WRN. 1992. Direct measurement of net radiation and photosynthetically active radiation absorbed by a single tree. *Agricultural and Forest Meteorology* **62**: 87-107.

Medlyn BE. 1998. The physiological basis of the light use efficiency model. *Tree Physiology* **18**: 167-186.

Medlyn B. 2004. Radiation conversion. In: M. Mencuccini ed. *Forests at the Land-Atmosphere Interface*. Wallingford, U.K.: CABI Publications, 33-37.

Medrano H, Escalona JM, Bota J, Gulias J, Flexas J. 2002. Regulation of photosynthesis of C_3 plants in response to progressive drought: stomatal conductance as a reference parameter. *Annals of Botany* **89**: 895-905.

Mena-Petite A, Robredo A, Alcalde S, Dunabeitia MK, Gonzalez-Moro MB, Lacuesta M, Munoz-Rueda A. 2003. Gas exchange and chlorophyll fluorescence responses of *Pinus radiata* D.Don seedlings during and after several storage regimes and their effects on post-planting survival. *Trees* **17**: 133-143.

Menzies MI, Bond SMC, Dibley M. 1991. Factors affecting radiata pine seed germination. In: P. Coolbear, C. A. Cornford, K. M. Pollock eds. *Seed Symposium-Seed Development and Germination. Special Publication No. 9*. Tauranga: Agronomy Society of New Zealand.

Milner KS, Coble DW. 1996. A mechanistic approach to modelling the effects of grass competition on seedling growth and survival. In: J. V. Skovsgaard, V. K. Johannsen eds. *Modelling Regeneration Success and Early Growth of Forest Stands. Proceedings from the IUFRO Conference, held in Copenhagen, 10-13 June 1996*. Horsholm: Danish Forest and Landscape Research Institute, 68-76.

Minko G. 1986. Seed cover and emergence, survival and growth of radiata pine seedlings. In: *Forestry Technical Papers No. 30*. Melbourne: State Forests and Lands Service, Victoria. 45-48.

Minko G, Aeberli BC. 1986. Spread of vegetation into indigenous vegetation in North-eastern Victoria. In: *Forestry Technical Papers No. 30*. Melbourne: State Forests and Lands Department, Victoria. 17-25.

Monteith JL. 1972. Solar radiation and productivity in tropical ecosystems. *Journal of Applied Ecology* **9**: 744-766.

Monteith JL. 1977. Climate and the efficiency of crop production in Britain. *Philosophical Transactions of the Royal Society London* **281**: 277-294.

Monteith JL, Unsworth MH. 1990. *Principles of Environmental Physics*. Oxford: Butterworth-Heinemann.

Moulds FR. 1955. Monterey pine seedling establishment under varying conditions of crown cover and soil treatment. *Australian Forestry* **19**: 100-116.

Murray JD, Lea-Cox JD, Ross DS. 2002. Time domain reflectometry accurately monitors and controls irrigation water applications in soilless substrates. *Acta Horticulturae* **633**: 75-82.

Myers BJ. 1988. Water stress integral--a link between short-term stress and long-term growth. *Tree Physiology* **4**: 315-323.

Nambiar EKS, Bowden GD, Sands R. 1979. Root regeneration and plant water status of *Pinus radiata* D.Don seedlings transplanted to different soil temperatures. *Journal of Experimental Botany* **30**: 1119-1131.

Ni B-R, Bradford KJ. 1992. Quantitative models characterizing seed germination responses to abscisic acid and osmoticum. *Plant Physiol.* **98**: 1057-1068.

Norgren O, Elfving B, Olsson O. 1995. Non-destructive biomass estimation of tree seedlings using image analysis. *Scandinavian Journal of Forest Research* **10**: 347-352.

Norman HC, Cocks PS, Smith FP, Nutt BJ. 1998. Reproductive strategies in Mediterranenan annual clovers: germination and hardseededness. *Australian Journal of Agricultural Research* **49**: 973-982.

O'Brien MJ, O' Hara KL, Erbilgin N, Wood DL. 2007. Overstory and shrub effects on natural regeneration processes in native *Pinus radiata* stands. *Forest Ecology and Management* **240**: 178-185.

Ow LF, Whitehead D, Walcroft AS, Turnbull MH. Undated. Thermal acclimation of photosynthesis and respiration in radiata pine. *Unpublished*.
Page AI. 1970. The re-establishment of radiata pine at Kaingaroa Forest. *New Zealand Journal of Forestry* **15**: 69-78.
Passioura JB. 2006. The perils of pot experiments. *Functional Plant Biology* **33**: 1075-1079.
Peper PJ, McPherson EG. 2003. Evaluation of four methods for estimating leaf area of solated trees. *Urban Forestry Urban Green* **2**: 19-29.
Perry DA. 1994. *Forest Ecosystems*. Baltimore, MD: The Johns Hopkins University Press.
Phelps K, Finch-Savage WE. 1997. A statistical perspective on threshold type germination models. In: R. H. Ellis, M. Black, A. J. Murdoch, T. D. Hong eds. *Basic and Applied Aspects of Seed Biology*. Dordrecht: Kluwer, 361-368.
Pomeroy KB. 1949. The germination and initial establishment of loblolly pine under various surface soil conditions. *Journal of Forestry* **47**: 541-543.
Poorter H, Nagel O. 2000. The role of biomass allocation in the growth response of plants to different levels of light, CO_2, nutrients and water; a quantitative review. *Australian Journal of Plant Physiology* **27**: 595-607.
Price DT, Zimmerman NE, van der Meer PJ, Lexer MJ, Leadley P, Jorritsma ITM, Schaber J, Clark DF, Lasch P, McNulty S, Wu J, Smith B. 2001. Regeneration in gap models:priority issues for studying forest responses to climate change. *Climatic Change* **51**: 475-508.
R Development Core Team. 2004. *R: A Language and Environment for Statistical Computing*. Vienna, Austria: R Foundation for Statistical Computing.
R Development Core Team. 2007. *R: A Language and Environment for Statistical Computing*. Vienna, Austria: R Foundation for Statistical Computing.
Reynolds JF, Bugmann H, Pitelka LF. 2001. How much physiology is needed in forest gap models for simulating long-term vegetation response to global change? Challenges, limitations and potentials. *Climatic Change* **51**: 541-557.
Richardson B. 1993. Vegetation management practices in plantation forests of Australia and New Zealand. *Canadian Journal of Forest Research* **23**: 1989-2005.
Richardson B, Vanner A, Ray J, Davenhill N, Coker G. 1996. Mechanisms of *Pinus radiata* growth suppression by some common forest weed species. *New Zealand Journal of Forestry Science* **26**: 421-437.
Richardson DM, Higgins SI. 1998. Pines as invaders in the Southern Hemisphere. In: D. M. Richardson ed. *Ecology and Biogeography of Pinus*. Cambridge, United Kingdom: Cambridge University Press, Chapter 22. pp 450-473.
Rimbawanto A, Coolbear P, Dourado AM, Firth A. 1988. Seed maturation precedes cone ripening in New Zealand *Pinus radiata*. *New Zealand Journal of Forestry Science* **18**: 139-148.
Robakowski P, Montpied P, Dreyer E. 2003. Plasticity of morphological and physiological traits in response to different levels of irradiance in seedlings of silver fir (*Abies alba* Mill) *Trees* **17**: 431-441.
Roberts EH. 1988. Temperature and seed germination. In: S. P. Long, F. I. Woodward eds. *Symposia of the Society for Experimental Biology*. Cambridge: Society for Experimental Biology (U.K.), 109-132.

Rook DA. 1969. The influence of growing temperature on photosynthesis and respiration of Pinus radiata seedlings. *New Zealand Journal of Botany* **7**: 43-55.

Rowse HR, Finch-Savage WE. 2003. Hydrothermal threshold models can describe the germination response of carrot (*Daucus carota*) and onion (*Allium cepa*) seed populations across both sub- and supra-optimal temperatures. *New Phytologist* **158**: 101-108.

Roy DF. 1966. *Silvical Characteristics of Monterey Pine (Pinus radiata D.Don). U.S. Forest Service Research Paper PSW-31*. Berkeley, California: Pacific Southwest Forest and Range Experimental Station. Forest Service, U.S. Department of Agriculture.

Ruehle JL, Marx DH, Muse HD. 1984. Calculated non-destructive indices of growth response for young pine seedlings. *Forest Science* **30**: 469-474.

Russell G, Jarvis PG, Monteith JL. 1989. Absorption of radiation by canopies and stand growth. Chapter 2. In: G. Russell, B. Marshall, P. G. Jarvis eds. *Plant Canopies: their Growth, Form and Function*. New York, USA; Melbourne, Australia: The Press Syndicate of the University of Cambridge, 21-39.

Ryan MG, Hunt ER, McMurtrie RE, Ågren GI, Aber JD, Friend AD, Rastetter EB, Pulliam W, Raison J, Lindner. S. 1996. Comparing Models of Ecosystem Function for Temperate Conifer Forests. I. Model Description and Validation In: A. Breymeyer, D. O. Hall, J. M. Melillo, G. I. Ågren eds. *SCOPE 56 - Global Change: Effects on Coniferous Forests and Grasslands*. New York: John Wiley & Sons, 313-362.

Sack L. 2004. Responses of temperate woody seedlings to shade and drought: do trade-offs limit potential niche differentiation? *Oikos* **107**: 110-127.

Sager JC, McFarlane JC. 1997. Radiation. In: R. W. Langhans, T. W. Tibbits eds. *Plant Growth Chamber Manual. North Central Regional Research Publication No. 340*. Ames, Iowa: Iowa State University.

Sahin U, Anapali O, Ercisli S. 2002. Physico-chemical and physical propoeries of some substrates used in horticulture. *Gartenbauwissenschaft* **67**: 55-60.

Sands PJ. 1995. Modelling canopy production II. From single-leaf photosynthetic parameters to daily canopy photosynthesis. *Australian Journal of Plant Physiology* **22**: 603-614.

Sands R, Kriedemann PE, Cotterill PP. 1984. Water relations and photosynthesis in three families of radiata pine seedlings known to differ in their response to weed control. *Forest Ecology and Management* **9**: 173-184.

Sasaki S, Kozlowski TT. 1968. The role of cotyledons in early development of pine seedlings. *Canadian Journal of Botany* **46**: 1173-1183.

Sharpe P. 1990. Forest modeling approaches: compromises between generality and precision In: R. Dixon, R. Mehldahl, G. Ruark, W. Warren eds. *Process Modeling of Forest Growth Responses to Environmental Stress*: Timber Press, 180–191

Sheriff DW, Mattay JP. 1995. Simultaneous effects of foliar nitrogen, temperature, and humidity on gas exchange in *Pinus radiata*. *Australian Journal of Plant Physiology* **22**: 615-626.

Sinclair TR. 2005. Theoretical analysis of soil and plant traits influencing daily plant water flux on drying soils. *Agronomy Journal* **97**: 1148-1152.

Smolander S, Stenberg P. 2001. A method for estimating light interception by a conifer shoot. *Tree Physiology* **21**: 797-803.
Squire RO, Attiwill PM, Neales TF. 1987. Effects of changes of available water and nutrients on growth, root development and water use in *Pinus radiata* seedlings. *Australian Forest Research* **17**: 99-111.
Squire RO, Neales TF, Loveys BR, Attiwill PM. 1988. The influence of water deficits on needle conductance, assimilation rate and abscisic acid concetration on seedlings of *Pinus radiata* D.Don. *Plant, Cell and Environment* **11**: 13-19.
Stephens SL, Piirto DD, Caramagno D. 2004. Fire regimes and resultant forest structure in the native Ano Nuevo Monterey pine (*Pinus radiata*) forest, California. *The American Midland Naturalist* **152**: 25-36.
Storer AJ, Wood DL, Gordon TR, Libby WJ. 2001. Restoring native Monterey pine forests in the presence of an exotic pathogen. *Journal of Forestry* **99**: 14-18.
Tamura N, Yoshida T, Tanaka A, Sasaki R, Bando A, Toh S, Lepiniec L, Kawakami K. 2006. Isolation and characterisation of high temperature-resistant germination mutants of *Aridopsis thaliana*. *Plant Cell Physiology* **47**: 1081-1094.
Taylor JR, Roundy BA, Allen PS, Meyer SE. 2004. Predicting seedling emergence using soil moisture and temperature sensors. In: A. L. Hild, N. L. Shaw, S. E. Meyer, D. T. Booth, E. D. McArthur eds. *Seed and Soil Dynamics in Shrubland Systems*. Laramie, Wyoming: USDA Forest Service Rocky Mountain Research Station, Ogden, Utah, 140-145.
Ter-Mikaelian M, Parker WC. 2000. Estimating biomass of white spruce seedlings with vertical photo imagery. *New Forests* **20**: 145-162.
Thomson AP, Prior KW. 1958. Natural regeneration of *P.radiata* following the Balmoral forest fire. *New Zealand Journal of Forestry* **7**: 51-70.
Townend J, Reeve MJ, Carter A. 2000. Water release characteristic. In: K. A. Smith, C. E. Mullins eds. *Soil and Environmental Analysis: Physical Methods*. New York: Marcel Dekker.
Trudgill DL, Honek A, Li D, Straalen NMv. 2005. Thermal time-concepts and utility. *Annals of Applied Biology* **146**: 1-14.
Vale FXR, Fernandes EIF, Liberato JR. 2003. QUANT - A software for plant disease severity assessment. *ICPP 2003, 8th International Congress of Plant Pathology*. Christchurch, New Zealand.
von Caemmerer S. 2000. Chapter2. Modelling C_3 photosynthesis. *Biochemical Models of Leaf Photosynthesis*. Collingwood, Victoria: CSIRO Publishing, 29-70.
Wahbi A, Sinclair TR. 2007. Transpiration response of Arabidopsis, maize and soybean to drying of artificial and mineral soil. *Environmental and Experimental Botany* **59**: 188-192.
Walcroft AS, Whitehead D, Silvester WB, Kelliher FM. 1997. The response of photosynthetic model parameters to temperature and nitrogen concentration in *Pinus radiata* D.Don. *Plant, Cell and Environment* **20**: 1338-1348.
Waring RH. 1987. Characteristics of trees predisposed to die. *BioScience* **37**: 569-574.
Watt AS. 1947. Pattern and process in the plant community. *Journal of Ecology* **35**: 1-22.
Watt MS, Whitehead D, Mason EG, Richardson B, Kimberley MO. 2003a. The influence of weed competition for light and water on growth and dry matter

partitioning of young *Pinus radiata*, at a dryland site. *Forest Ecology and Management* **183**: 363-376.

Watt MS, Whitehead D, Richardson B, Mason EG, Leckie AC. 2003b. Modelling the influence of weed competition on the growth of young *Pinus radiata*, at a dryland site. *Forest Ecology and Management* **178**: 271-286.

Weiner J. 2004. Allocation, plasticity and allometry in plants. *Perspectives in Plant Ecology, Evolution and Systematics* **6**: 207-215.

Wetzel S, Burgess D. 2001. Understorey environment and vegetation response after partial cutting and site preparation in *Pinus strobus* L. stands. *Forest Ecology and Management* **151**: 43-59.

Wilson JW. 1981a. Analysis of growth, photosynthesis, and light interception for single plants and stands. *Annals of Botany* **48**: 507-512.

Wilson JW. 1981b. Analysis of light interception by single plants. *Annals of Botany* **48**: 501-505.

Wood GR, Brittain EG. 1973. Photosynthesis, respiration and transpiration of radiata pine. *New Zealand Journal of Forestry Science* **3**: 181-190.

Wullschleger SD, Jackson RB, Currie WS, Friend AD, Luo Y, Mouillot F, Pan Y, Shao G. 2001. Below-ground processes in gap models for simulating forest reponse to global change. *Climatic Change* **51**: 449-473.

Yoda K, Kira T, Ogawa H, Hozami K. 1963. Self thinning in overcrowded pure stands under cultivated and natural conditions. *Journal of Biology, Osaka City University.* **14**: 107-129.

Zou C, Sands R, Buchan G, Hudson I. 2000a. Least limiting water range: a potential indicator of physical quality of forest soils. *Australian Journal of Soil Research* **38**: 947-958.

Zou C, Sands R, Sun O. 2000b. Physiological responses of radiata pine roots to soil strength and soil water deficit. *Tree Physiology* **20**: 1205-1207.

Zutter BR, Gjerstad DH, Glover GR. 1986. Effects of interfering vegetation on biomass, fasicle morphology, and leaf area of loblolly pine seedlings. *Forest Science* **32**: 1016-1031.

9 APPENDICES

All appendices are contained in the CD stored on the inside back cover of this document.

Appendix 1 Settings for LiCor 6400.

Appendix 2 Germination data, Chapter 3.

Appendix 3 Seedling biomass, Chapter 4.

Appendix 4 PPFD measurements, Chapter 4.

Appendix 5 Seedling silhouette areas, Chapter 4.

Appendix 6 Calculation of seedling RUE, Chapter 4.

Appendix 7 Seedling biomass, Chapter 5.

Appendix 8 Seedling silhouette area and projected leaf areas, Chapter 5.

Appendix 9 PPFD measurements, Chapter 5.

Appendix 10 Calculation of seedling RUE, Chapter 5.

Appendix 11 Soil moisture characteristic for the sand/perlite mixture, Chapter 5.

Appendix 12 Soil water measurements, Chapter 5.

Appendix 13 Seedling RUE versus soil water content, Chapter 5.

Appendix 14 Gas exchange measurements, Chapter 5.